UNIVERSIDADE DE SÃO PAULO
Instituto de Ciências Matemáticas e de Computação

Multiscale methods for oil reservoir simulation

Rafael Trevisanuto Guiraldello

Tese de Doutorado do Programa de Pós-Graduação em Ciências de Computação e Matemática Computacional (PPG-CCMC)

ICMC USP
SÃO CARLOS

Rafael Trevisanuto Guiraldello

Multiscale methods for oil reservoir simulation

Thesis submitted to the Institute of Mathematics and Computer Sciences – ICMC-USP – in accordance with the requirements of the Computer and Mathematical Sciences Graduate Program, for the degree of Doctor in Science. *FINAL VERSION*

Concentration Area: Computer Science and Computational Mathematics

Advisor: Prof. Dr. Roberto Federico Ausas

USP – São Carlos
February 2019

Ficha catalográfica elaborada pela Biblioteca Prof. Achille Bassi
e Seção Técnica de Informática, ICMC/USP,
com os dados inseridos pelo(a) autor(a)

G965m

Guiraldello, Rafael Trevisanuto
Multiscale methods for oil reservoir simulation / Rafael Trevisanuto Guiraldello; orientador Roberto Federico Ausas. -- São Carlos, 2019.
128 p.

Tese (Doutorado - Programa de Pós-Graduação em Ciências de Computação e Matemática Computacional) -- Instituto de Ciências Matemáticas e de Computação, Universidade de São Paulo, 2019.

1. Porous Media. 2. Darcy Flows. 3. Robin boundary conditions. 4. Multiscale Methods. I. Ausas, Roberto Federico, orient. II. Título.

Bibliotecários responsáveis pela estrutura de catalogação da publicação de acordo com a AACR2:
Gláucia Maria Saia Cristianini - CRB - 8/4938
Juliana de Souza Moraes - CRB - 8/6176

Rafael Trevisanuto Guiraldello

Métodos multiescala para simulação de reservatórios de petróleo

Tese apresentada ao Instituto de Ciências Matemáticas e de Computação – ICMC-USP, como parte dos requisitos para obtenção do título de Doutor em Ciências – Ciências de Computação e Matemática Computacional. *VERSÃO REVISADA*

Área de Concentração: Ciências de Computação e Matemática Computacional

Orientador: Prof. Dr. Roberto Federico Ausas

USP – São Carlos
Fevereiro de 2019

To Ana Maria and Antonio with all the love of my heart.

ACKNOWLEDGEMENTS

I would like to thank all the people who have somehow contributed to the development of this thesis. Firstly, I would like to thank Dr. Felipe Pereira for accepting me in this postgraduate program and for introducing me to this research area, which was the motivation for all the academic research that is part of this thesis. I would also like to thank my academic advisor Dr. Roberto Ausas for all the cooperative work, always friendly and helpful with feedback and insightful ideas in the development of this research.

In order to develop this work a range of basic knowledge was essential, and in this sense I thank Dr. Gustavo Buscaglia, Dr. Roberto Ausas and Dr. Fabricio Sousa for all the knowledge transmitted in the graduate disciplines. Here a special thanks to Dr. Gustavo Buscaglia for the care to direct my studies on related topic to my research project whenever possible within these disciplines.

I would like to thank the Institute of Mathematical and Computer Sciences (ICMC) and the University of São Paulo (USP) for all the resources and facilities offered for the developments of this research. Thanks also to the University of Texas at Dallas (UT-Dallas) for making its facilities available, where part of this work was developed in an internship under the supervision of Dr. Felipe Pereira, which I thank for the academic collaboration during this period and for contributing immensely in my stay in the city of Dallas.

I would also like to thank the Center for Applied Mathematical Sciences for Industry (CEPID - CeMEAI) through Dr. José Cuminato for the financial support in my participation in international congresses, thus contributing to the dissemination of my results.

I had the opportunity to work in collaboration with Dr. Felipe Pereira, Dr. Roberto Ausas, Dr. Fabricio Sousa and Dr. Gustavo Buscaglia through the development of this project and in the development of academic articles whom I thank for the scientific collaboration, always with a friendly and cooperative atmosphere, contributing to my development as a scientist.

Finally, I would like to thank my parents, Ana Maria and Antonio, and also my lifemate Vanessa for all the love and support, without you none of this would be possible.

“Therefore the problem is not so much, to see what nobody has yet seen,
but rather to think concerning that which everybody sees, what nobody has yet thought..”
(Arthur Schopenhauer)

RESUMO

GUIRALDELLO, R. T. **Métodos multiescala para simulação de reservatórios de petróleo**. 2019. 130 p. Tese (Doutorado em Ciências – Ciências de Computação e Matemática Computacional) – Instituto de Ciências Matemáticas e de Computação, Universidade de São Paulo, São Carlos – SP, 2019.

Nesta tese é proposto um método misto multiescala visando a aproximação precisa de campos de velocidade e pressão em meios porosos altamente heterogêneos, o método Multiscale Robin Coupled Method (MRCM). Este procedimento é baseado em um novo método de decomposição de domínio no qual os problemas locais são definidos com condições de contorno de Robin. O método permite a definição independente de espaços de interface para pressão e fluxo sobre o esqueleto da decomposição que pode ser escolhida com grande flexibilidade para acomodar características locais dos campos de permeabilidade subjacentes. Simulações numéricas são apresentadas visando ilustrar várias características do novo método. Ilustramos a possibilidade de recuperar a solução multiescala de dois métodos bem conhecidos da literatura, a saber, o Multiscale Mortar Mixed Finite Element Method (MMMFEM) e o Multiscale Hybrid-Mixed (MHM) Finite Element Method por escolhas adequadas do parâmetro β nas condições da interface de Robin. Os resultados mostram que a precisão do MRCM depende da escolha deste parâmetro algorítmico, bem como da escolha dos espaços de interface. Uma extensa avaliação numérica do MRCM é conduzida com dois tipos de espaços de interface, os usuais espaços polinomiais por partes e os espaços informados, este último obtidos a partir da redução de dimensionalidade de conjutos de espaços de *snapshots*. Diferentes distribuições de incógnitas entre pressão e fluxo são exploradas. Os resultados mostram que β, adequadamente adimensionalizado, pode ser fixado em unidade para evitar qualquer indeterminação no método. Além disso, com ambos os tipos de espaços, observa-se que uma distribuição equilibrada de incógnita entre pressão e fluxo nas interfaces torna o MRCM bastante atraente tanto em precisão quanto em custo computacional, competitivo com outros métodos multiescala da literatura. As soluções MRCM são, em geral, apenas globalmente conservativas. Dois procedimentos de pós-processamento são propostos para recuperar a conservação local dos campos de velocidade multiescala. Investigamos a aplicabilidade de tais métodos em campos de permeabilidade altamente heterogêneos na modelagem do transporte de contaminantes na subsuperfície. Esses métodos são comparados a um procedimento padrão da literatura. Os resultados indicam que os métodos propostos têm o potencial de produzir resultados mais precisos do que o método padrão com custo computacional similar ou reduzido.

Palavras-chave: Meio porosos, Fluxos de Darcy, Condições de fronteira de Robin, Aproximação multiescala, Simulação de reservatórios.

ABSTRACT

GUIRALDELLO, R. T. **Multiscale methods for oil reservoir simulation**. 2019. 130 p. Tese (Doutorado em Ciências – Ciências de Computação e Matemática Computacional) – Instituto de Ciências Matemáticas e de Computação, Universidade de São Paulo, São Carlos – SP, 2019.

In this thesis a multiscale mixed method aiming at the accurate approximation of velocity and pressure fields in heterogeneous porous media is proposed, the Multiscale Robin Coupled Method (MRCM). The procedure is based on a new domain decomposition method in which the local problems are subject to Robin boundary conditions. The method allows for the independent definition of interface spaces for pressure and flux over the skeleton of the decomposition that can be chosen with great flexibility to accommodate local features of the underlying permeability fields. Numerical simulations are presented aiming at illustrating several features of the new method. We illustrate the possibility to recover the multiscale solution of two well-known methods of the literature, namely, the Multiscale Mortar Mixed Finite Element Method (MMMFEM) and the Multiscale Hybrid-Mixed (MHM) Finite Element Method by suitable choices of the parameter β in the Robin interface conditions. Results show that the accuracy of the MRCM depends on the choice of this algorithmic parameter as well as on the choice of the interface spaces. An extensive numerical assessment of the MRCM is conduct with two types of interface spaces, the usual piecewise polynomial spaces and the informed spaces, the latter obtained from sets of snapshots by dimensionality reduction. Different distributions of the unknowns between pressure and flux are explored. The results show that β, suitably non-dimensionalized, can be fixed to unity to avoid any indeterminacy in the method. Further, with both types of spaces, it is observed that a balanced distribution of the interface unknowns between pressure and flux renders the MRCM quite attractive both in accuracy and in computational cost, competitive with other multiscale methods from the literature. The MRCM solutions are in general only global conservative. Two postprocessing procedures are proposed to recover local conservation of the multiscale velocity fields. We investigate the applicability of such methods in highly heterogeneous permeability fields in modeling the contaminant transport in the subsurface. These methods are compared to a standard procedure. Results indicate that the proposed methods have the potential to produce more accurate results than the standard method with similar or reduced computational cost.

Keywords: Porous media, Darcy Flow, Robin boundary conditions, Multiscale approximation, Reservoir simulation.

LIST OF FIGURES

LIST OF TABLES

LIST OF ABBREVIATIONS AND ACRONYMS

2LM	Two-Lagrange Multiplier Method
MHM	Multiscale Hybrid-Mixed Finite Element Method
MMMFEM	Multiscale Mortar Mixed Finite Element Method
MRCM	Multiscale Robin Coupled Method
MsFEM	Multiscale Finite Element Method
MuMM	Multiscale Mixed Method
VMM	Variational Multiscale Method

CONTENTS

CHAPTER

1

INTRODUCTION

The computational modeling of transport phenomena in porous media still presents major mathematical and numerical challenges and is, therefore, a current research topic of interest both in academia and industry. Such type of problems have a remarkable complexity that requires multiphysics and multiscale approach. Among the relevant phenomena that need to be considered are: (i) the fluid flow includes various phases such as oil, gas, and water, (ii) the presence of chemical reactions and phase transitions in which thermodynamics, energy, and mass transport must be considered, (iii) the heterogeneity on the properties of the porous medium such as permeability, porosity as well as mechanical properties such as geological faults and fractures at different scales need to be taken into account, (iv) the coupling between fluid transport and rock deformation, (v) the spatial and temporal multiscale nature of the phenomena being considered, ranging from the micropore scale to kilometer scales spatially and from the scale of the few seconds, due to rapid geological events or production, due to human intervention, to scales of many years temporally. On top of everything mentioned, (vi) the high uncertainty on the physical and material properties of the porous medium and the initial and the boundary conditions to be applied in order to solve the problem. The uncertainty in the determination of the coefficients of the governing equations on reservoir flow problems implies that deterministic predictions for this class of problems are of limited use. In general, the properties of the medium can be characterized statistically, defining quantities like the mean and covariance (GELHAR, 1993; GELHAR, 1989; ZHANG; LU, 2004) to carry out uncertainty quantification studies (SMITH, 2013; LAW; STUART; ZYGALAKIS, ; GINTING; PEREIRA; RAHUNANTHAN, 2014) which are the key concept to realistically estimate the expected error in the numerical predictions. However, in these studies, thousands of individual simulations typically involving several million or even billions of unknowns each need to be performed. It is clear here the need for the development of high-performance simulators together with robust and accurate numerical methods to allow such simulations to be made in a feasible time with high precision.

Depending on each of the above mentioned cases, different mathematical models are

needed to describe the different physical phenomena. Among these, the Darcy model is a basic ingredient and the development and analysis of efficient numerical schemes to approach this model is the central theme of this thesis. The solution to the porous media problem is not only relevant in the simulation of oil and gas reservoirs, but also in other applications such as contaminant transport in aquifers, the capture of CO2, the storage of nuclear waste and also in resin injection processes in industry, just to name a few.

Excellent references that describes in detail the mathematical and numerical treatment of the above themes can be found in (CHAVENT; JAFFRÉ, 1986; TRANGENSTEIN; BELL, 1989b; TRANGENSTEIN; BELL, 1989a; CHEN, 2007; CHEN, 2005; CHEN; HUAN; MA, 2006; COUSSY, 2010; HOU; WU, 1997; EFENDIEV; HOU, 2008; DURLOFSKY; GERRITSEN, 2006) among others.

In the next sections we introduce the mathematical problem to be handled as well as the key concepts for a multiscale approximation of the problem.

1.1 The Darcy flow problem

Consider the single-phase incompressible case with no effects of gravity, for simplicity (see (CHEN; HUAN; MA, 2006)). The problem for the pressure p and the velocity $\mathbf{u}$ based on Darcy's law is given by:

$$\nabla \cdot \mathbf{u} = f \quad \text{in } \Omega \tag{1.1}$$

$$\mathbf{u} = -K\nabla p \quad \text{in } \Omega \tag{1.2}$$

$$p = g_D \quad \text{on } \Gamma_D \tag{1.3}$$

$$\mathbf{u} \cdot \mathbf{n} = g_N \quad \text{on } \Gamma_N \tag{1.4}$$

$$-\beta \mathbf{u} \cdot \mathbf{n} + p = g_R \quad \text{on } \Gamma_R \tag{1.5}$$

where $\Omega \subset \mathbb{R}^d$, $d = 2$ or 3 is the problem's domain, K is a symmetric, uniformly positive definite tensor with components in $L^\infty(\Omega)$, $\mathbf{u}$ is the fluid velocity, p is the pressure, $f \in L^2(\Omega)$ the source/sink terms, g_D, g_N and g_R are the pressure boundary data, the normal velocity data and the Robin boundary condition data, respectively, where β is positive function defined on Γ_R and $\mathbf{n}$ is the outer normal vector to $\partial\Omega$. Eq. (1.1) is the mass conservation equation and Eq. (1.2) is the Darcy law. The extension to the multiphase case, i.e., problems in which two or more fluids are present can be seen, for example, in (CHAVENT; JAFFRÉ, 1986; CHEN; HUAN; MA, 2006).

Consider now the following spaces

$$W = \mathrm{L}^2(\Omega),\ \mathbf{V} = \mathrm{H}(div, \Omega) \text{ e } \mathbf{V}^{g_N} = \{\mathbf{v} \in \mathbf{V}; \mathbf{v} \cdot \mathbf{n} = g_N \text{ on } \Gamma_N\}$$

where

$$\mathrm{H}(div, \Omega) = \left\{\mathbf{q} \in \mathrm{L}^2(\Omega)^d; \nabla \cdot \mathbf{q} \in \mathrm{L}^2(\Omega)\right\}.$$

The mixed variational formulation of problem (1.1-1.5) is given by: Find $\mathbf{u} \in \mathbf{V}^{g_N}$ and $p \in W$, such that:

$$\begin{aligned} \int_\Omega K^{-1}\mathbf{u}\cdot\mathbf{v} + \int_{\Gamma_R} \beta(\mathbf{u}\cdot\mathbf{n})(\mathbf{v}\cdot\mathbf{n}) - \int_\Omega p\nabla\cdot\mathbf{v} &= -\int_{\Gamma_D} g_D\mathbf{v}\cdot\mathbf{n} - \int_{\Gamma_R} g_R\mathbf{v}\cdot\mathbf{n} \quad \forall \mathbf{v}\in\mathbf{V}^0 \\ \int_\Omega \nabla\cdot\mathbf{u}\, w &= \int_\Omega f w \qquad\qquad\qquad\qquad \forall w \in W, \end{aligned} \tag{1.6}$$

where we assume that g_D and g_R are regular enough so that problem (1.6) is well posed (see (KöNNö; SCHOETZAU; STENBERG, 2011)). Note that the pressure and Robin boundary condition happens to be introduced in a natural way in formulation (1.6), that is why in the context of finite elements these conditions are called the natural boundary conditions. On the other hand, the flux boundary condition needs to be included in the test space $\mathbf{V}^{g_N}$ and is called an essential boundary condition. Formulation (1.6) involves the divergence of the solution and test functions, but not arbitrary first order derivatives. This allow us to work with $\mathrm{H}(div,\Omega)$, i. e., a space spanned by polynomial vectors by parts that are only required to have their normal components to be continuous, an important fact for the finite element approximation of this problem.

1.2 Multiscale methods

The direct simulation of the three-dimensional problem (1.6) in the reservoir scale taking into account the spatial scales of permeability K can result in very large discrete problems, involving up to billions of unknowns to produce a consistent approximation. To resolve this issue and incorporate the fine-scale information in the numerical simulations, in the context of methods based on variational formulations, two lines of work have appeared: The multiscale finite element methods (MsFEM) and variational multiscale methods (VMM). Although the methods have been introduced separately, similarities, and in some cases equivalences, are observed.

The basic idea in the multiscale finite element method was introduced by Babuska and Osborn in (BABUSKA; OSBORN, 1983). In this work, the concept of generalized basis functions was introduced, where local problems are solved at element level and fine-scale information is introduced into the solution. From here, the idea was generalized and extended to numerous problems.

As mentioned by Aarnes in (AARNES, 2006), the work of Hou and Wu (HOU; WU, 1997) was one of the first to recognize the potential on these methods to solve two and three-dimensional elliptic problems with coefficients that exhibit high spatial variations, both in the context of Darcy's problem and compositive material problems in solid mechanics. In the case of an elliptic problem with 2D periodic coefficients the multiscale solution was proved to converge to the solution of the problem according to the homogenization theory. In the linear case, the solution of local problems can be done in an offline stage and the basis functions used a posteriori

to solve a global problem. In the nonlinear case, this can not be done in principle, but the methodology still has advantages because the solution of all local problems can be performed much more efficiently (e.g., in parallel) when compared to the complete solution of the problem in the fine mesh.

Similarly, multiscale variational methods were introduced for the purpose of capturing fine scale phenomena. The method was originally proposed by Hughes in (HUGHES, 1995; HUGHES *et al.*, 1998). Considering an abstract problem $\mathscr{L}(u) = f$ (+ boundary conditions), the idea to separate the scales in the associated variational problem is to split the search and test spaces as direct sum of the function space for the large scales $\bar{V}$ and a space for the fine scales V'. The solution is then written as the sum of a part that will be solved numerically via a finite element method plus a part that will be solved "analytically" (or in practice by some localization process) to incorporate the effect of fine scales, i.e., the solution $u \in V = \bar{V} \oplus V'$, $u = \bar{u} + u'$, $\bar{u} \in \bar{V}$, $u' \in V'$. The problem to be solved for u' in the fine scale uses the residual of the differential equation in the large scale given by $\mathscr{L}(\bar{u}) - f$. From here the method has been applied and extended to several areas. A full and detailed description of this type of method can be found in the references cited above. One of the interesting aspects to be considered is the relation of the method with several formulations of stabilized finite elements, providing a general and formal framework for its development.

Applications of the mixed and mixed-hybrid forms were studied later in both cases as can be seen, for example, in (CHEN; HOU, 2003; ARBOGAST *et al.*, 2007; ARBOGAST, 2004) among others. Extension for the finite volume formulations were also considered (see (JENNY; LEE; TCHELEPI, 2003; LUNATI; JENNY, 2006; LEE; ZHOU; TCHELEPI, 2009; HAJIBEYGI; TCHELEPI, ; BOSMA *et al.*, 2017)). It is worth mentioning here the interesting work of (KIPPE; AARNES; LIE, 2008) where these and other methods are compared in terms of accuracy.

The focus of this thesis is on the multiscale finite element methods based on domain decomposition (DD) schemes in which the domain Ω is decomposed into non-overlapping subdomains $\Omega_i, i = 1, \ldots, m$ and local problems are solved in each Ω_i, due to their potential to solve efficiently elliptic problems with rapidly varying coefficients in parallel multi-core computers.

To describe such type of MsFEM, consider problem (1.1-1.5) but now, for simplicity, with only pressure boundary conditions, given by

$$\begin{aligned} \nabla \cdot \mathbf{u} &= f && \text{in } \Omega \\ \mathbf{u} &= -K\nabla p && \text{in } \Omega \\ p &= g_D && \text{in } \partial\Omega \end{aligned} \quad . \tag{1.7}$$

To produce a multiscale approximation of the above problem one need:

- A domain decomposition scheme;

- A discrete solver for the Darcy problem.

In the next sections we recall these concepts, then we use then to produce an example of a multiscale method.

1.2.1 Domain decomposition schemes

In the study of transport in porous media a consistent approximation of the solution of differential equations, such as (1.7), usually requires a fine enough mesh to capture the spatial variation in small scales of the coefficient K, leading to large linear systems involving several millions or even billions unknowns, as mentioned earlier. Solving such a type of system directly implies an extremely high computational cost and/or processing time. To reduce such a computational burden, domain decomposition methods becomes an interesting alternative. The domain decomposition methods are a set of "divide and conquer" schemes used to find numerical solutions of partial differential equations, mainly elliptic and parabolic, that can be classified according to the choice of the domain partition as overlapping and non-overlapping methods. In (QUARTERONI; VALLI, 1999) and (MATHEW, 2008) there is a complete discussion on such type of methods. In this work we focus on non-overlapping methods due to its natural parallelization. In such type of methods, the domain Ω is decomposed into non-overlapping subdomains $\{\Omega_i\}$, $i = 1, \ldots, m$ and local problems are solved in each Ω_i. At the so-called skeleton Γ of the partition (the union of all internal interfaces $\Gamma_{i,j} = \overline{\Omega_i} \cap \overline{\Omega_j}$) compatibility conditions need to be satisfied, i.e.,

$$\mathbf{u}^i \cdot \mathbf{n}^i + \mathbf{u}^j \cdot \mathbf{n}^j = 0\,, \tag{1.8}$$

$$p^i - p^j = 0\,, \tag{1.9}$$

for the collection of local solutions $\{\mathbf{u}^i, p^i\}$ to be a solution of (1.7).

By restricting problem (1.7) to the subdomains Ω_i results in the domain decomposition problem given by: Find $\mathbf{u}^i \in \tilde{V}$ and $p_i \in \tilde{W}$

$$\begin{aligned}
\nabla \cdot \mathbf{u}^i &= f && \text{in } \Omega_i \\
\mathbf{u}^i &= -K\nabla p^i && \text{in } \Omega_i \\
p^i &= g_D && \text{on } \partial\Omega_i \cap \partial\Omega\,, \\
p_i = p_j &\doteq p_{ij} && \text{on } \Gamma_{ij} \\
\mathbf{u}^i \cdot \mathbf{n}^i = -\mathbf{u}^j \cdot \mathbf{n}^j &\doteq J_{ij} && \text{on } \Gamma_{ij}
\end{aligned} \tag{1.10}$$

where $\tilde{V}$ and $\tilde{W}$ are adequate spaces. We assume that f is regular enough such that problems (1.7) and (1.10) are equivalent.

We now want to formulate a set of local problems in Ω_i equivalent to problem (1.10). For this we must satisfy two conditions. Firstly, the restrictions of $\mathbf{u}^i$ and p^i must satisfy each local

problem. Secondly, every local problem should be well posed. We now need to define a coupling strategy between subdomains. Different subdomain coupling strategies were extensively studied during the last years. An overview of these studies is described, for example, in (LIONS, 1990; CHEN *et al.*, 2011; COWSAR; WHEELER, 1991).

Consider the following strategy: Find $\mathbf{u}^i \in \tilde{V}$, $p^i \in \tilde{W}$ and $\lambda \in M$, for $i = 1,..,m$, such that

$$\begin{aligned} \nabla \cdot \mathbf{u}^i &= f^i && \text{in } \Omega_i \\ \mathbf{u}^i &= -K\nabla p^i && \text{in } \Omega_i \\ p^i &= g_D && \text{on } \partial\Omega_i \cap \partial\Omega \\ p^i &= \lambda && \text{on } \Gamma_i \end{aligned} \tag{1.11}$$

that satisfy

$$\mathbf{u}^i \cdot \mathbf{n}^i + \mathbf{u}^j \cdot \mathbf{n}^j = 0 \text{ on } \Gamma_{ij}, i \neq j. \tag{1.12}$$

where $\Gamma_i = \partial\Omega_i \cap \Gamma$ and M is a suitable interface space. That is, we have defined the local problems (1.11) by given a unique pressure boundary condition λ defined over Γ. Note that, by doing so, we are automatically satisfying condition (1.9) and is left for us to a find the unique pressure in Γ that satisfy condition (1.8), i.e., the jump on the normal component of the velocity in Γ, as described in Eq. (1.12).

If one choose appropriate function spaces, we can multiply the above equations by test functions (including the jump restriction) and obtain the following variational problem: Find $\mathbf{u}^i \in \tilde{V}$, $p^i \in \tilde{W}$ and $\lambda \in M$, for $i = 1,..,m$, such that

$$\begin{aligned} \int_{\Omega_i} K^{-1}\mathbf{u}^i \cdot \mathbf{v} - \int_{\Omega_i} p^i \nabla \cdot \mathbf{v} + \int_{\Gamma_i} \lambda \mathbf{v} \cdot \mathbf{n}^i &= \int_{\partial\Omega_i \cap \Gamma_D} g_D \mathbf{v} \cdot \mathbf{n}^i && \forall \mathbf{v} \in \tilde{V} \\ \int_{\Omega_i} \nabla \cdot \mathbf{u}^i w &= \int_{\Omega_i} f_i w && \forall w \in \tilde{W} \\ \sum_{i=1}^m \int_{\Gamma_i} \mu\, \mathbf{u}^i \cdot \mathbf{n}^i &= 0 && \forall \mu \in M \end{aligned} \quad , \tag{1.13}$$

which is a mixed-hybrid variational formulation that is well posed if the involved spaces are

$$\tilde{V} = \bigoplus_i^n V_i, \qquad \tilde{W} = \bigoplus_{i=1}^n \mathrm{L}^2(\Omega_i),$$

$$M = \left\{ \mu \in \mathrm{H}^{1/2}(\Gamma), \mu|_\Gamma \in (V_i \cdot \mathbf{n}_i)' \right\},$$

where

$$V_i = \mathrm{H}(div; \Omega_i),$$

where $(\cdot)'$ denotes the dual space.

This formulation was originally proposed by (GLOWINSKI; WHEELER, 1988) as a domain decomposition method combined with mixed finite elements and is the basis for the multiscale formulation of (ARBOGAST *et al.*, 2007; GANIS; YOTOV, 2009). Other possible

options using the compatibility Eq.(1.8) - (1.9) is to define local problem with flux boundary conditions leading to the problem of satisfy the pressure jumps in Γ. This method is explored in (BERNARDI; MADAY; PATERA, 1994; BELGACEM, 1999) for the primal variational formulation and is the basis of the multiscale method of (HARDER; PAREDES; VALENTIN, 2013; ARAYA *et al.*, 2013). One can also consider a linear combination of the compatibility conditions, leading to local problems defined with Robin boundary conditions type, a possibility explored in (DOUGLAS *et al.*, 1993; LOISEL, 2013) that is the basis of the multiscale method of (FRANCISCO *et al.*, 2014; GUIRALDELLO *et al.*, 2018b).

1.2.2 Fine mesh discretization schemes

We are interested in numerical approximations of Darcy problems like (1.7), i.e., to approximate a pressure p and a velocity $\mathbf{u}$ with the requirement that the velocity field preserves the property of being continuous on every element of the triangulation and has continuous normal component between adjacent elements. A velocity field of this type is called a mass conservative and is appropriate to solve the governing transport equations of different scalar fields, such as concentrations of passive tracers in the linear case to saturation fields in nonlinear cases.

Mass conservative formulations are essential to avoid the spurious creation/destruction of fluid, and thus, to accurately predict the long-term evolution (days or even years of physical time) of a reservoir. For problem (1.7), we have this property when we consider its mixed variational formulation and ask for its solution in discrete subspace of $\mathbf{V} = H(div,\Omega)$, i.e., given a regular mesh $\mathscr{T}_h$ of $\bar{\Omega}$ in T elements, an approximation in finite elements consist in choose discrete subspaces $V_h \subset \mathrm{H}(div,\Omega)$ and $W_h \subset W = \mathrm{L}^2(\Omega)$ and solve the following problem:
Find $\mathbf{u}_h \in V_h \subset \mathbf{V}$ and $p_h \in W_h \subset W$ such that:

$$\begin{aligned} \int_\Omega K^{-1}\mathbf{u}_h \cdot \mathbf{v}_h - \int_\Omega p_h \nabla\cdot \mathbf{v}_h &= -\int_{\Gamma_D} g_D \mathbf{v}_h \cdot \mathbf{n} \quad \forall \mathbf{v}_h \in \mathbf{V}_h \\ \int_\Omega \nabla\cdot \mathbf{u}_h w_h &= \int_\Omega f w_h \qquad \forall w_h \in W \end{aligned} . \tag{1.14}$$

The most popular discrete spaces that satisfy this property are the Raviart-Thomas (RT) (RAVIART; THOMAS, 1977) and Brezzi-Douglas-Marini (BDM) (BREZZI; DOUGLAS; MARINI, 1985) spaces. Different formulations using these discrete spaces can be found in (RAVIART; THOMAS, 1977; NEDELEC, 1980; BREZZI *et al.*, 1987b; BREZZI *et al.*, 1987a; ARBOGAST *et al.*, 2000; DOUGLAS *et al.*, 1993) and their citations, and the books of (BREZZI; FORTIN, 1991; ROBERTS; THOMAS, 1991; QUARTERONI; VALLI, 1999).

In addition to finite element methods, finite volume methods are of interest because they are very popular in the industry and there is a complete range of codes available that can solve complete problems, including the multiphase nonlinear case, which can be used in the development of multiscale methods. The equivalence between these methods can be established for several cases (see (CHAVENT; JAFFRÉ, 1986; EYMARD; GALLOUËT; HERBIN, 2000;

RUSSEL; WHEELER, 1983; ARBOGAST; WHEELER; YOTOV, 1997; VOHRALÍK, 2006; BARANGER; MAITRE; OUDIN, 1996) and references therein).

1.2.3 A multiscale method

Now we put together the above ingredients and describe a multiscale method to approximate problem (1.7). Let us start by recalling the domain decomposition variational formulation (1.13) given by: Find $\mathbf{u}^i \in \tilde{V}$, $p^i \in \tilde{W}$ and $\lambda \in M$, for $i = 1,..,m$, such that

$$\begin{array}{rcll} \int_{\Omega_i} K^{-1}\mathbf{u}^i \cdot \mathbf{v} - \int_{\Omega_i} p^i \nabla\cdot\mathbf{v} + \int_{\Gamma_i} \lambda\, \mathbf{v}\cdot\mathbf{n}^i & = & \int_{\partial\Omega_i\cap\Gamma_D} g_D \mathbf{v}\cdot\mathbf{n}^i & \forall \mathbf{v}\in\tilde{V} \\ \int_{\Omega_i} \nabla\cdot\mathbf{u}^i\, w & = & \int_{\Omega_i} f_i\, w & \forall w\in\tilde{W}\ . \\ \sum_{i=1}^m \int_{\Gamma_i} \mu\ \mathbf{u}^i\cdot\mathbf{n}^i & = & 0 & \forall \mu\in M \end{array} \tag{1.15}$$

To discretize this problem, consider a triangulation $\mathscr{T}_h$ of $\Omega \subset \mathbb{R}^d, d = 2,3$, into d-dimensional simplexes. From this, consider a conform partition of Ω into m subdomains Ω_i, such that each simplex $T \in \mathscr{T}_h$ belong to one and only one subdomain and define $\mathscr{T}_{h,i}$ as the triangulation correspondent to Ω_i.

For each Ω_i, consider the lowest-order Raviart-Thomas spaces for velocity and pressure given by $\mathbf{V}_h^i = \mathrm{RT}_0(\Omega_i)$ and $W_h^i = \left\{w \in L^2(\Omega_i), w(\mathbf{x})|_T \in \mathbb{P}_0)\right\}$. As we have a global conform mesh, it naturally induces a unique partition in the skeleton Γ. Consider the space given by

$$F_h(S_h) = \{f : S_h \to \mathbb{R} \mid f|_e \in \mathbb{P}_0\ ,\ \forall e \in S_h\}, \tag{1.16}$$

in which S_h is any set o faces/edges of $\mathscr{T}_h$. Notice that $F_h(\partial\Omega_i)$ is the space of normal traces of $\mathbf{V}_h^i$. Let Γ_h be the set of all faces/edges over Γ and define $M_h = F_h(\Gamma_h)$.

The multiscale method reads as: Find $\mathbf{u}_h^i \in \mathbf{V}_h^i$, $p_h^i \in W_h^i$ and $\lambda_H \in M_H \subset M_h$ for each $i = 1,\ldots,m$, such that:

$$\begin{array}{rcll} \int_{\Omega_i} K^{-1}\mathbf{u}_h^i \cdot \mathbf{v} - \int_{\Omega_i} p_h^i\, \nabla\cdot\mathbf{v} + \int_{\Gamma_i} \lambda_H\, \mathbf{v}\cdot\mathbf{n}_i & = & -\int_{\partial\Omega_i\cap\Gamma_D} g_D\, \mathbf{v}\cdot\mathbf{n}_i & \forall \mathbf{v}\in\mathbf{V}_h^i \\ \int_{\Omega_i} \nabla\cdot\mathbf{u}_h^i\, w & = & \int_{\Omega_i} f\, w & \forall\, w\ \in W_h^i\ . \\ \sum_{i=1}^m \int_{\Gamma_i} \mathbf{u}_h^i\cdot\mathbf{n}^i\, \mu & = & 0 & \forall \mu\in M_H \end{array} \tag{1.17}$$

The above multiscale method is nothing but a particular case of the MMMFEM (see (ARBOGAST *et al.*, 2000; ARBOGAST *et al.*, 2007)). Notice that the first two equation of (1.17) accounts for the local problem in $\{\Omega_i\}$ where the local meshe $\mathscr{T}_{h,i}$ are fine enough to capture the small scale variations in the permeability without any approximation (or upscaling) of K. These are small problems when compared to the global problem in Ω and are usually solved in parallel. By choosing a low-dimensional space $M_H \subset M_h$, all local problems can be uncoupled, leaving us to find the interface pressure $\lambda_H \in M_H$ that solves the third equation of (1.17), which accounts for the flux jump between subdomain in a weak sense and couples the subdomain solutions, reducing the number of unknowns to N_P, the dimension of $M_H = \mathrm{span}\{\phi_1,\ldots,\phi_{N_P}\}$. If one take

$M_H = M_h$, we retrieve the domain decomposition method of (GLOWINSKI; WHEELER, 1988) in which for the above defined spaces has a unique solution equivalent to the non-decomposed problem ($m = 1$).

1.3 Outline

This thesis is mainly composed of scientific articles co-authored by the thesis's author produced in the development of this doctoral project and organized as chapters. Thus, each chapter contains its own introduction and conclusion regarding the scope of the article. In addition, the thesis has an introductory chapter and a closing chapter highlighting the main contributions and is organized as follows:

- Chapter 1 describes the background and purpose of this thesis.
- In Chapter 2 a multiscale mixed method aiming at the accurate approximation of velocity and pressure fields in heterogeneous porous media is proposed. This chapter is based on the publication "The Multiscale Robin Coupled Method for porous media flows"(MRCM) (GUIRALDELLO *et al.*, 2018b).
- Chapter 3 presents an extensive numerical assessment of the MRCM, exploring the flexibility of the method in order to increase its accuracy. This chapter is based on the following publication "Interface spaces for the Multiscale Robin Coupled method in reservoir simulation" (GUIRALDELLO *et al.*, 2018a).
- Chapter 4 presents two new downscaling (or postprocessing) procedures to recover local conservation and compatibility of the velocity field at fine grid level. These new procedures are compared with an usual procedure in multiscale solutions produced by global conservative multiscale methods and evaluated in the case of passive tracers. This chapter is based on the manuscript "Velocity postprocessing schemes for the Multiscale Robin Coupled method for contaminant transport in subsurface flows" submitted to the a renowned international journal.
- Chapter 5 summarizes the main result obtained and discuss future works.

CHAPTER

2

THE MULTISCALE ROBIN COUPLED METHOD FOR FLOWS IN POROUS MEDIA

A multiscale mixed method aiming at the accurate approximation of velocity and pressure fields in heterogeneous porous media is proposed. The procedure is based on a new domain decomposition method in which the local problems are subject to Robin boundary conditions. The domain decomposition procedure is defined in terms of two independent spaces on the skeleton of the decomposition, corresponding to interface pressures and fluxes, that can be chosen with great flexibility to accommodate local features of the underlying permeability fields. The well-posedness of the new domain decomposition procedure is established and its connection with the method of *Douglas et al., Numer. Math., 65(1):95–108, 1993*, is identified, also allowing us to reinterpret the known procedure as an optimized Schwarz (or Two-Lagrange-Multiplier) method. The multiscale property of the new domain decomposition method is indicated, and its relation with the Multiscale Mortar Mixed Finite Element Method (MMMFEM) and the Multiscale Hybrid-Mixed (MHM) Finite Element Method is discussed. Numerical simulations are presented aiming at illustrating several features of the new method. Initially we illustrate the possibility of switching from MMMFEM to MHM by suitably varying the Robin condition parameter in the new multiscale method. Then we turn our attention to realistic flows in high-contrast, channelized porous formations. We show that for a range of values of the Robin condition parameter our method provides better approximations for pressure and velocity than those computed with either the MMMFEM and the MHM. This is an indication that our method has the potential to produce more accurate velocity fields in the presence of rough, realistic permeability fields of petroleum reservoirs.

2.1 Introduction

Multiscale formulations of the porous media equations have been developed over the last twenty years motivated by the practical needs of the energy and environmental sectors. High-resolution permeability data are generated by geologists and hydrologists from seismic data, pointwise sampling and statistical models. These data are highly heterogeneous, with no scale separation, so that simplifications of the model by rigorous homogenization techniques cannot be applied. Reservoir simulators thus resort to numerical multiscale methods to obtain coarsened models (with much fewer degrees of freedom) that nevertheless incorporate the fine-grid details of the permeability field.

Consider the single-phase porous media problem

$$\mathbf{u} = -K\nabla p \qquad \text{in } \Omega \tag{2.1}$$

$$\nabla\cdot\mathbf{u} = f \qquad \text{in } \Omega \tag{2.2}$$

$$p = g \qquad \text{on } \partial\Omega_p \tag{2.3}$$

$$\mathbf{u}\cdot\mathbf{n} = z \qquad \text{on } \partial\Omega_u \tag{2.4}$$

where $\Omega\subset\mathbb{R}^d$, $d=2$ or 3 is the problem's domain, K is a symmetric, uniformly positive definite tensor with components in $L^\infty(\Omega)$, $\mathbf{u}$ is the fluid velocity, p is the pressure, $f\in L^2(\Omega)$ the source, $g\in H^{\frac{1}{2}}(\partial\Omega_p)$ the pressure boundary data, $z\in H^{-\frac{1}{2}}(\partial\Omega_u)$ the normal velocity data and $\mathbf{n}$ is the outer normal to $\partial\Omega$.

Of the multiscale formulations available in the literature, the focus here is on those based on domain decomposition (DD) techniques, in which the domain Ω is decomposed into non-overlapping subdomains $\{\Omega_i\}$, $i=1,\ldots,m$ and local problems are solved in each Ω_i. At the so-called skeleton Γ of the partition (the union of all interfaces $\Gamma_{i,j}=\overline{\Omega_i}\cap\overline{\Omega_j}$) compatibility conditions need to be satisfied, i.e.,

$$\mathbf{u}^i\cdot\check{\mathbf{n}}^i+\mathbf{u}^j\cdot\check{\mathbf{n}}^j = 0\,, \tag{2.5}$$

$$p^i-p^j = 0\,, \tag{2.6}$$

for the collection of local solutions $\{\mathbf{u}^i,p^i\}$ to be a solution of (2.1)-(2.4).

The finite element literature shows two main DD-based multiscale formulations: MMMFEM and MHM.

The first one, introduced by Arbogast and co-authors (ARBOGAST *et al.*, 2007), is based on the mixed formulation of (2.1)-(2.4) and its discretization by div-stable elements in each subdomain. It is known as MMMFEM, for Multiscale Mortar Mixed Finite Element Method. The local problems have *pressure boundary conditions* at each $\partial\Omega_i\cap\Gamma$. The Lagrange multiplier λ that enforces the continuity of fluxes across Γ is nothing but the interface pressure $p|_\Gamma$. This procedure is turned into a *multiscale formulation* by restricting λ to belong to a suitable low-dimensional space Λ_H, where H refers to the size of the partition. Inside each subdomain,

velocity and pressure are approximated with fine-grid spaces $\mathbf{V}_h^i \times Q_h^i$, where h is the size of the fine grid, assumed much smaller than H. In MMMFEM the pressure compatibility condition (2.6) is satisfied (weakly) at the fine-grid level, whereas the flux compatibility condition (2.5) is relaxed to

$$\int_\Gamma \left(\mathbf{u}^i \cdot \check{\mathbf{n}}^i + \mathbf{u}^j \cdot \check{\mathbf{n}}^j\right) \mu_H \;=\; 0\,, \qquad \forall\, \mu_H \in \Lambda_H\,. \tag{2.7}$$

As a consequence, there is a lack of accuracy in flux conservation at Γ that takes place even if the numerical scheme inside each subdomain is exactly conservative (such as RT_k or BDM_k finite elements (RAVIART; THOMAS, 1977; BREZZI; DOUGLAS; MARINI, 1985), or finite volume schemes). Cures for this crucial problem have been sought through post-processing (SILVA; LOULA, 2002; CORREA; LOULA, 2007) or *downscaling* techniques (JENNY; LEE; TCHELEPI, 2003; FRANCISCO *et al.*, 2014).

The Multiscale Hybrid-Mixed Finite Element Method (MHM), on the other hand, was introduced by Harder *et al* in 2013 (HARDER; PAREDES; VALENTIN, 2013; ARAYA *et al.*, 2013) and starts from the mortar formulation as introduced by Bernardi and co-workers in (BERNARDI; MADAY; PATERA, 1994) and Belgacem in (BELGACEM, 1999). In MHM the local problems have *flux boundary conditions*, i.e., $\mathbf{u}^i \cdot \check{\mathbf{n}}^i$ is assigned the value of an unknown Lagrange multiplier θ at $\partial\Omega_i \cap \Gamma$. A fine-grid is used in each subdomain as in the MMMFEM, but in the case of the MHM formulation it is the flux θ that is restricted to belong to a coarse space Θ_H, yielding a field θ_H that approximates the flux across Γ. As a consequence, (2.5) is (weakly) satisfied with fine-grid accuracy, whereas $p^i - p^j$ is only enforced to satisfy

$$\int_\Gamma (p^i - p^j)\, \zeta_H \;=\; 0\,, \qquad \forall\, \zeta_H \in \Theta_H\,. \tag{2.8}$$

The drawback is a lack of accuracy in the pressure compatibility condition (2.6).

The MHM formulation is more involved than the MMMFEM formulation because one has to deal with the non-existence of solution of the local problems unless the imposed boundary flux values at each $\partial\Omega_i$ exactly balance the source term integrated over Ω_i. The practical implementation adds one global unknown per subdomain, a constant-pressure mode, increasing the dimension of the global interface problem to $\dim(\Theta_H) + m$.

In this context it is natural to look for methods that combine the good properties of the two formulations described above, in which the error in satisfying (2.5)-(2.6) is distributed over the two equations, trying to find a convenient compromise between the flow conservation properties of the MHM method and the simplicity of the MMMFEM.

In this article, we elaborate on the formulation known as Multiscale Mixed Method (MuMM) (FRANCISCO *et al.*, 2014), which is based on a domain decomposition technique introduced by Douglas et al (DOUGLAS *et al.*, 1993). The local problems are subject to *Robin boundary conditions* on Γ, which are generally written as

$$-\beta_i\, \mathbf{u}^i \cdot \check{\mathbf{n}}^i + p^i = g_R \tag{2.9}$$

where β_i is the Robin condition parameter and g_R the prescribed value. As in the original MuMM, we assume that a global *fine* mesh $\mathscr{T}_h$ exists and that the subdomains are obtained by partitioning $\mathscr{T}_h$ into m regions $\{\Omega_i\}$ of size H, much larger than h. A discrete multiscale variational formulation is introduced for the MuMM allowing its generalization to arbitrary interface spaces, a possibility that was not studied in the original publication. The proposed method, named Multiscale Robin Coupled Method (MRCM) is then compared to the MMMFEM and MHM, which are shown to be limit cases of the MRCM as $\beta \to 0$ and $\beta \to \infty$, and suitable values of the Robin condition parameter are identified.

2.2 Numerical scheme

Domain decomposition methods are usually presented by first introducing the formulation at the continuous level and then approximating it by a finite-dimensional counterpart arising, for example, from finite elements. In the case of Robin interface conditions, as noted by Douglas et al (DOUGLAS *et al.*, 1993), the trace spaces of the continuous problem are unclear so that interface integrals can only be written formally, without rigorous justification. To avoid this theoretical setback, we present the *new* domain decomposition formulation directly in the discrete case, assuming a structured fine mesh of lowest-order Raviart-Thomas element RT_0 and a diagonal mobility tensor, which up to a quadrature error is equivalent to the most popular cell-centered finite volume method. This domain decomposition formulation is interesting in itself, especially due to its connections with Douglas et al's iterative scheme (DOUGLAS *et al.*, 1993) and with the Optimized Schwarz and Two-Lagrange-Multiplier methods (LOISEL, 2013).

2.2.1 The domain decomposition formulation

Let $\mathscr{T}_h$ be a subdivision of the domain $\Omega \subset \mathbb{R}^d$ into a Cartesian mesh of d-dimensional rectangles. From this mesh, a partitioning of Ω is made into subdomains $\{\Omega_i\}_{i=1,\dots,m}$, such that each rectangle $K \in \mathscr{T}_h$ belongs to one and only one of the subdomains. The submesh corresponding to Ω_i is denoted by $\mathscr{T}_h^i$.

On each Ω_i we define the lowest-order Raviart-Thomas spaces for velocity and pressure,

$$\begin{aligned} \mathbf{V}_h^i &= \{\mathbf{v} \in H(\mathrm{div}, \Omega_i)\ ,\ v_j(\mathbf{x})|_K = p_{j1}(x_1)p_{j2}(x_2)\dots\ ,\forall K \in \mathscr{T}_h^i\ , \\ &\qquad \text{with } p_{jk} \in \mathbb{P}_1 \text{ if } j = k\ , p_{jk} \in \mathbb{P}_0 \text{ if } j \neq k\ \} \qquad (2.10) \\ Q_h^i &= \{q \in L^2(\Omega_i)\ ,\ q(\mathbf{x})|_K \in \mathbb{P}_0\}\ , \qquad (2.11) \end{aligned}$$

where $\mathbb{P}_k$ is the space of polynomials of degree $\leq k$. Because the submeshes are a partition of a unique div-conformal mesh, the space of normal traces of $\{\mathbf{V}_h^i\}$ onto the skeleton Γ is uniquely defined. Let S_h be any subset of edges/faces of $\mathscr{T}_h$ (e.g., Γ), then we define

$$F_h(S_h) = \{f : S_h \to \mathbb{R} \mid f|_e \in \mathbb{P}_0\ ,\ \forall e \in S_h\}\ . \qquad (2.12)$$

Notice that $F_h(\partial\Omega_i)$ is the space of normal traces of $\mathbf{V}_h^i$. We assume that $\partial\Omega_u$ and $\partial\Omega_p$ coincide with subsets of $\mathscr{T}_h \cap \partial\Omega$ and introduce

$$\mathbf{V}_{hy}^i \;=\; \{\mathbf{v} \in \mathbf{V}_h^i \,,\, \mathbf{v}\cdot\check{\mathbf{n}} = y \text{ on } \partial\Omega_i \cap \partial\Omega_u\} \,, \tag{2.13}$$

where we have assumed that y belongs to $F_h(\partial\Omega_u)$ (if not, it should be replaced by its projection). Now, let $\mathscr{E}_h$ be the set of all faces/edges of $\mathscr{T}_h$ contained in Γ. On each face/edge $e \in \mathscr{E}_h$ we also introduce a unique normal $\check{\mathbf{n}}$, which is the exterior normal to $\partial\Omega$ if $e \in \partial\Omega$, and if e belongs to some $\Gamma_{i,j} \subset \Gamma$ then it is defined as the unit normal exterior to the subdomain with smallest index, $\min\{i,j\}$.

We need to define spaces for pressure and fluxes at subdomain interfaces:

$$\mathscr{P}_h \;=\; F_h(\mathscr{E}_h) \tag{2.14}$$

$$\mathscr{U}_h \;=\; \{V_h \in F_h(\mathscr{E}_h) \mid V_h = 0 \text{ on } R_h\} \tag{2.15}$$

where R_h is *the set of edges in* $\mathscr{E}_h$ *which have* $\beta = 0$ *on both sides*. When discussing matters not connected to the boundary conditions, the discrete spaces $\mathbf{V}_{hz}^i$ and $\mathbf{V}_{h0}^i$ will be denoted generically by $\mathbf{V}_h^i$. The (global) direct product of the subdomain spaces $\mathbf{V}_h^i$ and Q_h^i will be denoted by $\mathbf{V}_h$ and Q_h, respectively,

$$\mathbf{V}_h = \Pi_{i=1}^m \mathbf{V}_h^i \,, \qquad Q_h = \Pi_{i=1}^m Q_h^i \,. \tag{2.16}$$

The discrete variational formulation we consider is the following: Let $\mathscr{U}$ and $\mathscr{P}$ be **arbitrary** subspaces of $\mathscr{U}_h$ and $\mathscr{P}_h$, respectively. Find $(\mathbf{u}_h^i, p_h^i) \in \mathbf{V}_{hz}^i \times Q_h^i$, for $i = 1,\ldots,m$, and $(U,P) \in \mathscr{U} \times \mathscr{P}$ such that

$$(K^{-1}\mathbf{u}_h^i, \mathbf{v})_{\Omega_i} - (p_h^i, \nabla\cdot\mathbf{v})_{\Omega_i} + (P - \beta_i U\check{\mathbf{n}}^i\cdot\check{\mathbf{n}} + \beta_i\,\mathbf{u}_h^i\cdot\check{\mathbf{n}}^i, \mathbf{v}\cdot\check{\mathbf{n}}^i)_{\partial\Omega_i\cap\Gamma} \;=\; -(g, \mathbf{v}\cdot\check{\mathbf{n}}^i)_{\partial\Omega_i\cap\partial\Omega_p} \,, \tag{2.17}$$

$$(q, \nabla\cdot\mathbf{u}_h^i)_{\Omega_i} \;=\; (f,q)_{\Omega_i} \,, \tag{2.18}$$

$$\sum_{i=1}^m (\mathbf{u}_h^i\cdot\check{\mathbf{n}}^i, M)_{\partial\Omega_i\cap\Gamma} \;=\; 0 \,, \tag{2.19}$$

$$\sum_{i=1}^m (\beta_i\,(\mathbf{u}_h^i\cdot\check{\mathbf{n}}^i - U\check{\mathbf{n}}\cdot\check{\mathbf{n}}^i), V\check{\mathbf{n}}^i\cdot\check{\mathbf{n}})_{\partial\Omega_i\cap\Gamma} \;=\; 0 \,, \tag{2.20}$$

hold for all $(\mathbf{v},q) \in \mathbf{V}_{h0}^i \times Q_h^i$, $\forall\, i = 1,\ldots,m$, for all $M \in \mathscr{P}$ and for all $V \in \mathscr{U}$. A weak imposition of the boundary flux conditions on $\partial\Omega_u$ could also be considered.

Let us explain the conceptual basis for this formulation. Notice first that, if $\beta_i = 0$ for all i, then (2.20) reduces to $0 = 0$ and the formulation is simply the Mortar Mixed Finite Element Method (GLOWINSKI; WHEELER, 1988; ARBOGAST *et al.*, 2000), P being the Lagrange multiplier on Γ, which has the physical interpretation of a pressure. Clearly, the unknown U is completely undetermined if all β_i's are zero. Now consider $\beta_i > 0$. Considering P and U known, Eq. (2.17) is a discretization of (2.1) in subdomain Ω_i with Robin boundary condition

$$p - \beta_i\,\mathbf{u}\cdot\check{\mathbf{n}}^i = P - \beta_i U\,\check{\mathbf{n}}\cdot\check{\mathbf{n}}^i \,. \tag{2.21}$$

With respect to the case $\beta_i = 0$, we have a new unknown U, so that the problem is not closed by adding just the flux-continuity equation (2.19). The required additional equation, that in fact determines U, comes from requiring **pressure continuity** weakly. From (2.21) we see that

$$\tilde{p}^i \stackrel{\text{def}}{=} P - \beta_i U\, \check{\mathbf{n}} \cdot \check{\mathbf{n}}^i + \beta_i\, \mathbf{u}_h^i \cdot \check{\mathbf{n}}^i \tag{2.22}$$

is a *recovered boundary pressure* for Ω_i. It is then natural to impose pressure continuity weakly at an interface $\Gamma_{i,j}$ as

$$(P - \beta_i U\, \check{\mathbf{n}} \cdot \check{\mathbf{n}}^i + \beta_i\, \mathbf{u}_h^i \cdot \check{\mathbf{n}}^i, V\check{\mathbf{n}} \cdot \check{\mathbf{n}}^i) = (P - \beta_j U\, \check{\mathbf{n}} \cdot \check{\mathbf{n}}^j + \beta_j\, \mathbf{u}_h^j \cdot \check{\mathbf{n}}^j, V\check{\mathbf{n}} \cdot \check{\mathbf{n}}^i)\ ,\ \ \forall V \in \mathscr{U}\ . \tag{2.23}$$

Cancelling out P, and using $\check{\mathbf{n}}^j = -\check{\mathbf{n}}^i$ one arrives at (2.20). It is interesting to notice that (2.20) implies

$$U|_{\Gamma_{i,j}} = \Pi_U\, \frac{\beta_i \mathbf{u}_h^i \cdot \check{\mathbf{n}} + \beta_j \mathbf{u}_h^j \cdot \check{\mathbf{n}}}{\beta_i + \beta_j}\ , \tag{2.24}$$

where Π_U stands for the L^2-projection onto $\mathscr{U}$. A connection may be established with the decomposition methods proposed in (LEIVA; BLANCO; BUSCAGLIA, 2010; BLANCO; LEIVA; BUSCAGLIA, 2013) which also introduce two unknown fields per interface for the coupling.

Proposition 1. The solution $(\{\mathbf{u}_h^i, p_h^i\}, U, P)$ to the discrete formulation (2.17)-(2.20) is unique in $\Pi_{i=1}^m (\mathbf{V}_{hz}^i \times Q_h^i) \times \mathscr{U} \times \mathscr{P}$.

Proof. Assume $g = z = f = 0$, take $\mathbf{v} = \mathbf{u}_h^i$ in (2.17), $q = p_h^i$ in (2.18), $M = -P$ in (2.19) and $V = -U$ in (2.20). Adding up all the resulting equations one gets

$$\sum_{i=1}^m \left[(K^{-1}\mathbf{u}_h^i, \mathbf{u}_h^i)_{\Omega_i} + \| \sqrt{\beta_i}\, (\mathbf{u}_h^i \cdot \check{\mathbf{n}} - U) \|^2_{\partial\Omega_i \cap \Gamma} \right] = 0\ . \tag{2.25}$$

From this one concludes that $\mathbf{u}_h^i = 0$ for $i = 1, \ldots, m$, and that $U = 0$. We are thus left with

$$(p_h^i, \nabla \cdot \mathbf{v})_{\Omega_i} = (P, \mathbf{v} \cdot \check{\mathbf{n}}^i)_{\partial\Omega_i \cap \Gamma}\ , \qquad \forall \mathbf{v} \in \mathbf{V}_{h0}^i\ ,\ \forall i\ , \tag{2.26}$$

to prove that $p_h^i = 0$ and that $P = 0$. Take $\mathbf{v}$ such that $\mathbf{v} \cdot \check{\mathbf{n}}^i = 0$ on $\partial\Omega_i$ and such that $\nabla \cdot \mathbf{v} = p_h^i - D_i$, where D_i is the mean of p_h^i over Ω_i. Then $\int_{\Omega_i} p_h^i (p_h^i - D_i) = 0$ which implies that $p_h^i = D_i$, constant per subdomain. Inserting this into (2.26) and integrating by parts one gets $(D_i - P, \mathbf{v} \cdot \check{\mathbf{n}}^i)_{\partial\Omega_i \cap \Gamma} = 0$, which implies $D_i = P$ on $\partial\Omega_i \cap \Gamma$ because (since $\mathscr{P} \subset \mathscr{P}_h$) $P|_{\partial\Omega_i \cap \Gamma}$ belongs to the normal trace space of V_{h0}^i. The fact that P is constant over each $\partial\Omega_i \cap \Gamma$ for all i implies that $P = C$, a constant over the whole of Γ. This then allows to conclude that $p_h^i = C$ for all i. Going back once again to (2.26), now with $P = p_h^i = C$, taking $\mathbf{v}$ as the restriction to Ω_i of any $\mathbf{w} \in \mathbf{V}_{h0} \cap H(\mathrm{div}, \Omega)$ and then adding over all subdomains one finally obtains

$$C \int_{\partial\Omega_p} \mathbf{w} \cdot \check{\mathbf{n}} = 0\ , \qquad \forall \mathbf{w} \in \mathbf{V}_{h0} \cap H(\mathrm{div}, \Omega)\ .$$

If $\partial\Omega_p$ consists of at least one edge of $\mathscr{T}_h$ this implies $C = 0$. □

Remark 1. It is noteworthy that the well-posedness of the MRCM formulation does not require any compatibility condition between the spaces $\mathscr{U}$ and $\mathscr{P}$. In fact, $\mathscr{U}$ does not even need to be a subspace of $\mathscr{U}_h$. The situation for $\mathscr{P}$ is different, since in the proof one needs a compatibility condition between $\mathscr{P}$ and $\mathbf{V}_h^i$ to conclude, from $(D_i - P, \mathbf{v}\cdot\check{\mathbf{n}}^i)_{\partial\Omega_i\cap\Gamma} = 0$, that $D_i = P$. This compatibility condition is nothing but the usual inf-sup condition of the mixed mortar method,

$$\inf_{0\neq P\in\mathscr{P}} \sup_{\mathbf{v}\in\mathbf{V}_{h0}^i} \left(P, \mathbf{v}\cdot\check{\mathbf{n}}^i\right)_{\partial\Omega_i\cap\Gamma} > 0\,,$$

which in the proposed formulation is automatically satisfied because $\mathscr{P}\subset\mathscr{P}_h$.

We now show that the proposed formulation is indeed a domain decomposition method, i.e., it yields the same solution as the non-decomposed formulation if $\mathscr{U} = \mathscr{U}_h$ and $\mathscr{P} = \mathscr{P}_h$.

Proposition 2. Let $(\{\mathbf{u}_h^i, p_h^i\}, U_h, P_h)$ be the solution of the discrete formulation (2.17)-(2.20) with $\mathscr{U} = \mathscr{U}_h$ and $\mathscr{P} = \mathscr{P}_h$, and let $(\mathbf{u}_h, p_h) \in (\mathbf{V}_{hz}\cap H(\mathrm{div},\Omega))\times Q_h$ be the solution of the non-decomposed discrete problem ($m = 1$), which satisfies

$$(K^{-1}\mathbf{u}_h, \mathbf{v})_\Omega - (p_h, \nabla\cdot\mathbf{v})_\Omega = -(g, \mathbf{v}\cdot\check{\mathbf{n}})_{\partial\Omega_p}\,, \tag{2.27}$$

$$(q, \nabla\cdot\mathbf{u}_h)_\Omega = (f, q)_\Omega\,, \tag{2.28}$$

for all $\mathbf{v}\in\mathbf{V}_{h0}\cap H(\mathrm{div},\Omega)$ and all $q\in Q_h$.

Then, assuming β_i to be constant on each edge of $\mathscr{E}_h\cap\partial\Omega_i$,

$$\mathbf{u}_h^i = \mathbf{u}_h|_{\Omega_i} \tag{2.29}$$

$$p_h^i = p_h|_{\Omega_i} \tag{2.30}$$

$$U_h = \mathbf{u}_h\cdot\check{\mathbf{n}} \qquad \text{on } \Gamma\setminus R_h \tag{2.31}$$

Proof. Let us show that $(\mathbf{u}_h, p_h)$, restricted to each subdomain, satisfies (2.17)-(2.20). Because $\mathbf{u}_h\in H(\mathrm{div},\Omega)$ we know that $\bar{\mathbf{u}}_h^i \overset{\text{def}}{=} \mathbf{u}_h|_{\Omega_i}$ satisfies (2.19). This implies, from the assumption on β_i, that $\bar{U}_h \overset{\text{def}}{=} \bar{\mathbf{u}}_h^i\cdot\check{\mathbf{n}}$ satisfies (2.20) and the two terms containing β_i cancel out in (2.17).

Because $(\bar{\mathbf{u}}_h^i, \bar{p}_h^i)$ is the restriction to Ω_i of the global solution $(\mathbf{u}_h, p_h)$, there exists a unique $\bar{P}_h^i$ in the restriction of $\mathscr{P}_h$ to $\partial\Omega_i\cap\Gamma$ such that

$$(K^{-1}\bar{\mathbf{u}}_h^i, \mathbf{v}^i)_{\Omega_i} - (\bar{p}_h^i, \nabla\cdot\mathbf{v}^i)_{\Omega_i} + (\bar{P}_h^i, \mathbf{v}^i\cdot\check{\mathbf{n}}^i)_{\partial\Omega_i\cap\Gamma} = -(g, \mathbf{v}^i\cdot\check{\mathbf{n}}^i)_{\partial\Omega_i\cap\partial\Omega_p}\,, \qquad \forall\,\mathbf{v}^i\in\mathbf{V}_{h0}^i\,. \tag{2.32}$$

Adding over subdomains we get

$$\sum_{i=1}^m \left[(K^{-1}\bar{\mathbf{u}}_h^i, \mathbf{v}^i)_{\Omega_i} - (\bar{p}_h^i, \nabla\cdot\mathbf{v}^i)_{\Omega_i} + (g, \mathbf{v}^i\cdot\check{\mathbf{n}}^i)_{\partial\Omega_i\cap\partial\Omega_p}\right] + \sum_{i=1}^m (\bar{P}_h^i, \mathbf{v}^i\cdot\check{\mathbf{n}}^i)_{\partial\Omega_i\cap\Gamma} = 0\,. \tag{2.33}$$

Take now $\mathbf{v}^i = \mathbf{v}|_{\Omega_i}$, with $\mathbf{v}\in\mathbf{V}_{h0}\cap H(\mathrm{div},\Omega)$ an element of the unbroken global velocity space. From the definition of $\bar{\mathbf{u}}_h^i$ such $\mathbf{v}^i$s make the first sum in (2.33) to vanish, and so

$$\left(\ \mathbf{v}^i\cdot\check{\mathbf{n}}^i + \mathbf{v}^j\cdot\check{\mathbf{n}}^j = 0\,,\quad \forall\,\Gamma_{i,j}\ \right) \ \Rightarrow\ \sum_{i=1}^m (\bar{P}_h^i, \mathbf{v}^i\cdot\check{\mathbf{n}}^i)_{\partial\Omega_i\cap\Gamma} = 0\,.$$

This can only happen if $\bar{P}_h^i = \bar{P}_h^j$ on every $\Gamma_{i,j}$, and thus a single-valued $\bar{P}_h \in \mathscr{P}_h$ can be defined that makes (2.17) to hold. The uniqueness of solution for (2.17)-(2.20) makes $\mathbf{u}_h^i = \bar{\mathbf{u}}_h^i$, $p_h^i = \bar{p}_h^i$, $U_h = \bar{U}_h$ and $P_h = \bar{P}_h$. □

Remark 2. If all β_i are positive, then $\mathscr{P}_h = \mathscr{U}_h = F_h(\mathscr{E}_h)$. Denoting

$$\lambda_h^i = P_h|_{\partial\Omega_i\cap\Gamma} - \beta_i U_h|_{\partial\Omega_i\cap\Gamma}\check{\mathbf{n}}\cdot\check{\mathbf{n}}^i \,, \tag{2.34}$$

then one has, for any $\Gamma_{i,j} \subset \Gamma$,

$$P_h = \frac{\beta_j\lambda_h^i + \beta_i\lambda_h^j}{\beta_i+\beta_j} \,, \qquad U_h\check{\mathbf{n}}\cdot\check{\mathbf{n}}^i = \frac{\lambda_h^j - \lambda_h^i}{\beta_i+\beta_j} \,. \tag{2.35}$$

Using this, formulation (2.17)-(2.20) can be rewritten as: Find $(\mathbf{u}_h^i, p_h^i, \lambda_h^i) \in \mathbf{V}_{hz}^i \times Q_h^i \times F_h(\mathscr{E}_h\cap\partial\Omega_i)$, for $i = 1,\ldots,m$, such that

$$(K^{-1}\mathbf{u}_h^i,\mathbf{v})_{\Omega_i} - (p_h^i,\nabla\cdot\mathbf{v})_{\Omega_i} + (\beta_i\mathbf{u}_h^i\cdot\check{\mathbf{n}}^i,\mathbf{v}\cdot\check{\mathbf{n}}^i)_{\partial\Omega_i\cap\Gamma} + (\lambda_h^i,\mathbf{v}\cdot\check{\mathbf{n}}^i)_{\partial\Omega_i\cap\Gamma} = -(g,\mathbf{v}\cdot\check{\mathbf{n}}^i)_{\partial\Omega_i\cap\partial\Omega_p} \,, \tag{2.36}$$

$$(q,\nabla\cdot\mathbf{u}_h^i)_{\Omega_i} = (f,q)_{\Omega_i} \,, \tag{2.37}$$

$$\sum_{i=1}^m (\mathbf{u}_h^i\cdot\check{\mathbf{n}}^i, M_h)_{\partial\Omega_i\cap\Gamma} = 0 \,, \tag{2.38}$$

$$\sum_{i=1}^m (\beta_i\mathbf{u}_h^i\cdot\check{\mathbf{n}}^i + \lambda_h^i, V_h\check{\mathbf{n}}^i\cdot\check{\mathbf{n}})_{\partial\Omega_i\cap\Gamma} = 0 \,, \tag{2.39}$$

hold for all $(\mathbf{v},q) \in \mathbf{V}_{h0}^i$ and for all $(M_h,V_h) \in F_h(\mathscr{E}_h)\times F_h(\mathscr{E}_h)$.

This can be identified as the variational formulation that underlies the domain decomposition algorithm proposed by Douglas et al (DOUGLAS *et al.*, 1993). In fact, their iterative algorithm assumes a red-black colouring of the subdomains with an initial value of λ_h^i for all red Ω_i's. This allows to solve (2.36)-(2.37) for $\mathbf{u}_h^i$ and p_h^i. Then (2.38)-(2.39) are considered at all interfaces $\Gamma_{i,j}$, where Ω_j is a black subdomain, which yield the update formula for λ_h^j as

$$\lambda_h^j = \lambda_h^i + \beta_i\mathbf{u}_h^i\cdot\check{\mathbf{n}}^i - \beta_j\mathbf{u}_h^j\cdot\check{\mathbf{n}}^j = \lambda_h^i + (\beta_i+\beta_j)\mathbf{u}_h^i\cdot\check{\mathbf{n}}^i \,.$$

The process can then be iterated switching the roles of the black and red subdomains.

Remark 3. Equations (2.36)-(2.39) also provide the variational formulation of the so-called Two-Lagrange-Multiplier (2LM) method, or Optimized Schwarz method (LOISEL, 2013; LOISEL; NGUYEN; SCHEICHL, 2015; MADAY; MAGOULÈS, 2006). The λ_h^i, of which there exist two at each edge of each internal interface $\Gamma_{i,j}$, are the two Lagrange multipliers that give the method its name (notice that in our formulation there is no unknown shared by more than two subdomains).

The 2LM formulation (2.36)-(2.39) may be seen as more concise, and perhaps more elegant, than the proposed (equivalent if $\mathscr{U} = \mathscr{P} = F_h(\mathscr{E}_h)$) formulation (2.17)-(2.20). The latter

is however more powerful, since the separate roles of the interface pressure P_h and of the interface flow U_h can be clearly identified. As explained in the next section, this allows for the design of multiscale formulations with different spaces for $\mathscr{P}$ and $\mathscr{U}$, which is not possible if the start point is (2.36)-(2.39).

2.2.2 The multiscale formulation

Multiscale variants of domain decomposition formulations, such as the MMMFEM and the MHM method, follow the strategy of creating two discretization scales by restricting the Lagrange multiplier space, which roughly speaking is $F_h(\mathscr{E}_h)$ in the fine grid, to a much coarser space defined at a scale $H \gg h$. Usually, H is the size of the individual subdomains.

Take for example the Mortar Mixed Finite Element Method (GLOWINSKI; WHEELER, 1988; ARBOGAST *et al.*, 2000), which is nothing but our DD formulation (2.17)-(2.20) with $\mathscr{P} = \mathscr{P}_h$ and $\beta_i = 0$ for all i. In this case, one obtains the fine grid solution, whereas taking $\mathscr{P} = \mathscr{P}_H$ (a coarse subspace of $\mathscr{P}_h$) one obtains its multiscale version, the MMMFEM. Similarly, the MHM method is obtained from the Mortar Method (BELGACEM, 1999) by taking a coarse subspace $\mathscr{U}_H$ for the Lagrange multiplier, which in this case is U. Notice that the Mortar Method is (intuitively) the limit of our DD formulation when $\beta_i \to +\infty$, which makes the unknown P to disappear.

Following the same strategy, **the multiscale approach we propose simply consists of taking coarse spaces $\mathscr{U} = \mathscr{U}_H$ and $\mathscr{P} = \mathscr{P}_H$ in (2.17)-(2.20) while keeping the fine-scale spaces $\mathbf{V}_h^i$ for velocity and Q_h^i for pressure inside each Ω_i**. Let us follow the tradition and give a name to the proposed method. Be it Multiscale Robin Coupled method, MRCM, which as shown in Prop. 1 yields a well–posed discrete problem with the sole condition that $\mathscr{P}_H \subset \mathscr{P}_h$ (see Remark 1).

When the interface spaces are coarsened, the computational cost is greatly alleviated in both calculations and message passing operations. The solution is certainly quite different from that computed on the fine mesh, unless the interface subspaces happen to approximate very well the fine mesh solution. A unique feature of MRCM is that coarse spaces for **both** interface pressure and flux can be chosen arbitrarily, while MMMFEM only allows the user to select $\mathscr{P}_H$ and MHM only allows to select $\mathscr{U}_H$.

Piecewise polynomial interface spaces were the first to be explored in multiscale formulations (GANIS; YOTOV, 2009; HARDER; PAREDES; VALENTIN, 2013) and are the ones implemented in this work, since they are easy to code and allow for rigorous analysis. More precisely, our interface spaces $\mathscr{U}_H$ and $\mathscr{P}_H$ are projections of piecewise polynomial spaces onto $F_h(\mathscr{E}_h)$. For highly heterogeneous media a convenient alternative to piecewise polynomial spaces are *informed spaces*, in which fine-mesh solutions are precomputed at some neighborhood (oversampling) of each interface $\Gamma_{i,j}$, and from them some reduction technique is applied to

build $\mathscr{P}_H$ and/or $\mathscr{U}_H$. This alternative has been explored recently by Chung et al (CHUNG; FU; YANG, 2016) for the MMMFEM, while it remains unexplored for the MHM method. The assessment of the MRCM with informed spaces is however left for future work.

2.2.3 The multiscale implementation

This section provides details on the implementation of the Multiscale Robin Coupled Method. The way followed to describe our implementation shares similarities to that used by Ganis and Yotov for the Multiscale Mortar Mixed Finite Element method in (GANIS; YOTOV, 2009). Referring to Fig. 1, let us consider a non-overlapping domain decomposition of Ω into subdomains Ω_i, $i = 1,\ldots,m$. Also consider associated to the skeleton Γ of this decomposition, a partition denoted by $\mathscr{T}_H$ (see Fig. 1 to visualize a possible partition of the skeleton) and to this partition coarse–scale spaces $\mathscr{U}_H$ and $\mathscr{P}_H$ for fluxes and pressure, respectively. Though not strictly necessary (see Remark 1), both $\mathscr{U}_H$ and $\mathscr{P}_H$ are taken as subspaces of $F_h(\mathscr{E}_h)$. This simplifies the coding and garantees, because $\mathscr{P}_H \subset \mathscr{P}_h = F_h(\mathscr{E}_h)$, that the discrete problem is well posed. As said, the size of the partition H is typically much larger than h, therefore the dimension of these subspaces is small as compared to that of $F_h(\mathscr{E}_h)$ as depicted in Fig. 1.

In order to explain the implementation, let us suppose at this stage $(U_H, P_H) \in \mathscr{U}_H \times \mathscr{P}_H$ known. This way, we can rewrite the local problems on each subdomain as: Find $(\mathbf{u}_h^i, p_h^i) \in \mathbf{V}_{hz}^i \times Q_h^i$, for $i = 1,\ldots,m$, such that

$$\begin{aligned}(K^{-1}\mathbf{u}_h^i,\mathbf{v})_{\Omega_i} - (p_h^i,\nabla\cdot\mathbf{v})_{\Omega_i} + (\beta_i\,\mathbf{u}_h^i\cdot\check{\mathbf{n}}^i,\mathbf{v}\cdot\check{\mathbf{n}}^i)_{\partial\Omega_i\cap\Gamma} &= -(P_H - \beta_i U_H\check{\mathbf{n}}^i\cdot\check{\mathbf{n}},\mathbf{v}\cdot\check{\mathbf{n}}^i)_{\partial\Omega_i\cap\Gamma} \\ &\quad -(g,\mathbf{v}\cdot\check{\mathbf{n}}^i)_{\partial\Omega_i\cap\partial\Omega_p}\,, \qquad (2.40)\\ (q,\nabla\cdot\mathbf{u}_h^i)_{\Omega_i} &= (f,q)_{\Omega_i}\,, \qquad (2.41)\end{aligned}$$

hold for all $(\mathbf{v},q) \in \mathbf{V}_{h0}^i \times Q_h^i$, $\forall\, i = 1,\ldots,m$. Now, we perform an additive decomposition of the solution $(\mathbf{u}_h^i, p_h^i)$ as

$$\begin{aligned}\mathbf{u}_h^i &= \widehat{\mathbf{u}}_h^i + \bar{\mathbf{u}}_h^i, \qquad (2.42)\\ p_h^i &= \widehat{p}_h^i + \bar{p}_h^i. \qquad (2.43)\end{aligned}$$

On the one hand, $(\bar{\mathbf{u}}_h, \bar{p}_h) \in \mathbf{V}_{hz}^i \times Q_h^i$ satisfies the subdomain problems with interface values U_H and P_H equal to zero and nonzero forcing terms, that is

$$\begin{aligned}(K^{-1}\bar{\mathbf{u}}_h^i,\mathbf{v})_{\Omega_i} - (\bar{p}_h^i,\nabla\cdot\mathbf{v})_{\Omega_i} + (\beta_i\,\bar{\mathbf{u}}_h^i\cdot\check{\mathbf{n}}^i,\mathbf{v}\cdot\check{\mathbf{n}}^i)_{\partial\Omega_i\cap\Gamma} &= -(g,\mathbf{v}\cdot\check{\mathbf{n}}^i)_{\partial\Omega_i\cap\partial\Omega_p}\,, \qquad (2.44)\\ (q,\nabla\cdot\bar{\mathbf{u}}_h^i)_{\Omega_i} &= (f,q)_{\Omega_i}\,, \qquad (2.45)\end{aligned}$$

hold for all $(\mathbf{v},q) \in \mathbf{V}_{h0}^i \times Q_h^i$, $\forall\, i = 1,\ldots,m$. On the other hand, $(\widehat{\mathbf{u}}_h^i, \widehat{p}_h^i) \in \mathbf{V}_{h0}^i \times Q_h^i$ satisfies the subdomain problems with forcing terms f and g identically equal to zero

$$\begin{aligned}(K^{-1}\widehat{\mathbf{u}}_h^i,\mathbf{v})_{\Omega_i} - (\widehat{p}_h^i,\nabla\cdot\mathbf{v})_{\Omega_i} + (\beta_i\,\widehat{\mathbf{u}}_h^i\cdot\check{\mathbf{n}}^i,\mathbf{v}\cdot\check{\mathbf{n}}^i)_{\partial\Omega_i\cap\Gamma,} &= -(P_H - \beta_i U_H\check{\mathbf{n}}^i\cdot\check{\mathbf{n}},\mathbf{v}\cdot\check{\mathbf{n}}^i)_{\partial\Omega_i\cap\Gamma} \\ &\qquad (2.46)\\ (q,\nabla\cdot\widehat{\mathbf{u}}_h^i)_{\Omega_i} &= 0, \qquad (2.47)\end{aligned}$$

hold for all $(\mathbf{v},q) \in \mathbf{V}^i_{h0} \times Q^i_h$, $\forall i = 1,\ldots,m$.

The local problems above, like (2.40)–(2.41) or any other considered in the rest of the article can be solved by choosing any standard discrete spaces for $\mathbf{V}^i_{h0}$ and Q^i_h. In this article we restrict ourselves to the two dimensional case and the lowest order Raviart-Thomas space RT_0 on quadrilateral cartesian grids of uniform cell size h (see Fig. 1). As known, the choice of this space and a combination of the midpoint and the trapezoidal rules for numerical integration produces a discrete system which only involves pressure unknowns and that is equivalent to a classical cell–centered finite volume method (see (ARBOGAST; WHEELER; YOTOV, 1997) for instance).

Let us provide some details of the final algebraic equations that are generated by problem (2.40)–(2.41) for our choice of finite element and mesh. We denote the pressure unknowns, located at the cell centers, by $p_{h,I,J}$ and the flux unknowns, located at the faces midpoints, by $u_{h,I\pm1/2,J}$ (for horizontal faces) or $u_{h,I,J\pm1/2}$ (for vertical faces). Assuming K to be elementwise constant, Eq. (2.40) translates into the following two-point formulas for any internal edge of the mesh:

$$\begin{aligned} u_{h,I+1/2,J} &= -\bar{K}_{I+1/2,J}\,\frac{p_{h,I+1,J}-p_{h,I,J}}{h}, \quad u_{h,I-1/2,J} = -\bar{K}_{I-1/2,J}\,\frac{p_{h,I,J}-p_{h,I-1,J}}{h}, \\ u_{h,I,J+1/2} &= -\bar{K}_{I,J+1/2}\,\frac{p_{h,I,J+1}-p_{h,I,J}}{h} \quad u_{h,I,J-1/2} = -\bar{K}_{I,J-1/2}\,\frac{p_{h,I,J}-p_{h,I,J-1}}{h}. \end{aligned} \tag{2.48}$$

The indices I and J above run through all fine scale cells of the local problems, and the $\bar{K}$'s are the harmonic means of the permeabilities at interelement faces, for example, $\bar{K}_{I+1/2,J} = 2\,K_{I,J}\,K_{I+1,J}/(K_{I,J}+K_{I+1,J})$. Turning to Eq. (2.41), for each fine scale cell it translates into

$$h\left(u_{h,I+1/2,J} - u_{h,I-1/2,J} + u_{h,I,J+1/2} - u_{h,I,J-1/2}\right) = h^2\, f_{I,J}. \tag{2.49}$$

As for the treatment of boundary conditions, those of the flux type are imposed directly by replacing the right hand side of the corresponding flux expression (Eq. (2.48)) by the prescribed value at boundary edges, which is consistent with the definition of V^i_{hy} in Eq. (2.13).

For boundary edges subject to pressure conditions Eq. (2.48) can be rewritten as

$$u_{h,I-1/2,J} = -K_{I,J}\,\frac{p_{I,J}-\pi_{I-1/2,J}}{h/2} \tag{2.50}$$

where $\pi_{I-1/2,J}$ is a face pressure which is set to the prescribed value. The case of a Robin boundary condition, given as in (2.9), also leads to Eq. (2.50), but with the value of $\pi_{I-1/2,J}$ now replaced by

$$\pi_{I-1/2,J} = g_R + \beta_i\,\mathbf{u}_h\cdot\check{\mathbf{n}}^i = g_R - \beta_i\,u_{h,I-1/2,J} \tag{2.51}$$

Though Eqs. (2.50) and (2.51) are specific to a West boundary, they readily extend to the others.

Inserting Eqs. (2.48) or (2.50) into (2.49) one ends up with a linear system only involving pressure unknowns. Suitable modifications of the scheme that deal with anisotropic (tensorial)

permeability coefficients can be found in (ARBOGAST; WHEELER; YOTOV, 1997). More sophisticated finite volume methods, known as Multipoint Flux Approximations (MPFA) are discussed in, for example, (VOHRALÍK, 2006).

Let us now turn to the next ingredient of the implementation, namely the construction of the coarse discrete spaces $\mathscr{U}_H$ and $\mathscr{P}_H$. Their respective finite element basis are denoted by $\{\phi^j\}_{1\leq j\leq n_U}$ and $\{\psi^j\}_{1\leq j\leq n_P}$, so that the unknowns U_H and P_H are written as

$$U_H = \sum_{\ell=1}^{n_U} X_\ell^U \, \phi^\ell, \quad P_H = \sum_{\ell=1}^{n_P} X_\ell^P \, \psi^\ell \,, \tag{2.52}$$

where $n_U = \dim(\mathscr{U}_H)$ and $n_P = \dim(\mathscr{P}_H)$. By considering Eqs. (2.19)-(2.20) that corresponds to weak flux and pressure continuity on Γ, now posed on the coarse scale H, we may simultaneously solve for all fields and subdomains. However, it is possible to eliminate the internal subdomain degrees of freedom, thus solving a relatively small system for the interface unknowns alone. This is accomplished by building multiscale basis functions on the different subdomains as explained next.

2.2.3.1 Multiscale basis functions and the interface linear system

We define multiscale basis functions by solving certain local problems in each subdomain. First, we need to introduce some notation. Let us define the global vector of interface unknowns $\underline{X} \in \mathbb{R}^n$, $n = n_U + n_P$, $\underline{X} = \left(\underline{X}^U, \underline{X}^P\right)^T$, $\underline{X}^U = \left(X_1^U, \ldots, X_{n_U}^U\right)$ and $\underline{X}^P = \left(X_1^P, \ldots, X_{n_P}^P\right)$. For subdomain Ω_i, $i = 1, \ldots, m$, let us also define $\mathscr{J}^i$ as the set of indices of global interface degrees of freedom associated to basis functions for $\mathscr{U}_H$ and $\mathscr{P}_H$ whose support is on the boundary $\partial\Omega_i \cap \Gamma$. The multiscale basis functions in Ω_i, denoted here as $\{\Phi_{k_j}^i, \Psi_{k_j}^i\}_{1\leq k_j\leq n_i}$, being $n_i = |\mathscr{J}^i|$ (the number of elements in $\mathscr{J}^i$) and $k_j = 1, \ldots, n_i$ a local subdomain numbering of the unknowns corresponding to global indices $j \in \mathscr{J}^i$, are obtained as solutions of problem (2.46)-(2.47) as follows. For $j \in \mathscr{J}^i$, if $1 \leq j \leq n_U$, basis function k_j of subdomain Ω_i is obtained by solving the local problem with boundary data $U_H = \phi^j$, $P_H = 0$, i.e., find $(\Phi_{k_j}^i, \Psi_{k_j}^i) \in \mathbf{V}_{h0}^i \times Q_h^i$, such that

$$(K^{-1}\Phi_{k_j}^i, \mathbf{v})_{\Omega_i} - (\Psi_{k_j}^i, \nabla\cdot\mathbf{v})_{\Omega_i} + (\beta_i \Phi_{k_j}^i \cdot \check{\mathbf{n}}^i, \mathbf{v}\cdot\check{\mathbf{n}}^i)_{\partial\Omega_i\cap\Gamma} = (\beta_i \phi^j \check{\mathbf{n}}^i \cdot \check{\mathbf{n}}, \mathbf{v}\cdot\check{\mathbf{n}}^i)_{\partial\Omega_i\cap\Gamma}, \tag{2.53}$$

$$(q, \nabla\cdot\Phi_{k_j}^i)_{\Omega_i} = 0, \tag{2.54}$$

hold for all $(\mathbf{v}, q) \in \mathbf{V}_{h0}^i \times Q_h^i$, whereas, if $n_U < j \leq n_U + n_P$, subdomain basis function k_j is obtained by solving the local problem with boundary data $U_H = 0$, $P_H = \psi^{j-n_U}$, i.e., find $(\Phi_{k_j}^i, \Psi_{k_j}^i) \in \mathbf{V}_{h0}^i \times Q_h^i$, such that

$$(K^{-1}\Phi_{k_j}^i, \mathbf{v})_{\Omega_i} - (\Psi_{k_j}^i, \nabla\cdot\mathbf{v})_{\Omega_i} + (\beta_i \Phi_{k_j}^i \cdot \check{\mathbf{n}}^i, \mathbf{v}\cdot\check{\mathbf{n}}^i)_{\partial\Omega_i\cap\Gamma} = -(\psi^{j-n_U}, \mathbf{v}\cdot\check{\mathbf{n}}^i)_{\partial\Omega_i\cap\Gamma}, \tag{2.55}$$

$$(q, \nabla\cdot\Phi_{k_j}^i)_{\Omega_i} = 0, \tag{2.56}$$

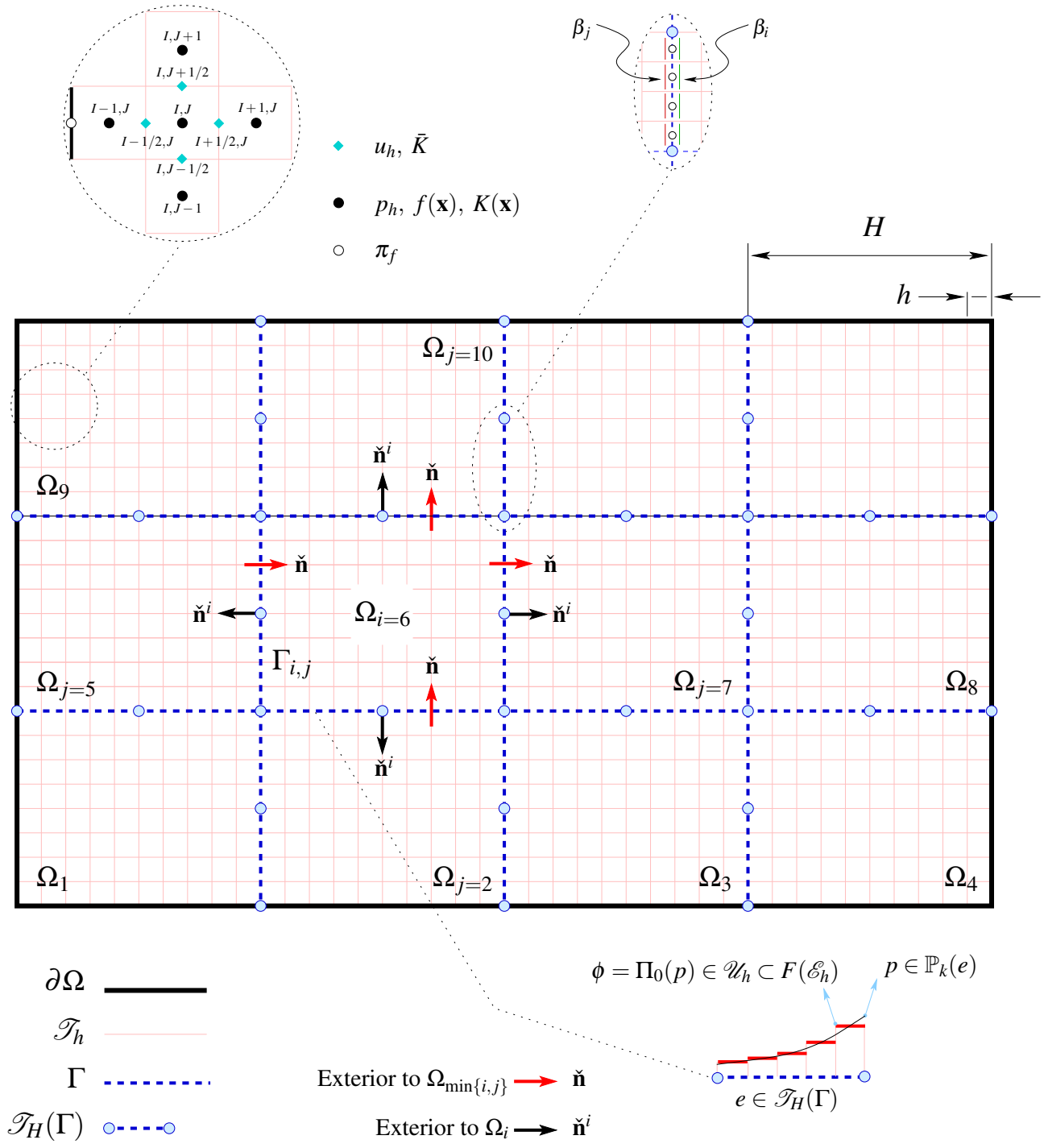

Source: Elaborated by the author.

Figure 1 – Computational domain, meshes used for discretization and relevant notation to implement the MRCM. The blue dots are only used to visualize a possible partition $\mathscr{T}_H$ of the skeleton Γ. They might or not be nodes to which an interface degree of freedom is associated.

hold for all $(\mathbf{v}, q) \in \mathbf{V}^i_{h0} \times Q^i_h$. Computation of these basis functions can be done off–line and is naturally parallelizable.

Now, we are ready to build the interface linear system. To this end, first note that by the

linearity of the problem, the local solutions on each subdomain can be written as

$$\widehat{\mathbf{u}}_h^i = \sum_{j\in\mathscr{J}^i} X_j \Phi_{k_j}^i, \quad \widehat{p}_h^i = \sum_{j\in\mathscr{J}^i} X_j \Psi_{k_j}^i. \tag{2.57}$$

Recalling the decomposition (2.42)-(2.43) and the weak flux and pressure continuity Eqs. (2.19)-(2.20) on the coarse scale, we write

$$\sum_{i=1}^{m} \left(\widehat{\mathbf{u}}_h^i \cdot \check{\mathbf{n}}^i, M_H\right)_{\partial\Omega_i\cap\Gamma} = -\sum_{i=1}^{m} \left(\bar{\mathbf{u}}_h^i \cdot \check{\mathbf{n}}^i, M_H\right)_{\partial\Omega_i\cap\Gamma}, \tag{2.58}$$

$$\sum_{i=1}^{m} (\beta_i (\widehat{\mathbf{u}}_h^i \cdot \check{\mathbf{n}}^i - U_h \check{\mathbf{n}}^i \cdot \check{\mathbf{n}}), V_H \check{\mathbf{n}}^i \cdot \check{\mathbf{n}})_{\partial\Omega_i\cap\Gamma} = -\sum_{i=1}^{m} (\beta_i (\bar{\mathbf{u}}_h^i \cdot \check{\mathbf{n}}^i), V_H \check{\mathbf{n}}^i \cdot \check{\mathbf{n}})_{\partial\Omega_i\cap\Gamma}. \tag{2.59}$$

Finally, by substituing (2.57) and testing with all basis functions of $\mathscr{U}_H$ and $\mathscr{P}_H$ we end up with the linear system

$$\underline{\underline{A}}\,\underline{X} = \underline{b}. \tag{2.60}$$

If a matrix–free method is used to solve the linear system, such as the Biconjugate Gradient or the GMRES method, no explicit computation of the matrix coefficients becomes necessary, otherwise, the entries of matrix $\underline{\underline{A}} = \left[a_{\ell j}\right] \in \mathbb{R}^{n\times n}$ are, for $j = 1,\ldots,n$

$$a_{\ell j} = \begin{cases} \sum_{i=1}^{m} (\beta_i (\Phi_{k_j}^i \cdot \check{\mathbf{n}}^i - \varphi^j \check{\mathbf{n}}^i \cdot \check{\mathbf{n}}), \phi^\ell \check{\mathbf{n}}^i \cdot \check{\mathbf{n}})_{\partial\Omega_i\cap\Gamma}, & \text{for } 1 \le \ell \le n_U \\ \sum_{i=1}^{m} \left(\Phi_{k_j}^i \cdot \check{\mathbf{n}}^i, \psi^{\ell-n_U}\right)_{\partial\Omega_i\cap\Gamma}, & \text{for } n_U < \ell \le n \end{cases} \tag{2.61}$$

where $\varphi^j = \phi^j$ if $1 \le j \le n_U$ and zero otherwise and recalling that for the i-th subdomain and for each k_j, j must belong to the set $\mathscr{J}^i$ for the corresponding term to make sense in (2.61). As for the right hand side vector $\underline{b} = [b_\ell] \in \mathbb{R}^n$, computing its entries involves the particular solutions $\bar{\mathbf{u}}_h^i$ previously found by solving (2.44)-(2.45), yielding

$$b_\ell = \begin{cases} -\sum_{i=1}^{m} (\beta_i (\bar{\mathbf{u}}_h^i \cdot \check{\mathbf{n}}^i), \phi^\ell \check{\mathbf{n}}^i \cdot \check{\mathbf{n}})_{\partial\Omega_i\cap\Gamma}, & \text{for } 1 \le \ell \le n_U \\ -\sum_{i=1}^{m} \left(\bar{\mathbf{u}}_h^i \cdot \check{\mathbf{n}}^i, \psi^{\ell-n_U}\right)_{\partial\Omega_i\cap\Gamma}, & \text{for } n_U < \ell \le n \end{cases} \tag{2.62}$$

Computing the integrals above is straightforward once all functions are piecewise constant on the set of edges of $\mathscr{T}_h$ contained in Γ. Also notice that, as pointed out by Ganis and Yotov (GANIS; YOTOV, 2009), during the resolution of the interface problem, storing the whole set of subdomain basis functions values may lead to an unnecessary memory burden, being that in this step only the fluxes and recovered pressure values at the edges lying on Γ are required. Consequently, the authors recommend to store only those values and after solving (2.60) perform a last subdomain solve to find $(\widehat{\mathbf{u}}_h^i, \widehat{p}_h^i)$ so the final global solution can be reconstructed.

2.3 Numerical experiments

This section presents a numerical assessment of the Multiscale Robin Coupled method and its comparison in some classical benchmark problems to the Multiscale Mortar Mixed and

Hybrid-Mixed Finite Element methods previously introduced. We aim to illustrate the possibility of switching from one method to the other by suitably varying the Robin condition parameter in the MRCM formulation and also show the possibility of choosing different (coarse) spaces $\mathscr{U}_H$ and $\mathscr{P}_H$ for flux and pressure on the interface. Three test examples are addressed. First, the classical quarter of a 5–spot problem is studied by considering a random (log normal) permeability field of moderate variability. Second, a problem with a manufactured solution proposed in (HARDER; PAREDES; VALENTIN, 2013) is presented in order to assess the convergence properties of the scheme. Finally, the MRCM formulation is assessed by solving several sections of the SPE10 benchmark with high contrast permeability fields that exhibit channelized regions. All numerical results are restricted to the two dimensional case assuming an isotropic diagonal permeability tensor. As for the construction of the discrete spaces $\mathscr{U}_H$ and $\mathscr{P}_H$ on the interface, we will restrict ourselves in this article to the following spaces for flux and pressure

$$\mathscr{U}_H = \{V_H,\, V_H|_e = \Pi_0(q), q \in \mathbb{P}_{\ell_U}(e),\, e \in \mathscr{T}_H\}, \tag{2.63}$$

$$\mathscr{P}_H = \{M_H,\, M_H|_e = \Pi_0(q), q \in \mathbb{P}_{\ell_P}(e),\, e \in \mathscr{T}_H\}, \tag{2.64}$$

where $\mathbb{P}_k$, $k = \ell_U$ or ℓ_P is the space of polynomials of degree k and Π_0 is the L^2–projection of a function of $\mathbb{P}_k(e)$ onto the space $F_h(e)$, $e \in \mathscr{T}_H$, i.e., $\mathscr{U}_H$ and $\mathscr{P}_H$ are made up of the elementwise constant fine grid representation of polynomials of degree k over the interface elements. These spaces will be denoted by $\mathscr{U}_{H,k}$ and $\mathscr{P}_{H,k}$ from now on. In most of the numerical examples below k is made either equal to 0 or 1. For simplicity, in the first two numerical experiments $\mathscr{T}_H$ is built by taking only one element per interface $\Gamma_{i,j}$ between subdomains. In the third numerical experiment we also consider the possibility of performing a simple refinement of the skeleton partition to better illustrate the properties and versatility of the scheme. More sophisticated choices for these spaces and other interface refinements of $\mathscr{T}_H$ are certainly possible and relatively easy to handle, but these are left for future work.

As for the Robin condition parameter, from dimensional analysis we can see that the value of β_i on subdomain i in our discrete formulation should be chosen as:

$$\beta_i(\mathbf{x}) = \frac{\alpha(\mathbf{x})L}{K(\mathbf{x})}, \tag{2.65}$$

where L is a characteristic length scale that in line with (FRANCISCO *et al.*, 2014) is chosen to be equal to the mesh size h. The non-dimensional function α and the permeability K are tunnable algorithmic parameters to be selected. Different choices are possible for this parameter, such as discontinuous or continuous functions at subdomain interfaces. A natural choice for K that is adopted in the first two numerical examples corresponds to using the local permeability $K_i(\mathbf{x})$ in (2.65), which yields in general different parameters for each subdomain. In the third numerical example, other options are explored, e.g., using the harmonic mean of the permeabilities between neighboring subdomains. A comprehensive survey on the choice of β_i and the possibility of selecting it adaptively is the subject of ongoing works.

2.3.1 The quarter of a 5-spot - Relation between methods

This first example intends to illustrate the behavior of the MRCM formulation as the Robin condition parameter α introduced in Eq. (2.65) is increased from very small values, where the method behaves as the MMMFEM formulation, up to very large values, where the MRCM is expected to behave as the MHM formulation. To this end, we consider the classical quarter of a 5-spot problem. The computational domain $\Omega = [0,1] \times [0,1]$ is considered with a point source located at the top left corner and a point sink located at the bottom right corner as displayed in Fig. 2. Boundary conditions correspond to no flow on $\partial\Omega$. A heterogeneous permeability field given by

$$K(\mathbf{x}) = e^{\gamma \xi(\mathbf{x})}, \tag{2.66}$$

is used, where γ controls the permeability contrast $K_{\max}/K_{\min}$ which is taken to be 2455.8 in this numerical example and $\xi(\mathbf{x})$ is a self similar Gaussian distribution with zero mean and covariance function $C(\mathbf{x},\mathbf{y}) = |\mathbf{x}-\mathbf{y}|^{-1/2}$. Figure 2 shows a particular realization of this permeability field used in the simulations with a logarithmic color scale to better appreciate the permeability contrast. The domain is decomposed into 4×4 subdomains also indicated in the figure, each one discretized by a 16×16 (fine) grid, thus having $H = 1/4$ and $h = H/16$. From this decomposition, subdomain basis functions $\{\Phi^i_{k_j}, \Psi^i_{k_j}\}$ are computed according to the numerical procedure explained in the previous section. At this point, it is interesting to illustrate the behavior of such functions. Let us consider, for instance, the interface spaces $\mathscr{U}_{H,1}$ and $\mathscr{P}_{H,1}$. For this case, Fig. 3 shows plots of four (out of sixteen) local flux and pressure basis functions for subdomain Ω_7, setting the Robin condition parameter α equal to 1. To enhance the visualization, the velocity field arrows have been plotted without any scale applied to them in order to simply appreciate the trend of flow field. The shape of these functions clearly reflects the complexity of the flow as a consequence of the random permeability field being considered.

We aim now to study the behavior of the MRCM method as the Robin condition parameter α in Eq. (2.65) is varied continuously and report the $L^2(\Omega)$ norm of the difference between the MRCM solution and those obtained by the MMMFEM and MHM methods, both, implemented into independent codes as explained in (ARBOGAST *et al.*, 2000) and (HARDER; PAREDES; VALENTIN, 2013) respectively. For the MMMFEM, the corresponding Lagrange multiplier μ_H is chosen in the coarse interface space $\mathscr{P}_{H,k}$, whereas for the MHM method, the corresponding Lagrange multiplier ζ_H is chosen in $\mathscr{U}_{H,k}$.

We report pressure and flux errors using $\mathscr{U}_{H,0}$, $\mathscr{P}_{H,0}$ and $\mathscr{U}_{H,1}$, $\mathscr{P}_{H,1}$ as coarse interface spaces in this experiment. As mentioned, a single element per interface between neighboring subdomains is used to create the partition $\mathscr{T}_H$ of the skeleton Γ. Results are shown in Fig. 4. This figure shows the difference between the MRCM and the MMMFEM formulations goes to zero as the algorithmic parameter α is reduced. Conversely, as α is increased the solution of the MRCM formulation becomes closer to that obtained by the MHM method. This numerical evidence indicates the MRCM formulation changes continuously from the MMMFEM to the

MHM method as the Robin parameter is varied. As commented, a rigorous proof of this fact, however, is out of the scope of the article. Figure 4 indicates that asymptotically the MRCM approaches the MMMFEM (as $\alpha \to 0$) and the MHM (as $\alpha \to \infty$) linearly with respect to the Robin condition parameter α. In order to further illustrate the behavior of the method, Fig. 5 shows the pressure error and arrows of the velocity field error for the MRCM formulation with respect to the fine grid solution, for three different values of the parameter α and the same coarse interface spaces previously used. Clearly, results that correspond to $\mathscr{U}_{H,0}$ and $\mathscr{P}_{H,0}$ exhibit the larger errors. Notice this error is somewhat more concentrated near subdomain boundaries in all cases, as can be expected once the discretization has been weakened precisely at the interfaces between subdomains. At least in this case, the MRCM method shows improved accuracy as the Robin condition parameter is increased. However, this is not always the case as we will see later on in the following numerical examples, which motivates the possibility of selecting β_i adaptively in the different regions so as to switch between methods according to their accuracy or improved performance at particular locations.

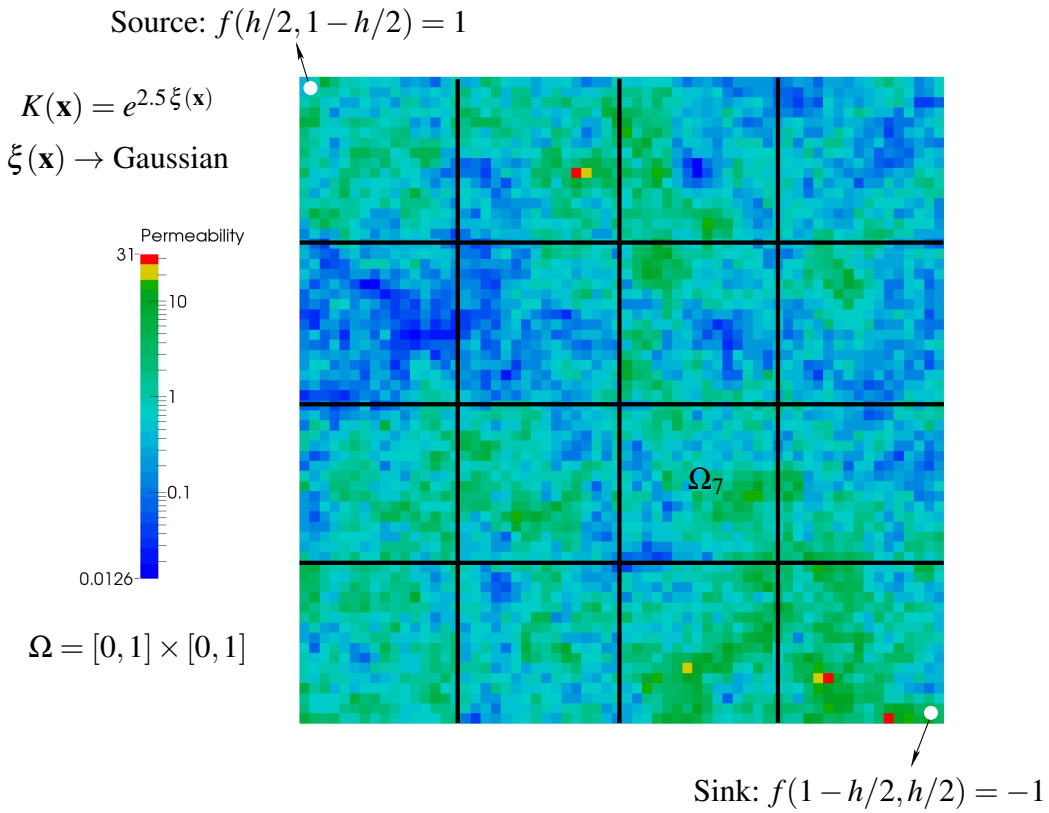

Source: Elaborated by the author.

Figure 2 – Problem setting and permeability field $K(\mathbf{x})$ for the quarter of a 5–spot problem.

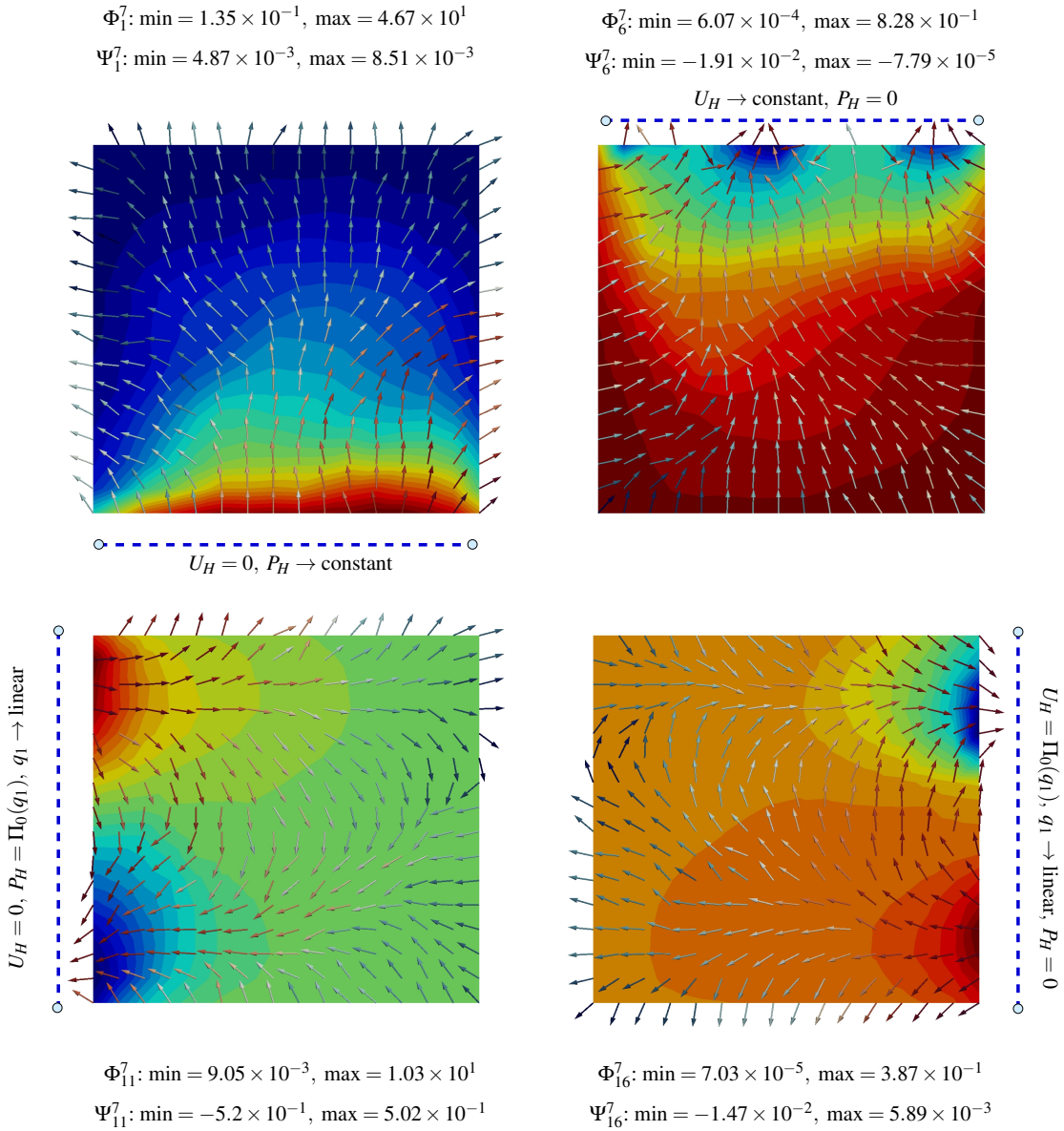

Source: Elaborated by the author.

Figure 3 – Pressure and flux basis functions of local indices $1, 6, 11$ and 16 corresponding to subdomain Ω_7 when using as interface spaces $\mathscr{U}_{H,1}$ and $\mathscr{P}_{H,1}$. The velocity field arrows are drawn without any scale applied to them in order to simply illustrate the trend of the flow field. The maximum (red) and minimum (blue) values of the Ψ's and vector magnitude of the Φ's are also indicated.

2.3.2 Problem with a manufactured solution - Convergence assessment

The second problem we consider corresponds to taking as computational domain the unit square, the following manufactured solution for the pressure

$$p = \cos(2\pi x_1)\cos(2\pi x_2) \tag{2.67}$$

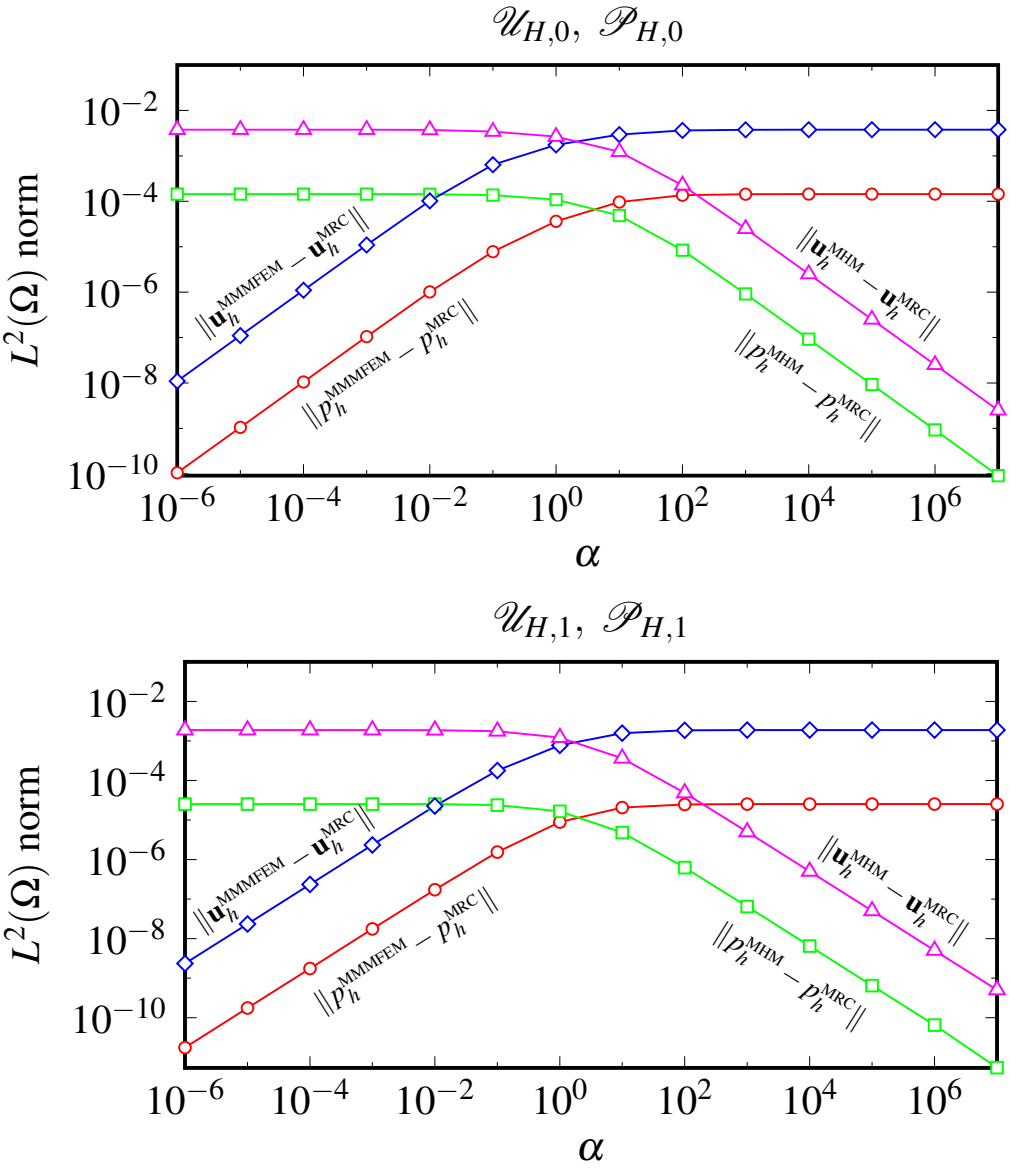

Source: Elaborated by the author.

Figure 4 – $L^2(\Omega)$ norm of the difference between the MRCM solution and the MMMFEM and MHM solutions as a function of the algorithmic parameter α for the quarter of a 5-spot problem.

and an uniform scalar permeability field $K = 1$, for which $f = 8\pi^2 \cos(2\pi x_1)\cos(2\pi x_2)$ must be given as the source term in (2.1)-(2.4). The solution satisfies homogeneous flux boundary conditions at all boundaries and has zero mean. From this problem we aim to assess the convergence properties of the MRCM method as the algorithmic parameter α in Eq. (2.65) is increased. First, mesh refinement is performed such that the ratio H/h is maintained constant, this is, by increasing the number of subdomains in each direction and simultaneously the number of fine grid cells in the same proportion. This way, the number of fine mesh cells in each subdomain is maintained constant. The first mesh in the sequence consists of 3×3 subdomains, each one subdivided into a fine mesh consisting of 20×20 elements, i.e., $H = 1/3$ and $h = H/20$. The rest

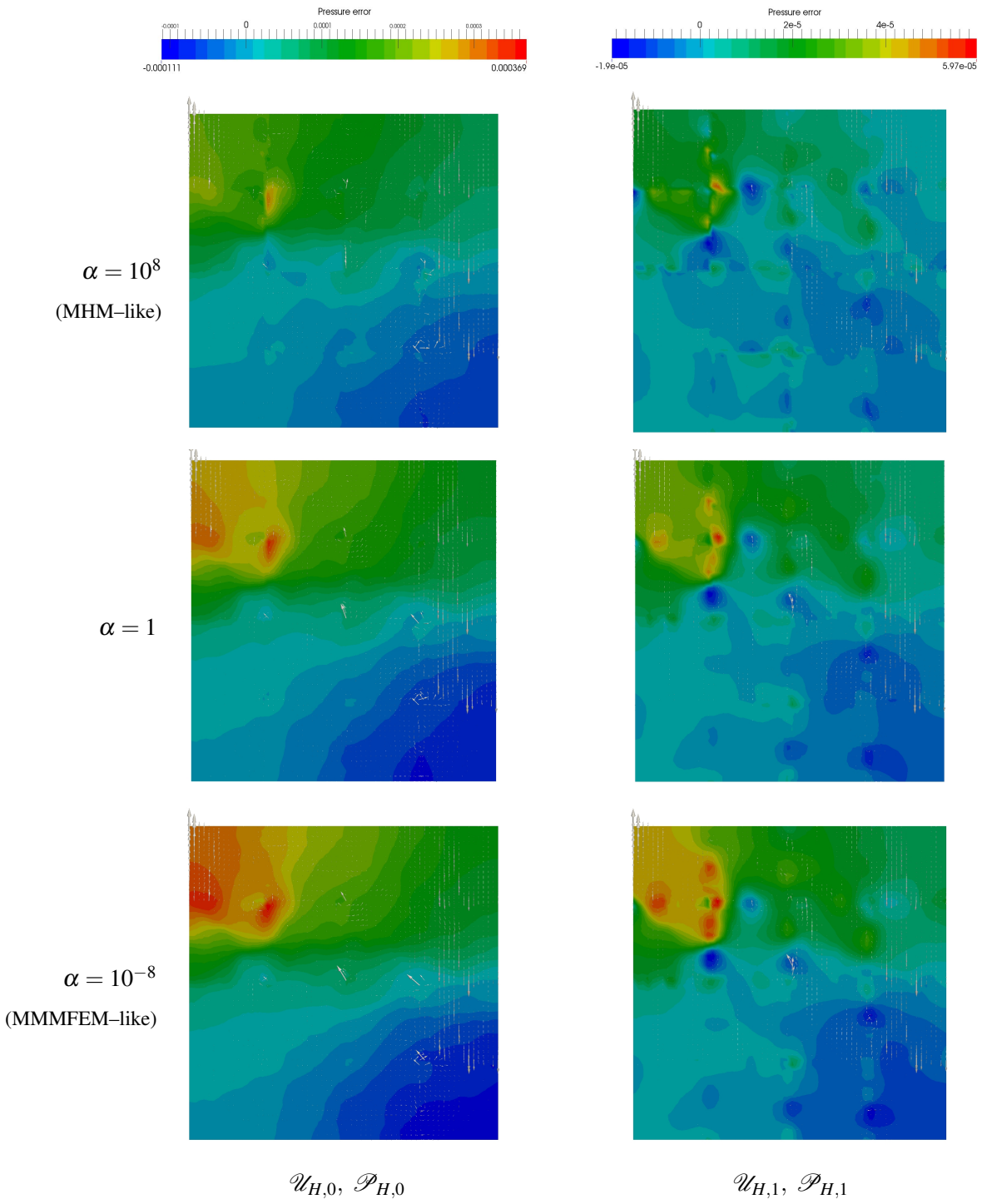

Source: Elaborated by the author.

Figure 5 – Contours of pressure error and arrows of velocity error of the MRCM solution with respect to the fine grid solution for different values of the Robin condition parameter α of Eq. (2.65) and different coarse interface spaces $\mathscr{U}_H$ and $\mathscr{P}_H$ in the quarter of a 5-spot problem.

of the meshes in the sequence are obtained by successively halving H and h. We report the $L^2(\Omega)$ error norms for pressure and velocity denoted respectively by $\|p - p_h\|_{L^2(\Omega)}$ and $\|\mathbf{u} - \mathbf{u}_h\|_{L^2(\Omega)}$

as functions of the partition characteristic size H. In the limiting cases, corresponding to $\alpha \to 0$ and $\alpha \to \infty$, we expect to recover respectively the convergence rates of the MMMFEM method (ARBOGAST *et al.*, 2000; ARBOGAST *et al.*, 2007) and those corresponding to the MHM method (HARDER; PAREDES; VALENTIN, 2013). These rates are summarized in table 1 for the particular cases that interest us in this article. A few comments are in order regarding these convergence rates: first, they assume that polynomial spaces are used on the mesh skeleton, although it is worth recalling that we are not using polynomials, but their projections onto $F(\mathscr{E}_h)$, as previously discussed. Second, for the MMMFEM formulation, the order H^2 for pressure is a superconvergence result obtained by a duality argument in (ARBOGAST *et al.*, 2000) precisely when the $L^2(\Omega)$–norm is used to measure the errors, that is the natural norm in our implementation. Finally, regarding the approximation properties of the local solvers, for the MMMFEM the estimates in (ARBOGAST *et al.*, 2000) consider a mixed formulation and for instance RT_k spaces (here, $k = 0$), whereas for the MHM method, according to (HARDER; PAREDES; VALENTIN, 2013), the convergence properties of the scheme are assessed by using an elliptic solver at the local level with a one element submesh and polynomial interpolation of degree $\ell + 1$ (here, $\ell \in \{0, 1\}$).

Table 1 – Expected convergence rates of the $L^2(\Omega)$ norm of the error for the MMMFEM and MHM formulations when polynomial spaces of degree $\ell = 0$ or 1 are used on the skeleton Γ.

	Pressure		*Flux*	
Method	$\ell = 0$	$\ell = 1$	$\ell = 0$	$\ell = 1$
MMMFEM (see (ARBOGAST *et al.*, 2000))	-	$\mathscr{O}(H^2)$	-	$\mathscr{O}(H)$
MHM (see (HARDER; PAREDES; VALENTIN, 2013))	$\mathscr{O}(H^2)$	$\mathscr{O}(H^3)$	$\mathscr{O}(H)$	$\mathscr{O}(H^2)$

Results are displayed in Fig. 6 and 7 that show the error norms corresponding to different combinations of the coarse interface spaces, namely, $\mathscr{U}_{H,\ell_U}$–$\mathscr{P}_{H,\ell_P}$ with ℓ_U and ℓ_P in $\{0, 1\}$. Lack of convergence is observed for the MMMFEM method for any combination of interface spaces where $\mathscr{P}_H = \mathscr{P}_{H,0}$. Conversely, the best results are obtained by taking moderate to large values of α and any combination of interface spaces where $\mathscr{P}_H = \mathscr{P}_{H,1}$. In the limiting case, that corresponds to taking $\alpha = 10^{-8}$, the error exhibits the expected convergence rate of the MMMFEM method, i.e., $\mathscr{O}(H^2)$ for pressure and $\mathscr{O}(H)$ for flux. In the other limiting case, that corresponds to taking $\alpha = 10^8$ the error exhibits the expected convergence rate of the MHM method, i.e., the error converges either with $\mathscr{O}(H^2)$ for pressure and $\mathscr{O}(H)$ for flux if the velocity space is $\mathscr{U}_{H,0}$, whereas if the velocity space $\mathscr{U}_{H,1}$ is used, the convergence rate is $\mathscr{O}(H^3)$ for pressure and $\mathscr{O}(H^2)$ for flux. We see that for all combinations of spaces considered, the error and convergences properties of the MRCM formulation improves as we increase the value of the Robin condition parameter, with one exception that corresponds to using $\mathscr{U}_{H,0}$ and $\mathscr{P}_{H,1}$ (see third column of Figs. 6 and 7), in which the method exhibits the same convergence rate irrespective of the value of α taken. In this case, we also note the error does not change monotonically with respect to α and that for $\alpha = 10^8$ (MHM-like solution) it exhibits greater

errors both for pressure and flux. Finally, for the choice of interface spaces $\mathscr{U}_{H,1}$ and $\mathscr{P}_{H,1}$ we observe that for low to intermediate values of the Robin condition parameter (tipically, $\lesssim 10$ for pressure and $\lesssim 30$ for flux) the convergence rate of the MRCM method never exceeds $\mathscr{O}(H^2)$ for pressure and $\mathscr{O}(H)$ for flux, but it reaches the MHM rates rapidly as we further increase α from those values, indeed coinciding with the values at which the MRCM begins to approach the MHM formulation linearly with respect to α as observed in the first numerical experiment (see Fig. 4).

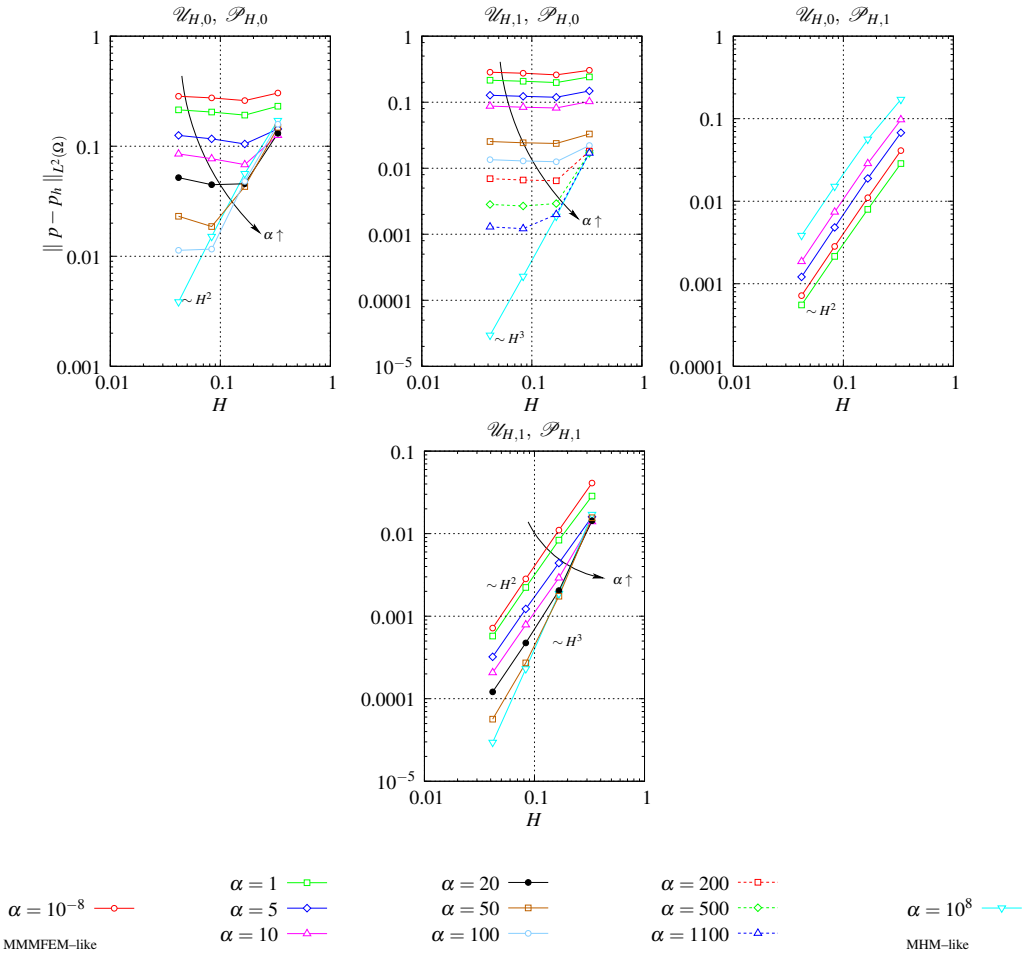

Source: Elaborated by the author.

Figure 6 – $L^2(\Omega)$ error norm of pressure $\|p - p_h\|_{L^2(\Omega)}$ as a function of the characteristic coarse interface mesh size H for the second numerical example maintaining the ratio H/h constant and considering different combinations of coarse interface spaces $\mathscr{U}_H$ and $\mathscr{P}_H$. Solution norm: $\| p \|_{L^2(\Omega)} = 1/2$.

The previous refinement procedure brings insight on the convergence properties of the method as the number of subdomains is increased, but the size of the local problems is left unchanged. From a HPC perspective, these results becomes thus relevant if we are interested in weak scaling speedup. A different refinement approach, consists in keeping the global fine grid partition $\mathscr{T}_h$ fix and then increase the number of subdomains, such that the local problems

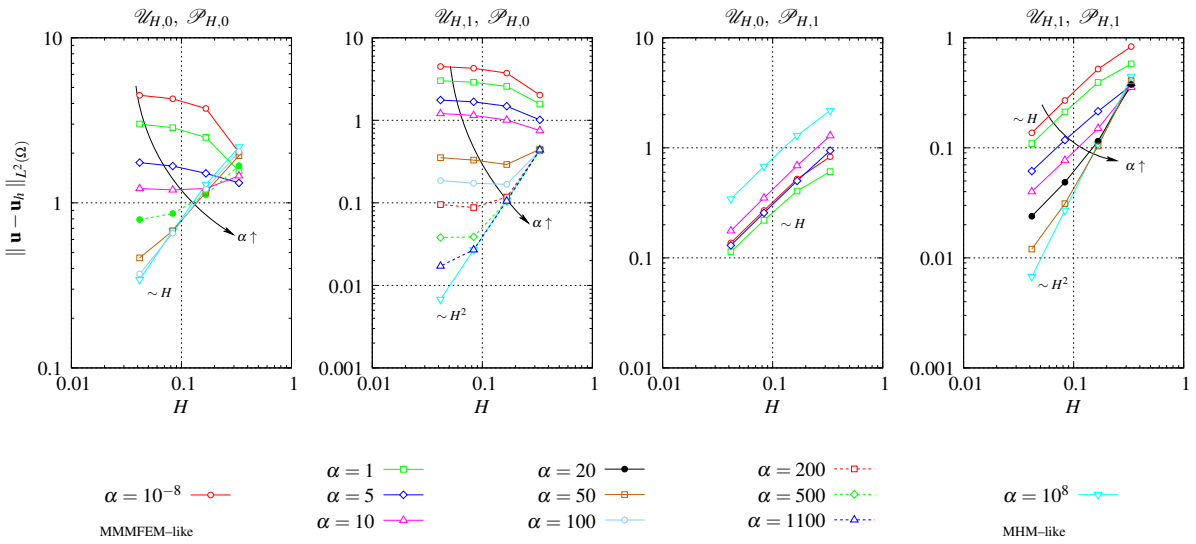

Source: Elaborated by the author.

Figure 7 – $L^2(\Omega)$ error norm of flux $\|\mathbf{u}-\mathbf{u}_h\|_{L^2(\Omega)}$ as a function of the characteristic coarse interface mesh size H for the second numerical example maintaining the ratio H/h constant and considering different combinations of interface spaces $\mathscr{U}_H$ and $\mathscr{P}_H$. Solution norm: $\|\mathbf{u}\|_{L^2(\Omega)} = \sqrt{2}\pi$.

become smaller at each refinement step. This may be relevant if we are interested in strong scaling speedup. To illustrate the convergence properties in this case, Fig. 8 shows the $L^2(\Omega)$ norm of the errors for pressure and flux using $\mathscr{U}_{H,1}$ and $\mathscr{P}_{H,1}$ as interface spaces. In contrast to the previous refinement study, now we observe a smoother increase of the convergence rate towards the MHM estimates, both for pressure and flux as we move to larger values of α. Interestingly, the MRCM asymptotically exhibits a significantly larger convergence rate and similar error for pressure ($\sim H^{2.72}$) for the intermediate value $\alpha = 5$ as compared to the case with $\alpha = 10^8$ (MHM–like), whose convergence rate deteriorates to something lower than $\mathscr{O}(H)$.

As a final convergence experiment, consider a fixed domain decomposition of Ω consisting of 4×4 subdomains (i.e., $H = 1/4$) and take as coarse interface spaces for flux and pressure $\mathscr{U}_{H,\ell}$ and $\mathscr{P}_{H,\ell}$ with $\ell = 0, 1, \ldots, 6$. For this experiment we adopt the value $\alpha = 100$ and report results for different fine grid discretizations, namely $h = H/20$, $h = H/40$ and $h = H/80$. Figure 9 shows the $L^2(\Omega)$ error norms of pressure and flux. Consider for example the curves corresponding to $h = H/20$. The pressure error decreases as ℓ is increased from 0 to 2 and then becomes essentially constant for $\ell > 2$. A similar behavior is observed for the flux error for $\ell > 3$. This means that taking $\ell = 3$ (6 unknowns per interface $\Gamma_{i,j}$, 3 for U_H and 3 for P_H) one gets results with the same accuracy as that of the fine grid solution. Considering that the fine grid solution involves 20 unknowns per interface (using Mortar or Mortar Mixed domain decomposition) the reduction in dimensionality is evident. For the case $h = H/80$ the reduction is even larger, since taking $\ell = 5$ (10 unknowns per interface) yields the same accuracy as that obtained with the 80 unknowns per interface of the fine grid.

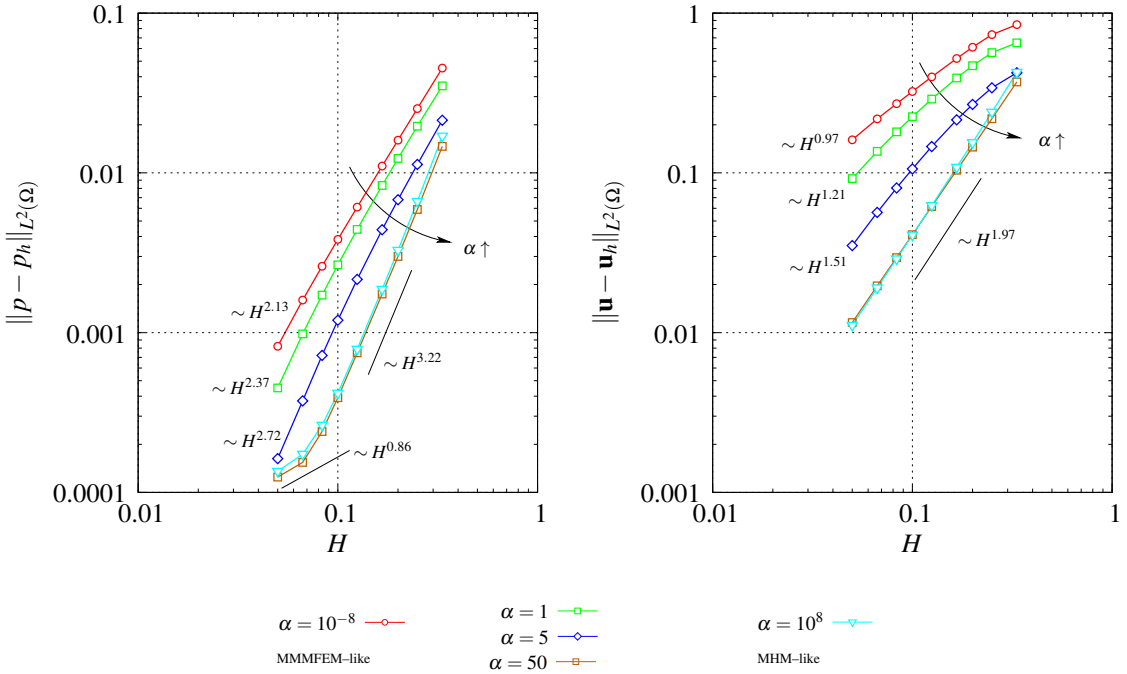

Source: Elaborated by the author.

Figure 8 – $L^2(\Omega)$ error norms of pressure and flux as a function of the characteristic coarse interface mesh size H for the second numerical example with fine grid size h maintained constant and using $\mathscr{U}_{H,1}$ and $\mathscr{P}_{H,1}$ as interface spaces. Solution norm: $\| p \|_{L^2(\Omega)} = 1/2$, $\| \mathbf{u} \|_{L^2(\Omega)} = \sqrt{2}\pi$.

2.3.3 The importance of the Robin condition parameter

Next we focus on two aspects of the MRCM. Through numerical experiments we will show that for a range of values of the Robin condition parameter the MRCM provides better approximations for pressure and velocity than those computed with the MRCM with extreme values of the Robin condition parameter. These extreme values produce numerical solutions close the the ones produced by the MMMFEM and MHM. Moreover, we perform a comprehensive number of tests aiming in illustrating the accuracy and robustness of the generalized MRCM formulation.

In the study reported here we use the permeability field provided by the SPE10 project (http://www.spe.org/web/csp), that is commonly employed to test subsurface codes. Released by the Society of Petroleum Engineers (SPE), it has become a recurrent benchmark in this field (CHRISTIE; BLUNT, 2001; FRANCISCO *et al.*, 2014). The original data contains $220 \times 60 \times 85$ cells and its physical dimensions are $2200 \times 1200 \times 170$ (ft). In our experiments the permeability contrast is $K_{\max}/K_{\min} \simeq 10^7$. For the purpose of our simulations and further investigations about the choice of the Robin condition parameter, 2D computations are performed in selected slices in the z direction. It is worth noting that most of the selected slices contains channelized structures that are particularly challenging for current multiscale methods. Moreover, if not stated otherwise, results were computed using linear spaces $\mathscr{P}_{H,1}$ and $\mathscr{U}_{H,1}$ for the underlying interface problems.

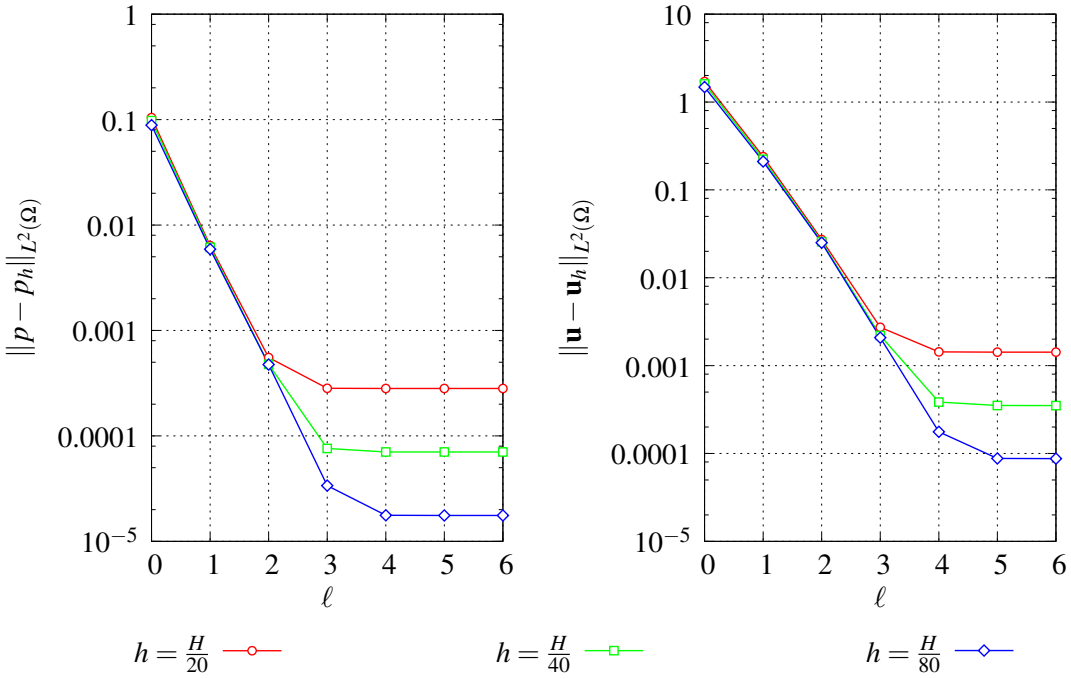

Source: Elaborated by the author.

Figure 9 – $L^2(\Omega)$ error norms of pressure and flux as a function of the polynomial order of the discrete interface spaces $\mathscr{U}_H$ and $\mathscr{P}_H$. Solution norm: $\| p \|_{L^2(\Omega)} = 1/2$, $\| \mathbf{u} \|_{L^2(\Omega)} = \sqrt{2}\pi$.

For all slices, the computational domain is set to be a rectangle $\Omega = [0, 11/3] \times [0, 1]$, and boundary conditions are no-flow at the top and bottom boundaries ($y = 0$ and $y = 1$), along with an imposed flux on the left ($x = 0$) and right ($x = 11/3$) boundaries.

As previously stated, the Robin condition parameter β_i appearing in the variational formulation (2.17)-(2.20), is computed as in Eq. (2.65), i.e. $\beta_i = \alpha h/K$, where α is a dimensionless parameter and K is the permeability field, that can be calculated on the interfaces $\Gamma_{i,j} \subset \Gamma$ in different ways. Although an optimal choice for the computation of this parameter demands a more thorough investigation, we consider here four simple choices for the evaluation of the permeability field aiming at showing the robustness and flexibility of our formulation. We consider the following options:

1. **Discontinuous**: The most obvious choice, since permeability fields are discontinuous along the grid edges/facets, is to compute

$$\beta_\ell(\mathbf{x}) = \frac{\alpha h}{K_\ell(\mathbf{x})}, \quad \ell \in \{i, j\},\ \mathbf{x} \in \Gamma_{i,j} \tag{2.68}$$

   so that β is constant by parts and different on each side of $\Gamma_{i,j}$ (an illustration is provided in the insert of figure 1).

2. **Harmonic**: Another approach is to take the same value on both sides of $\Gamma_{i,j}$ as the

harmonic average of permeability values, i.e.

$$\beta_\ell(\mathbf{x}) = \frac{\alpha h}{\overline{K}}, \quad \overline{K} = \frac{2K_i(\mathbf{x})K_j(\mathbf{x})}{K_i(\mathbf{x})+K_j(\mathbf{x})}, \quad \ell \in \{i,j\},\ \mathbf{x} \in \Gamma_{i,j}\ . \tag{2.69}$$

3. **One-sided**: Consists in setting β to zero in one side of $\Gamma_{i,j}$, and the other side dependent on a given parameter α. Thus

$$\beta_\ell(\mathbf{x}) = \begin{cases} 0, \text{ if } K_\ell(\mathbf{x}) < \max\left\{K_i(\mathbf{x}), K_j(\mathbf{x})\right\} \\ \dfrac{\alpha h}{K_\ell(\mathbf{x})}, \text{ otherwise.} \end{cases} \tag{2.70}$$

with $\ell \in \{i,j\}$ and $\mathbf{x} \in \Gamma_{i,j}$.

4. **Extreme**: Consists in setting the Robin condition parameter β as the extreme values (0 or ∞) in each side of the interface, such as

$$\beta_\ell(\mathbf{x}) = \begin{cases} 0, \text{ if } K_\ell(\mathbf{x}) < \max\left\{K_i(\mathbf{x}), K_j(\mathbf{x})\right\} \\ \infty, \text{ otherwise.} \end{cases} \tag{2.71}$$

with $\ell \in \{i,j\}$ and $\mathbf{x} \in \Gamma_{i,j}$.

We performed a series of numerical studies for a number of different slices, using the *Discontinuous* Robin condition parameter (Eq. (2.68)), varying the parameter α from 10^{-6} (where the MRCM behaves like the MMMFEM) to 10^6 (where the MRCM behaves like the MHM). For these studies, the domain is decomposed in 11×3 sub-domains of size $H = 1/3$, each containing 20×20 cells, so that $h = 1/60$. The $L^2(\Omega)$ errors are computed based on a reference fine grid solution of 220×60 grid cells. Figure 10 shows the behavior of the errors for pressure (top) and fluxes (bottom), alongside the (log-scaled) permeability field for a set of slices of the SPE10 model.

The first eye-catching conclusion that can be drawn from these results is that there is a range of alpha ($\alpha \in [1,100]$) values in which the errors for pressure and fluxes attain a minimum value. These errors are smaller than the errors of the MMMFEM-like and the MHM-like results, for all slices, using the standard discontinuous computation of β.

We have chosen slice number 36 to perform additional tests, in order to assess how the errors are affected by the choice of the Robin condition parameter and on the way the domain decomposition is performed. Figure 11 shows the error profiles obtained in this slice, for different computations of the Robin condition parameter. The results show that for the *Discontinuous* and *Harmonic* approaches we observe a similar behavior of the errors as we move from small values of α (MMMFEM-like solutions) to large values of this parameter (MHM-like solutions), with a small flux error improvement in the *Harmonic* approach for small values of α. For the *One-sided* and *Extreme* cases, distinct behaviors are observed, with no real improvement over

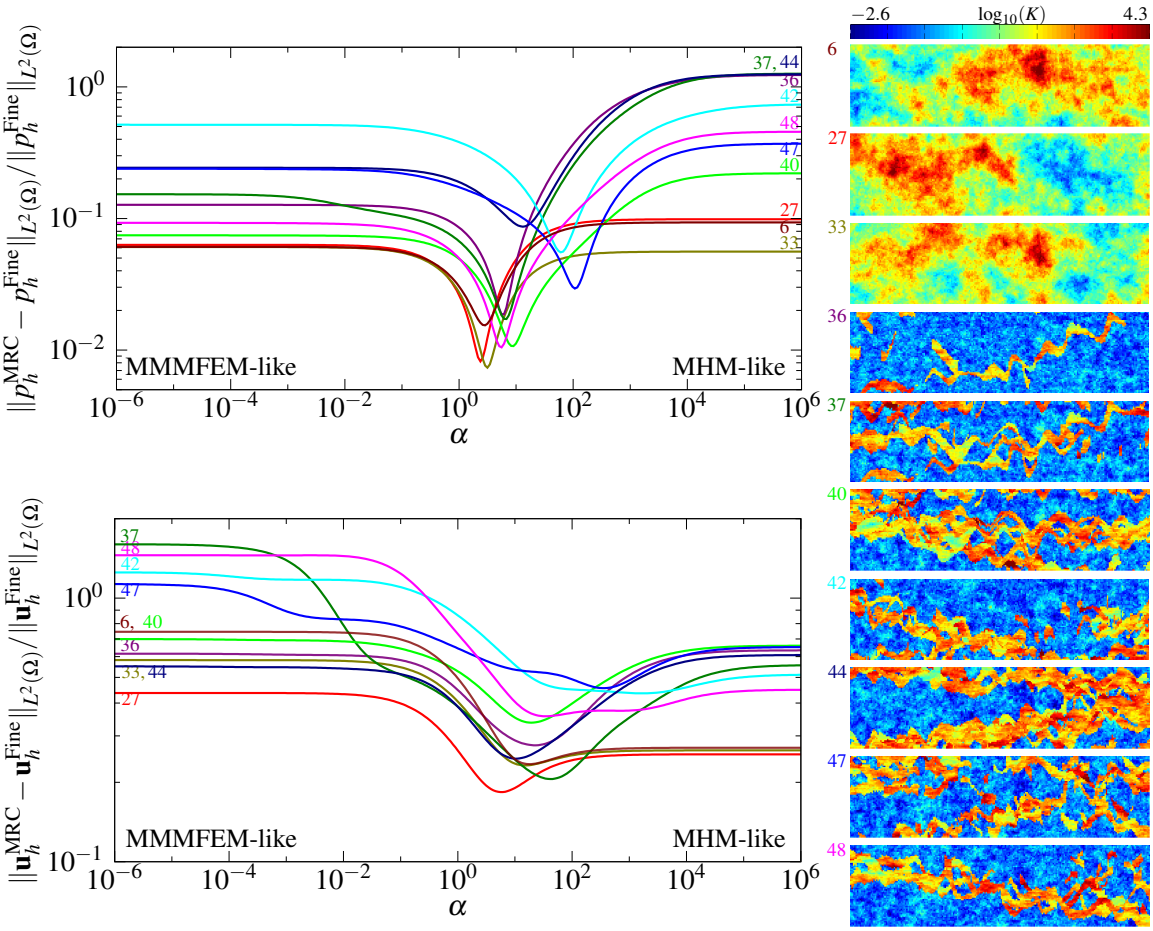

Source: Elaborated by the author.

Figure 10 – Relative $L^2(\Omega)$ errors for pressures (top) and fluxes (bottom), computed using the fine grid solution of SPE10 as a reference. Each curve shows the results of a different slice, depicted in the right-hand side. Note that the errors associated with the MRCM for intermediate values of α are considerably smaller than those associated with the MMMFEM and MHM.

previous choices. In the *One-sided* case, the minimum pressure error happens for a different α value, as compared to the α value leading to a minimum in the flux error. For the *Extreme* case, the error sensitivity to the variation of α parameter is less pronounced, with no significant error improvement. Nonetheless, these two cases illustrate the robustness of our formulation: the Robin condition parameters may be set in an arbitrary manner, with acceptable results produced by the MRCM formulation.

Another factor affecting the error profiles is the number of subdomains used to decompose the whole domain. The error profiles for different domain decompositions can be seen in figure 12, where pressure and flux erros for the 36th slice of SPE10 are shown. We consider subdivisions with 11×3 subdomains, yielding $H = 1/3$ and 20×20 fine grid cells inside each subdomain, 22×6 subdomains, with $H = 1/6$ and 10×10 fine grid cells per subdomain, and finally 44×12

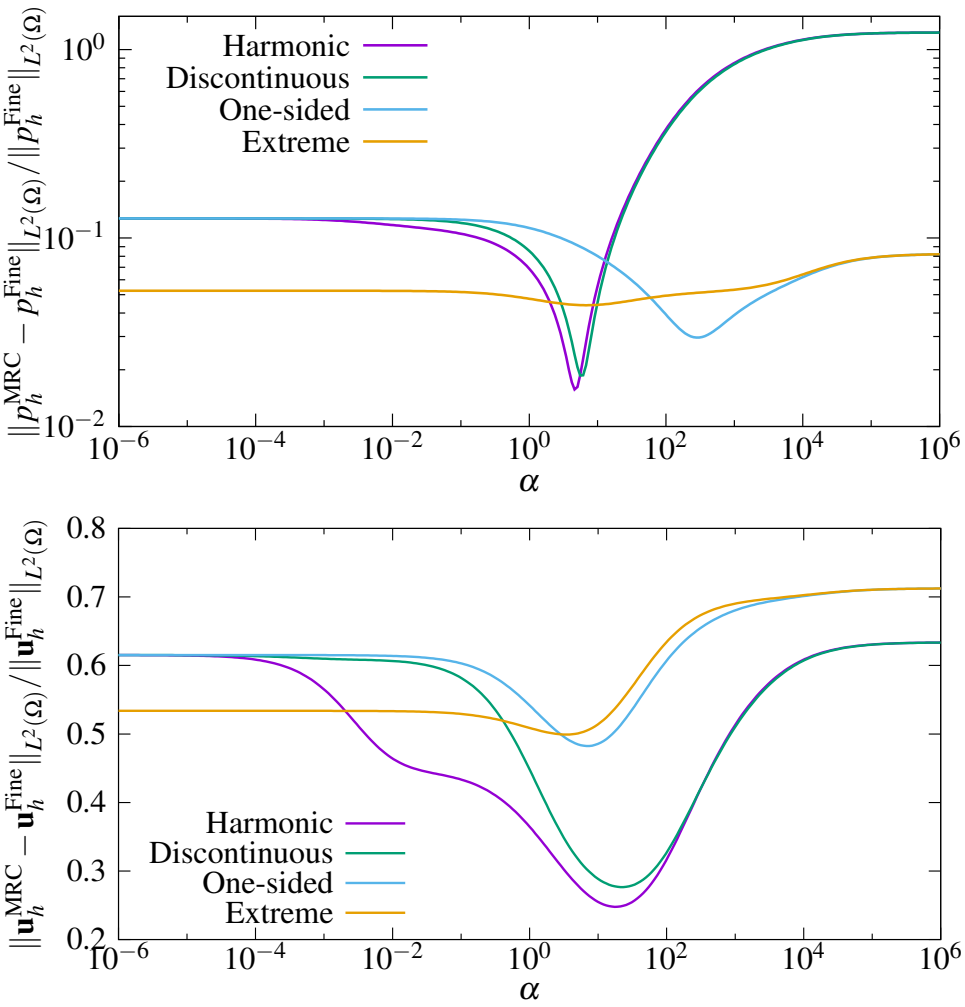

Source: Elaborated by the author.

Figure 11 – Relative pressure and flux error profiles for slice 36 as a function of α parameter, for different computations of the Robin condition parameter.

subdomains, with $H = 1/12$ and subdomains containing only 5×5 fine grid cells. The simulations were performed using the discontinuous computation of the Robin condition parameter. While the main trend is preserved throughout all simulated cases, one can easily see that the minimum for both pressure and flux is shifted towards the position $\alpha = 1$ by increasing the number of subdomains.

Following the ideas in (FRANCISCO *et al.*, 2014), we also test the introduction of an intermediate length scale $\overline{H}$ such that $h < \overline{H} < H$. While H still refers to the size of the subdomains, $\overline{H}$ is the size of a subdivision of each interface $\Gamma_{i,j}$ and defines a new partition $\mathscr{T}_{\overline{H}}$ of Γ. The piecewise polynomial spaces on $\mathscr{T}_{\overline{H}}$ are denoted by $\mathscr{P}_{\overline{H},k}$ and $\mathscr{U}_{\overline{H},k}$. Notice that Γ does not depend on $\overline{H}$, so that $\mathscr{P}_{\overline{H},k}$ is a refinement of $\mathscr{P}_{H,k}$ and $\mathscr{U}_{\overline{H},k}$ is a refinement of $\mathscr{U}_{H,k}$.

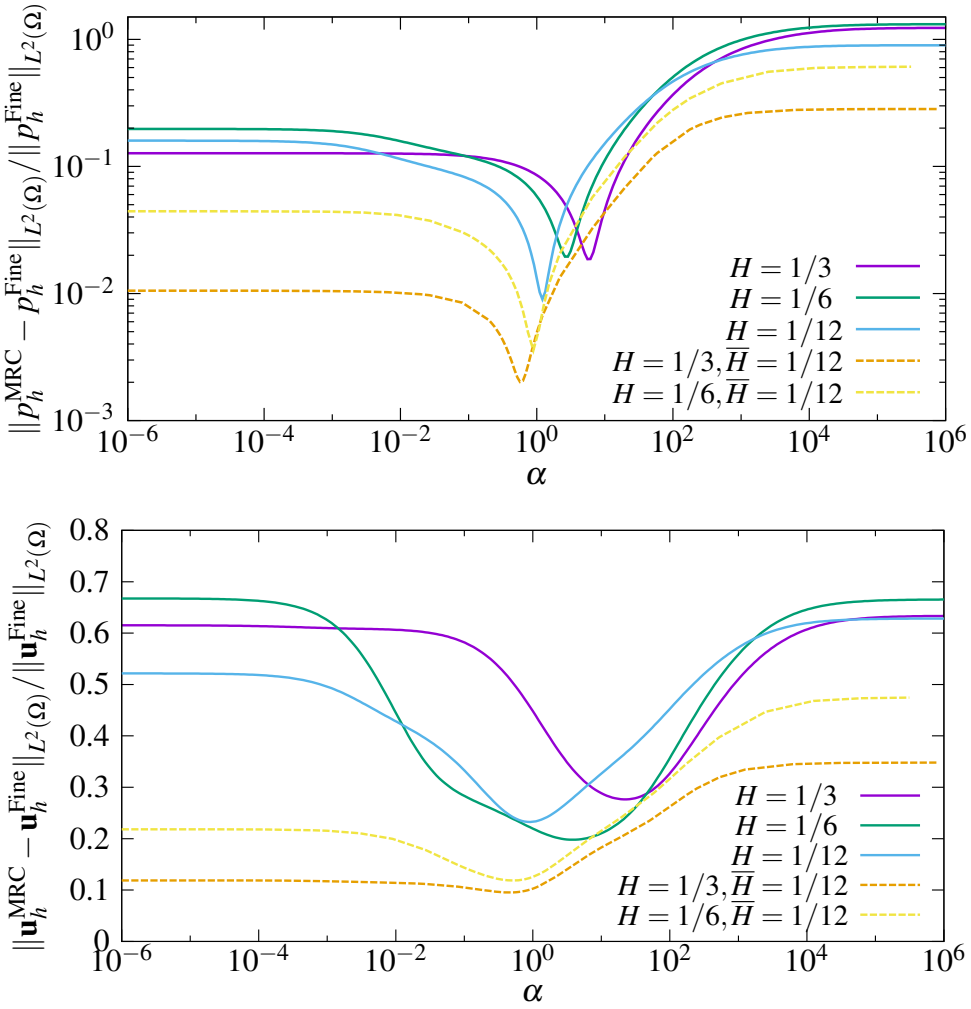

Source: Elaborated by the author.

Figure 12 – Relative pressure and flux error profiles for slice 36 as a function of α parameter, for different number of subdomains.

Results of two additional simulations with interface spaces $\mathscr{P}_{\overline{H},1}$ and $\mathscr{U}_{\overline{H},1}$ can be seen in figure 12 (in dashed lines). One is computed by setting $H = 1/3$ and $\overline{H} = 5h = H/4$ while the other is computed with $H = 1/6$ and $\overline{H} = 5h = H/2$. We remark on two of the main advantages resulting from the introduction of the intermediate length scale $\overline{H}$. First, pressure and flux errors are somewhat smaller as compared to the results obtained with the linear spaces $\mathscr{P}_{H,1}$ and $\mathscr{V}_{H,1}$. Second, and most importantly, the introduction of $\overline{H}$ scale alleviates the dependence of the minimum error location on the domain decomposition, as they are all near the value $\alpha = 1$.

We now focus on the results reported in figure 13, where one can see the error profiles for pressure and flux, for the computations performed with permeability field given by the 36th slice of the SPE10 field. We show details of the error distribution as inserts in this figure. These inserts

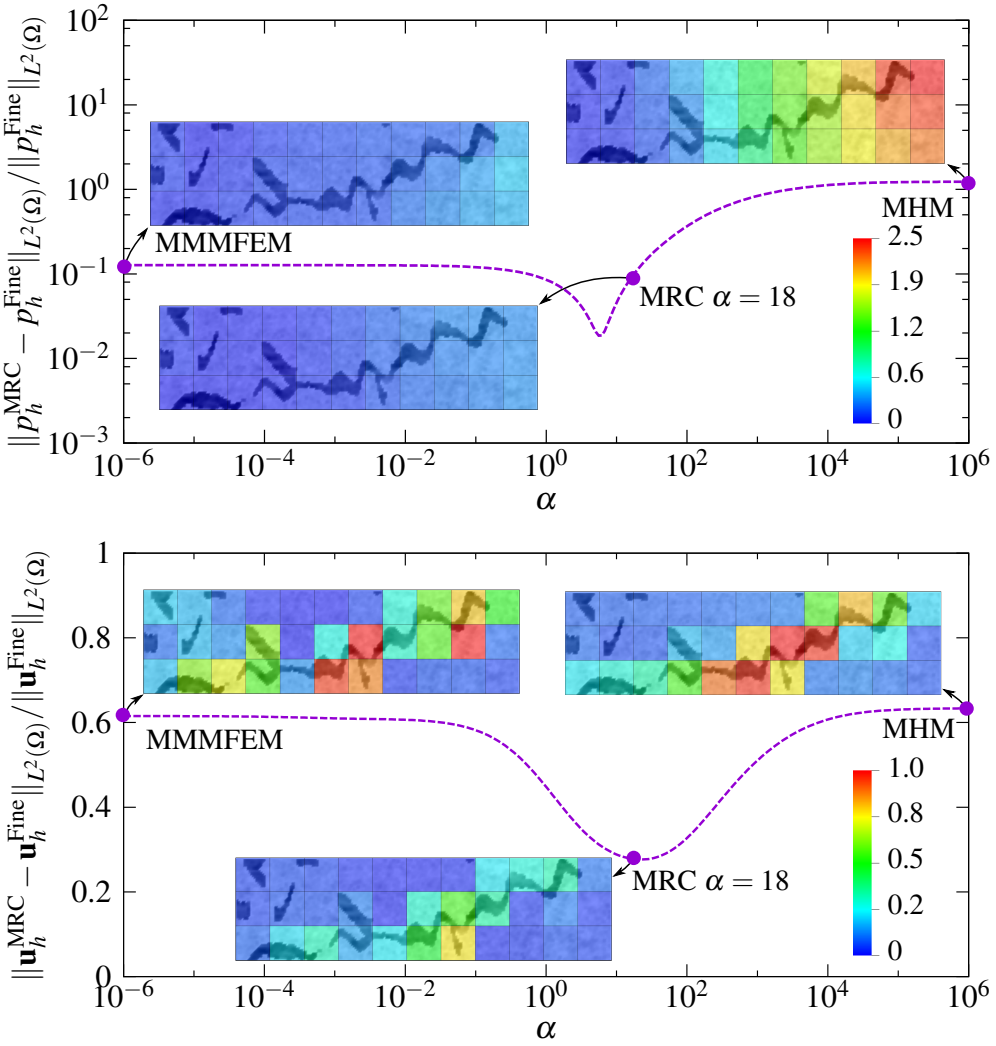

Source: Elaborated by the author.

Figure 13 – Relative pressure and flux error profiles for slice 36 as a function of α parameter. The inserts show the permeability field and the subdomains colored by the local norm $L^2(\Omega_i)$ for each subdomain Ω_i.

show the domain decomposition used (corresponding to $H = 1/3$) and the permeability field superimposed by the local errors, i.e., errors computed inside each domain Ω_i using a $L^2(\Omega_i)$ norm. We display the local errors for the MMMFEM and MHM methods, as well as the MRCM with a choice for α that minimizes the flux errors. For this selected slice of SPE10 and the chosen subdomain division ($H = 1/3$), the minimum flux happens around $\alpha = 18$, while the minimum pressure error is attained around $\alpha = 6$. Once in porous media flows minimizing flux errors is typically preferred over minimizing pressure errors, we show only detailed results for $\alpha = 18$. These results bring some insights about the error distribution in each method. Pressure errors are well-behaved, and small errors are obtained in all subdomains, for both MMMFEM and MRCM with small values of α. Large pressure errors are obtained for large α, including the result from the MHM method, with increasing pressure errors towards the fluid production (right) boundary. Flux errors are more insightful. One can easily see that for all methods, errors are concentrated around the channelized structures of the permeability field, with larger values attained for the MMMFEM and MHM methods. The choice $\alpha = 18$ brings the local flux errors down by a factor of at least 2, especially in the vicinity of the channelized structures.

We close this section with a study of the error for pressure and fluxes that result from distinct contrasts $K_{\max}/K_{\min}$ in the permeability field of slice number 36. We set this ratio from 10^5 until 10^9. The results displayed in figure 14 indicate robustness of the MRCM also in terms of this ratio. The errors for flux show only mild dependence on it, even for very heterogeneous formations.

2.4 Concluding remarks

We have introduced a new multiscale mixed finite element method, the Multiscale Robin Coupled method (MRCM), aiming at the accurate approximation of subsurface flows. The new method is based on a domain-decomposition procedure in which the subdomains are coupled by the Robin boundary condition. There appear two independent spaces on the skeleton of the decomposition, corresponding to interface pressures and fluxes, that can be chosen with great flexibility to accommodate local features of the underlying permeability fields. Initially the well-posedness of the proposed domain decomposition procedure is established and it is shown that it generalizes an existing domain decomposition procedure based on the Robin boundary condition. In fact, it allows one to interpret the existing procedure as a Two-Lagrange-Multiplier method. The multiscale property of the proposed domain decomposition method is discussed and its relation with existing multiscale mixed methods is pointed out.

Numerical experiments are presented and discussed. Initially we compare the numerical solutions of the MRCM to existing ones. We show that as the parameter in the Robin condition of our method is set to extreme values we recover results from two known methods (MMMFEM and MHM) as well as their convergence rates. Then we focus on the simulation of realistic flow

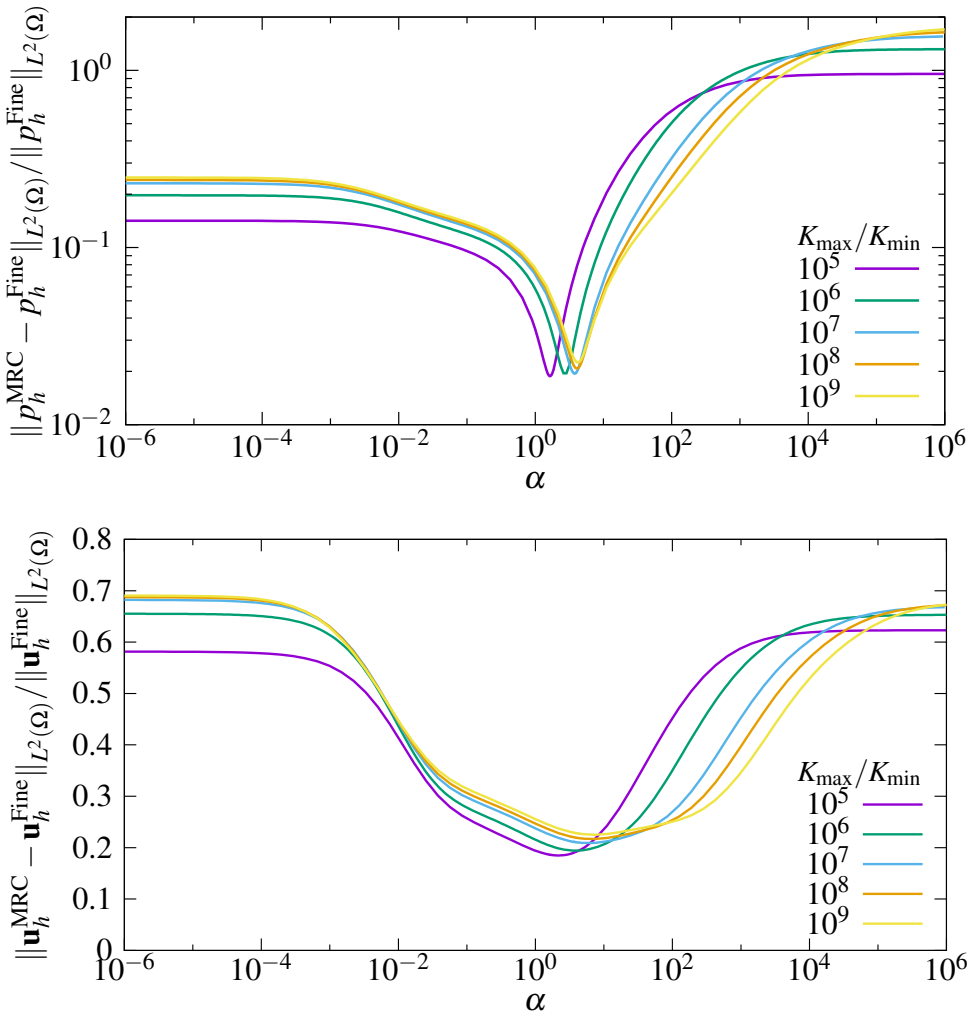

Source: Elaborated by the author.

Figure 14 – Relative pressure and flux error profiles for slice 36 as a function of α parameter, or different permeability contrast $K_{\max}/K_{\min}$.

in high-contrast channelized porous formations by considering several layers of the classical SPE10 permeability field. Two aspects of the MRCM are considered. First we show that for a range of values of the Robin condition parameter our method provides better approximations for pressure and velocity than those computed with the new procedure with extreme values of the Robin condition parameter. This is an indication that our method has the potential to produce more accurate velocity fields in the presence of rough, realistic permeability fields of petroleum reservoirs. Moreover, by selecting different expressions for the calculation of the Robin condition parameter, we indicate the robustness of the MRCM formulation.

CHAPTER

3

INFORMED SPACES FOR THE MULTISCALE ROBIN COUPLED METHOD IN RESERVOIR SIMULATION

The Multiscale Robin Coupled Method (MRCM) is a recent multiscale numerical method based on a non-overlapping domain decomposition procedure. One of its hallmarks is that the MRCM allows for the independent definition of interface spaces for pressure and flux over the skeleton of the decomposition. The accuracy of the MRCM depends on the choice of these interface spaces, as well as on an algorithmic parameter β in the Robin interface conditions imposed at the subdomain boundaries. This work presents an extensive numerical assessment of the MRCM in both of these aspects. Two types of interface spaces are implemented: usual piecewise polynomial spaces and informed spaces, the latter obtained from sets of snapshots by dimensionality reduction. Different distributions of the unknowns between pressure and flux are explored. Two non- dimensionalizations of β are tested. The assessment is conducted on realistic, high contrast, channelized permeability fields from a SPE benchmark database. The results show that β, suitably non-dimensionalized, can be fixed to unity to avoid any indeterminacy in the method. Further, with both types of spaces it is observed that a balanced distribution of the interface unknowns between pressure and flux renders the MRCM quite attractive both in accuracy and in computational cost, competitive with other multiscale methods from the literature.

3.1 Introduction

Multiscale domain decomposition methods have received considerable attention from the scientific community due to their potential to solve efficiently elliptic problems with rapidly varying coefficients in parallel multi-core computers. This class of methods approximates the exact solution by solving uncoupled local problems on non-overlapping subdomains, along with

one *global* problem (or *interface* problem) associated with the coupling between subdomains through their boundaries. In fact, consistency conditions require the imposition of some form of continuity of fluxes and of pressures at interfaces between neighbor subdomains. Different methods have been developed based on distinct approaches to address the continuity issue. We mention, for instance, the Multiscale Mortar Mixed Finite Element Method (MMMFEM) (ARBOGAST *et al.*, 2007) and the Multiscale Hybrid-Mixed Method (MHM) (ARAYA *et al.*, 2013; HARDER; PAREDES; VALENTIN, 2015), as some well known procedures of this type. In the MMMFEM, the pressure continuity is weakly satisfied in the fine-grid scale (the scale of the local grid of each subdomain, usually denoted by h), while normal flux continuity is ensured in a much larger scale ($H \gg h$), usually associated with the size of the subdomains. Conversely in the MHM, continuity of the normal fluxes is satisfied at the fine-grid h scale, while pressure continuity is only imposed at the larger H scale.

The design of accurate multiscale domain decomposition methods for channelized, high-contrast porous media, remains as an important challenge because in typical problems posed by the oil industry existing multiscale methods may produce inaccurate numerical approximations (GUIRALDELLO *et al.*, 2018b).

In our search for more accurate procedures, here we investigate an improved version of the recently proposed Multiscale Robin Coupled method (MRCM) (GUIRALDELLO *et al.*, 2018b). This method is based on the domain decomposition of Douglas et al. (DOUGLAS *et al.*, 1993) and on the Multiscale Mixed Method (MuMM) of Francisco et al. (FRANCISCO *et al.*, 2014), and ensures weak continuity of both normal fluxes and pressures through the imposition of Robin-type boundary conditions, namely

$$-\beta_i \mathbf{u}^i \cdot \check{\mathbf{n}}^i + p^i = \beta_j \mathbf{u}^j \cdot \check{\mathbf{n}}^j + p^j, \tag{3.1}$$

at the interface Γ_{ij} between subdomains (identified by i and j), usually in a scale that is larger than the fine-grid scale. In Eq. (3.1) p^i and $\mathbf{u}^i$ are pressure and velocity of subdomain i at the interface, and $\check{\mathbf{n}}^i = -\check{\mathbf{n}}^j$ is the outwards unit normal. The MRCM can be seen as a generalization of the above mentioned methods depending on the parameter β_i: the MMMFEM (respectively, the MHM) is recovered as $\beta_i \to 0$ (respectively, $\beta_i \to +\infty$) for all i.

The accuracy and cost of multiscale domain decomposition methods are mainly determined by the choice of the *interface* space, i.e., the space on which the global problem is posed. This space consists of functions defined on the collection of interfaces between subdomains, or *skeleton* of the partition, $\Gamma = \cup_{i \neq j} \Gamma_{ij}$, where Γ_{ij} denotes the interface between nearest-neighbor subdomains. For the MMMFEM the interface space is a **pressure** space $\mathscr{P}_H$, while for the MHM it is a **flux** space $\mathscr{U}_H$. A salient feature of the MRCM, with β_i different from 0 and $+\infty$, is that its global interface problem is posed on the direct product $\mathscr{P}_H \times \mathscr{U}_H$ of a pressure space and a flux space, both defined on the skeleton and which can be chosen independently. This allows us to explore an interesting question: Assume that one decides to allocate k unknowns at each

interface Γ_{ij} of the skeleton. How does their distribution between pressure unknowns and flux unknowns affect the accuracy and cost-effectiveness of the method?

Of course the approximation capabilities of the interface space depends not just on its dimension (i.e., number of unknowns) but also on the functions it consists of. The first reported implementations of MMMFEM, MHM and MRCM adopted piecewise polynomial spaces over the interfaces, which are the simplest to code and analyze. It is however accepted nowadays that polynomial spaces are not optimal for highly heterogeneous problems, and different kinds of problem-dependent approximation spaces (*informed spaces*, in short) have been proposed for multiscale finite element (BABUSKA; OSBORN, 1983; CHUNG; EFENDIEV; HOU, 2016) and finite volume (JENNY; LEE; TCHELEPI, 2003) methods. The latter was extended to several nonlinear complex cases, including the compressible and compositional cases as well as fractures (LUNATI; JENNY, 2006; LEE; ZHOU; TCHELEPI, 2009; HAJIBEYGI; TCHELEPI, ; BOSMA *et al.*, 2017). The combination of informed spaces with the MMMFEM has recently been studied by Chung et al. (CHUNG; FU; YANG, 2016), while it remains unexplored for the MHM. In line with this trend, this work explores a strategy for building informed spaces at the interfaces for the MRCM. In this way, we explore the question of optimal allocation of unknowns between pressure and flux not just with polynomials but also with spaces that are more suitable for highly heterogeneous media. Moreover, once the MHM is a particular case of the MRCM, a first study of combining the MHM with informed spaces is also produced.

Our numerical results indicate that, typically, the optimal accuracy is attained somewhere in between the MMMFEM (all unknowns for pressure) and the MHM (all unknowns for flux). In other words, the solution of minimal error is produced by the MRCM for some specific choice of its algorithmic parameters. Further, it is shown that through appropriate dimensional analysis it is possible to fix all parameters of the MRCM automatically, resulting in a fully-determined method that is competitive with known ones. In particular, it is recommended that the number of unknowns for interface pressure is equal to (or slightly smaller than) the number of unknowns for interface flux. In this way we arrive at a method that is effective for all layers in the SPE10 database. The construction of the informed spaces needs however to be improved, since the method exhibits comparable overall accuracy with polynomial and informed interface spaces. There exist multiscale iterative methods, that include global information on the multiscale basis functions and show improvements in terms of accuracy (see e.g. (CHUNG; EFENDIEV; LEUNG, 2018; HAJIBEYGI *et al.*, 2008)). The development and dicussion of such procedures for the MRCM is out of the scope of this article and is left for future work. However, we remark that informed interface spaces do show improved approximation of fluxes in regions of the domain with high-contrast formations.

The plan of this article is as follows: The MRCM is briefly recalled in Section 2, adopting a fine grid discretization consisting of lowest order Raviart-Thomas finite elements RT_0 and general spaces $\mathscr{P}_H$ and $\mathscr{U}_H$ at the skeleton Γ. The reader should recall that the RT_0 elements are

equivalent to the popular cell-centered finite volume method with two-point flux approximation. The strategy adopted for building the interface spaces is described in Section 3. It is similar to strategies proposed by other authors, such as the empirical interpolation technique used by Calo et al. (CALO *et al.*, 2014; CALO *et al.*, 2016) in the context of multiscale finite elements. With these elements at hand, Section 4 is then devoted to numerical experiments addressing the questions of selection of optimal algorithmic parameters and of optimal allocation of interface unknowns between pressures and fluxes. The geological data used in the experiments are two-dimensional slices of the SPE10 benchmark database, with different degrees of channelization.

3.2 The Multiscale Robin Coupled Method

3.2.1 Discrete variational formulation

Let us consider a fine grid $\mathscr{T}_h$, i.e., a subdivision of the domain $\Omega \subset \mathbb{R}^d$ consisting of d-dimensional cuboids of size h, and a decomposition of Ω in subdomains $\{\Omega_i\}_{i=1,\dots,m}$, of characteristic size $H \gg h$, such that each element $K \in \mathscr{T}_h$ belongs to one and only one of the subdomains. Moreover, let Γ be the skeleton of the domain decomposition, as the union of all interfaces $\Gamma_{i,j} = \overline{\Omega}_i \cap \overline{\Omega}_j$. The discrete variational formulation of the MRCM is written over the discrete lowest order Raviart-Thomas spaces for velocity and pressure, defined as

$$\begin{aligned}
\mathbf{V}_h^i = \{ & \mathbf{v} \in H(\mathrm{div}, \Omega_i) \ , \ v_j(\mathbf{x})|_K = p_{j1}(x_1) p_{j2}(x_2) \dots \ , \forall K \in \mathscr{T}_h^i \ , \\
& \text{with } p_{jk} \in \mathbb{P}_1 \text{ if } j = k \ , p_{jk} \in \mathbb{P}_0 \text{ if } j \neq k \ \} \ , \qquad (3.2) \\
\mathbf{V}_{hy}^i = \{ & \mathbf{v} \in \mathbf{V}_h^i \ , \ \mathbf{v} \cdot \check{\mathbf{n}} = y \ \text{ on } \ \partial\Omega_i \cap \partial\Omega_u \} \ , \qquad (3.3) \\
Q_h^i = \{ & q \in L^2(\Omega_i) \ , \ q(\mathbf{x})|_K \in \mathbb{P}_0 \} \ , \qquad (3.4)
\end{aligned}$$

with y being a piecewise constant function defined on the edges of $\partial\Omega_u$ and $\mathbb{P}_k$ the usual space of polynomials of degree up to k.

We denote by $\mathscr{E}_h$ the set of all edges/faces of $\mathscr{T}_h$ in the skeleton Γ. A unique normal $\check{\mathbf{n}}$ is defined as

$$\check{\mathbf{n}}(e) \doteq \text{exterior normal to } \partial\Omega_{\min\{i,j\}} \ , \ \text{ if } e \in \Gamma_{i,j} \qquad (3.5)$$

for every e in $\mathscr{E}_h$. The spaces for pressures and fluxes at subdomain interfaces that will be considered here consist of functions that are constant on each e of $\mathscr{E}_h$, i.e., they are subsets of

$$F_h(\mathscr{E}_h) = \{ f : \mathscr{E}_h \to \mathbb{R} \mid f|_e \in \mathbb{P}_0 \ , \ \forall e \in \mathscr{E}_h \} \ . \qquad (3.6)$$

To finally state the variational formulation of the MRCM, consider low-dimensional subspaces $\mathscr{U}_H$ and $\mathscr{P}_H$ of $F_h(\mathscr{E}_h)$. The MRCM consists in finding $(\mathbf{u}_h^i, p_h^i) \in \mathbf{V}_{hz}^i \times Q_h^i$, for

$i = 1, \ldots, m$, and $(U_H, P_H) \in \mathscr{U}_H \times \mathscr{P}_H$ such that

$$\begin{aligned} &\left(K^{-1}\mathbf{u}_h^i, \mathbf{v}\right)_{\Omega_i} - \left(p_h^i, \nabla\cdot\mathbf{v}\right)_{\Omega_i} \\ &+ \left(P_H - \beta_i U_H \check{\mathbf{n}}^i\cdot\check{\mathbf{n}} + \beta_i \mathbf{u}_h^i\cdot\check{\mathbf{n}}^i, \mathbf{v}\cdot\check{\mathbf{n}}^i\right)_{\partial\Omega_i\cap\Gamma} = -\left(g, \mathbf{v}\cdot\check{\mathbf{n}}^i\right)_{\partial\Omega_i\cap\partial\Omega_p} \end{aligned} \tag{3.7}$$

$$\left(q, \nabla\cdot\mathbf{u}_h^i\right)_{\Omega_i} = (f,q)_{\Omega_i} \tag{3.8}$$

$$\sum_{i=1}^{m}\left(\mathbf{u}_h^i\cdot\check{\mathbf{n}}^i, M_H\right)_{\partial\Omega_i\cap\Gamma} = 0 \tag{3.9}$$

$$\sum_{i=1}^{m}\left(\beta_i\left(\mathbf{u}_h^i\cdot\check{\mathbf{n}}^i - U_H\check{\mathbf{n}}^i\cdot\check{\mathbf{n}}\right), V_H\check{\mathbf{n}}^i\cdot\check{\mathbf{n}}\right)_{\partial\Omega_i\cap\Gamma} = 0 \tag{3.10}$$

hold for all $(\mathbf{v}, q) \in \mathbf{V}_{h0}^i \times Q_h^i$, $\forall i = 1, \ldots, m$, for all $M_H \in \mathscr{P}_H$ and for all $V_H \in \mathscr{U}_H$. Above, the symbol $(\cdot,\cdot)_A$ denotes the scalar product of $L^2(A)$.

The existence and uniqueness of the solution of this variational formulation is proved in (GUIRALDELLO *et al.*, 2018b). It only requires that

$$\sum_{i=1}^{m}(\beta_i V_H, V_H) > 0\,, \quad \forall V_H \in \mathscr{U}_H\,, \quad V_H \neq 0\,. \tag{3.11}$$

This condition is easy to check, since

$$\sum_{i=1}^{m}(\beta_i V_H, V_H) = \sum_{i=1}^{m}\int_{\partial\Omega_i\cap\Gamma}\beta_i V_H^2 = \int_\Gamma\left(\beta^+ + \beta^-\right)V_H^2\,, \tag{3.12}$$

where the plus and minus superscript refer to the two sides of Γ. If the functions β_i, assumed non-negative, are not identically zero *on both sides of* Γ and *on the whole support* of some V_H, then the solution is unique. In the extreme case that all β_i's are identically zero, then $\mathscr{U}_H$ must be zero for the problem to be well-posed. This reduces the formulation to the MMMFEM.

Remark 4. Actually, the variational formulation also holds without the conditions $\mathscr{P}_H \subset F_h(\mathscr{E}_h)$, $\mathscr{U}_H \subset F_h(\mathscr{E}_h)$. The necessary and sufficient conditions are, in fact, (3.12) together with the same inf-sup compatibility of the MMMFEM, namely that for each nonzero $M_H \in \mathscr{P}_H$ there exists i $(1 \leq i \leq m)$ such that

$$\sup_{\mathbf{v}\in\mathbf{V}_{h0}^i}\left(\mathbf{v}\cdot\check{\mathbf{n}}^i, M_H\right)_{\partial\Omega_i\cap\Gamma} > 0 \tag{3.13}$$

For the case of the RT_0 velocity approximation, this is equivalent to

$$\sup_{A_h\in F_h(\mathscr{E}_h)}(A_h, M_H)_\Gamma > 0\,,$$

which is automatically satisfied if $\mathscr{P}_H \subset F_h(\mathscr{E}_h)$. Otherwise condition (3.13) must be checked independently.

The implementation performed here strictly follows the one presented in (GUIRALDELLO *et al.*, 2018b), sharing similarities with the works of Ganis & Yotov (GANIS; YOTOV, 2009)

and Francisco et al. (FRANCISCO *et al.*, 2014). Note that the linear system associated with Eqs. (3.7)-(3.10) is of a size comparable to that of the original, undecomposed problem. However, the solution to the problem written in terms of Eqs. (3.7)-(3.10) can be, locally, expressed in terms of linear combinations of multiscale basis functions. The construction of such basis functions is naturally parallelizable.

By assuming that the interface variables (U_H, P_H) are known, one can uncouple Eqs. (3.7)-(3.8) from Eqs. (3.9)-(3.10). The first set of equations will produce local problems for the computation of the multiscale basis functions. The set of multiscale basis functions is then used on Eqs. (3.9)-(3.10) to generate a global linear system to be solved for the interface variables, coupling the local solutions while ensuring the compatibility conditions between subdomains. The final solution is then obtained by linear combination of the previously computed multiscale basis functions. The interested reader is referred to Guiraldello et al. (GUIRALDELLO *et al.*, 2018b) for a thorough explanation of the implementation of this numerical scheme.

3.3 Interface spaces: Polynomial and informed

The original implementation of the MRCM used piecewise polynomial spaces over the skeleton Γ of the domain decomposition, both for pressure $\mathscr{P}_H$ and flux $\mathscr{U}_H$. More precisely, we have considered spaces made up of the elementwise constant fine grid representation of polynomials over the interface elements

$$\mathscr{U}_H = \mathscr{U}_H^{\text{pol},\ell_U+1} = \{V_H,\, V_H|_e = \Pi_0(q), q \in \mathbb{P}_{\ell_U}(e),\, e \in \mathscr{T}_H\}, \tag{3.14}$$

$$\mathscr{P}_H = \mathscr{P}_H^{\text{pol},\ell_P+1} = \{M_H,\, M_H|_e = \Pi_0(q), q \in \mathbb{P}_{\ell_P}(e),\, e \in \mathscr{T}_H\}, \tag{3.15}$$

where $\mathbb{P}_k,\ k = \ell_U$ or ℓ_P, is the space of polynomials of degree $\leq k$ and Π_0 is the L^2–projection of a function of $\mathbb{P}_k(e)$ onto the space $F_h(e),\ e \in \mathscr{T}_H$. The superscript added to the symbol for each space contains the class of functions adopted ("pol" for polynomials, "inf" for informed) followed by the number of degrees of freedom on each edge of $\mathscr{T}_H$. Notice that $\mathscr{U}_H$ and $\mathscr{P}_H$ are defined independently at each edge (face in 3D), with no continuity at corner points.

One alternative to polynomial spaces is, as previously mentioned, informed spaces, whose construction is a two-step process: (i) construction of the so called *snapshot space* by solving local problems on regions containing the interfaces $\Gamma_{i,j}$ of the domain decomposition (i.e., oversampling) and considering some parameterisation (for example, on the boundary conditions of these local problems) and (ii) selection of the final *informed space* by applying a dimensionality reduction technique (SVD, POD, etc.) to end up with a coarsened interface problem of affordable size and whose solution appoximates well the fine grid solution.

By oversampling, we associate to each subdomain Ω_k a new region ω_k that contains it. Figure 15 shows a few examples of the oversampling regions ω_k for an interior subdomain and for a subdomain that intersects the boundary of Ω. This way, the ω_k's clearly contain the whole

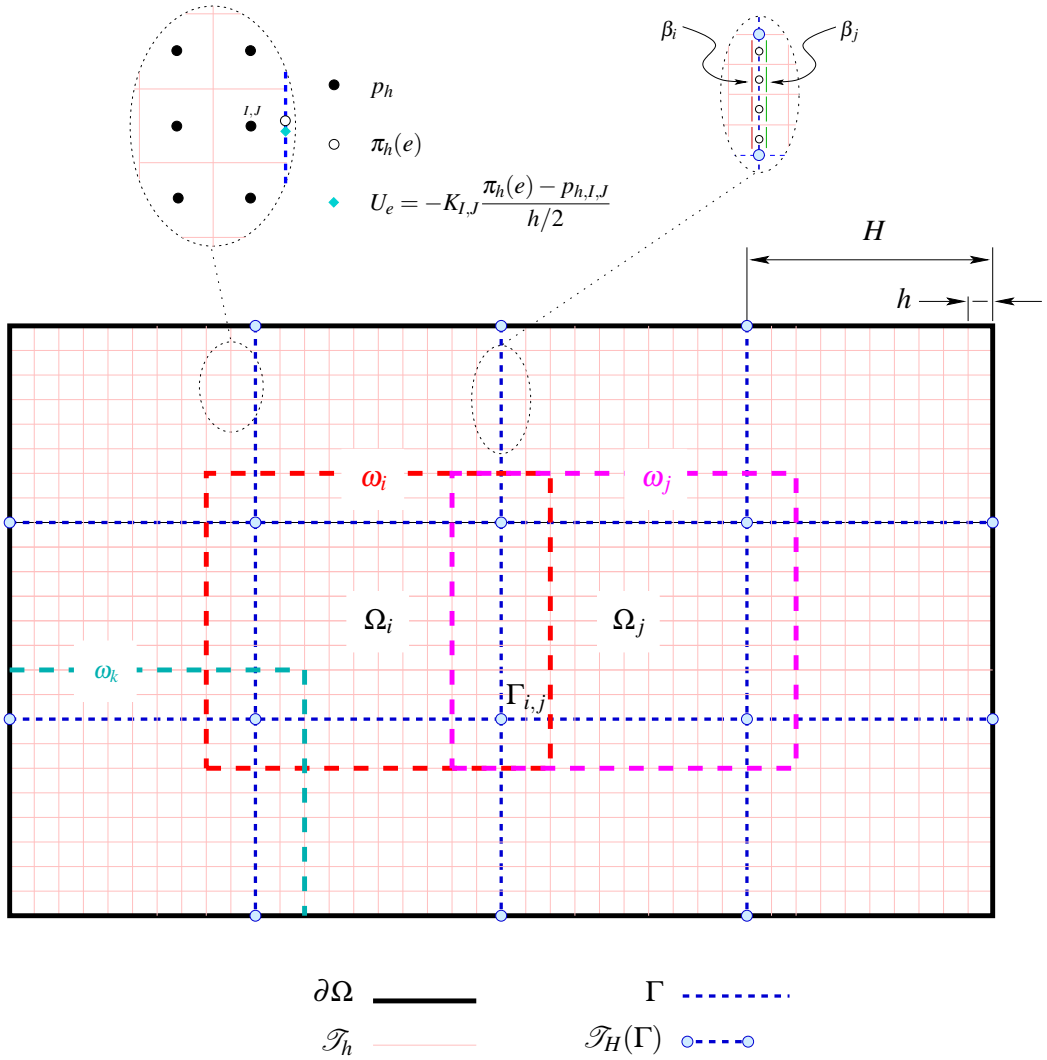

Source: Elaborated by the author.

Figure 15 – Computational domain decomposition and oversampling regions.

of $\partial\Omega_k \cap \Gamma$. This decomposition essentially follows the original domain decomposition of Ω by slightly augmenting the size of the local problems by just a few layers of fine grid cells that are now shared by several processes. This is expected to be efficient in terms of message passing and avoids dealing with more than one decomposition of Ω. Although in the linear case this would not be a serious drawback since this stage of the computation is done *offline*, in the non-linear case periodic recomputation of the basis functions is needed and switching dynamically between very distinct domain decompositions would lead to an undesirable computational burden.

Consider interface $\Gamma_{i,j}$ and corresponding subdomains ω_k, $k = i, j$. Their boundaries are formed by a collection of fine grid faces $e_m \in \mathscr{T}_h$, $m = 1, 2, \ldots, N_k$. In order to build the snapshot space for interface $\Gamma_{i,j}$ we solve N_K local Darcy problems on each oversampling region

ω_k ($k = i, j$), i.e.,

$$\begin{array}{rcll} \mathbf{u}_h^{k,m} & = & -K\nabla p_h^{k,m} & \text{in } \omega_k \\ \nabla \cdot \mathbf{u}_h^{k,m} & = & C_{k,m} & \text{in } \omega_k \\ \mathscr{B}(\mathbf{u}_h^{k,m}, p_h^{k,m}) & = & \delta_m(x) & \text{on } \partial\omega_k \end{array} \tag{3.16}$$

The function $\delta_m(x)$ takes the value 1 if $x \in e_m$ and 0 otherwise. In (3.16), $\mathscr{B}$ is a boundary operator which enforces either pressure boundary conditions on $\partial\omega_k$, i.e.,

$$\mathscr{B}(\mathbf{u}_h^{k,m}, p_h^{k,m}) = p_h^{k,m} \tag{3.17}$$

in which case the source term $C_{k,m}$ is identically equal to zero, or flux boundary conditions on $\partial\omega_k$, i.e.,

$$\mathscr{B}(\mathbf{u}_h^{k,m}, p_h^{k,m}) = \mathbf{u}_h^{k,m} \cdot \check{\mathbf{n}}_{\partial\omega_k} \tag{3.18}$$

and the source term $C_{k,m}$ satifies the compatibility condition

$$\int_{\omega_k} C_{k,m} = \int_{\partial\omega_k} \delta_m \, . \tag{3.19}$$

After solving these problems, we retrieve the corresponding fluxes through the faces $e \in \Gamma_{ij}$ as

$$U_e^{k,m} = \mathbf{u}_h^{k,m}(e) \cdot \check{\mathbf{n}}(e) \, . \tag{3.20}$$

We also retrieve the corresponding pressure at Γ_{ij}, but since for the RT_0 element the pressure nodes are located at the center of the computational cells, face pressure values must be recovered by using Darcy's law. This amounts to compute a face pressure at each fine grid cell that intersects the boundary $\Gamma_{i,j}$. For instance, for an east boundary and fine grid cell I, J (see Figure 15), we obtain the face pressure $\pi_h^{k,m}(e)$ by solving

$$U_e^{k,m} = -K_{I,J} \frac{\pi_h^{k,m}(e) - p_{h,I,J}^{k,m}}{h/2} \, . \tag{3.21}$$

In this way we end up, for each $\Gamma_{i,j}$, for each $k = i$ or j, and for each $m = 1, \ldots, N_k$, with two column arrays $\underline{\tilde{U}}^{k,m}$ and $\underline{\tilde{P}}^{k,m}$, each of dimension M_{ij} (the number of fine grid faces in $\Gamma_{i,j}$), whose components are $U_e^{k,m}$ and $\pi_h^{k,m}(e)$, respectively. We define new column arrays denoted by $\underline{U}^{k,m}$ and $\underline{P}^{k,m}$ by substracting the constant component of $\underline{\tilde{U}}^{k,m}$ and $\underline{\tilde{P}}^{k,m}$ which are finally used to build the snapshot matrices

$$\mathbb{A}_U^{\Gamma_{ij}} = \left[\underline{U}^{i,1}, \ldots, \underline{U}^{i,N_i}, \underline{U}^{j,1}, \ldots, \underline{U}^{j,N_j}\right]$$

$$\mathbb{A}_P^{\Gamma_{ij}} = \left[\underline{P}^{i,1}, \ldots, \underline{P}^{i,N_i}, \underline{P}^{j,1}, \ldots, \underline{P}^{j,N_j}\right]$$

The next step is to perform the SVD decomposition on the two matrices above. The SVD decomposition of a given matrix $\mathbb{A} \in \mathbb{R}^{m \times n}$ reads

$$\mathbb{A} = \mathbb{X}\Sigma\mathbb{Y}^T$$

where $\mathbb{X} \in \mathbb{R}^{m\times m}$ and $\mathbb{Y} \in \mathbb{R}^{n\times n}$ are orthogonal matrices and $\Sigma \in \mathbb{R}^{m\times n}$ is a diagonal matrix given by

$$\Sigma = \text{diag}(\sigma_1, .., \sigma_q, 0, .., 0) \tag{3.22}$$

where $\sigma_1 \geq \sigma_2 \geq ... \geq \sigma_q > 0$ are the singular values of the decomposition and q is the rank of matrix $\mathbb{A}$. This procedure is executed on both $\mathbb{A}_U^{\Gamma_{ij}}$ and $\mathbb{A}_P^{\Gamma_{ij}}$.

Finally, the informed space $\mathscr{U}_H^{\text{inf},k}$ (respectively, $\mathscr{P}_H^{\text{inf},k}$) is defined locally on each $\Gamma_{i,j}$ as the space of linear combinations of the first $k-1$ right singular vectors of $\mathbb{A}_U^{\Gamma_{ij}}$ (respectively, $\mathbb{A}_P^{\Gamma_{ij}}$) augmented with the constant function on the corresponding interface.

Two comments are in order for the procedure just described. First, the number of local problems of type (3.16) to be solved can be reduced significantly by adopting a different strategy to parameterize the solution, for instance, by grouping together several fine grid faces on $\partial\omega$ on which some specified boundary conditions can be applied. Also randomly sampling these fine grid faces is a possibility (CALO *et al.*, 2016). Second, in the proposed approach, the solutions of the local problems are considered all equally probable prior to computing the SVD decomposition. However, some strategy could be devised to discard solutions of small norm on the interface. These topics will be the subject of future studies.

3.4 Numerical experiments

We have performed a series of numerical experiments in a quarter of a 5-spot geometry in a rectangular 2D region with dimensions $[0, 11/3] \times [0, 1]$. We consider no-flow boundary conditions with an injection (production) well positioned at the top left (bottom right) corner of the computational region. For the absolute permeability we take distinct layers of the SPE10 project (http://www.spe.org/web/csp) (CHRISTIE; BLUNT, 2001). These are realistic, very heterogeneous fields typical of petroleum reservoirs.

The interface spaces are either polynomials or informed spaces obtained with oversampling of size h. We consider the flux boundary operator given by Eq. (3.18) and the average pressure is set to zero. The results are given in the form of graphs that display the relative $L^2(\Omega)$ error norm (computed with respect to the fine grid solution) for the pressure and flux variables. We first investigate the adequate characteristic length scale for the adimensionalization of the numerial parameter β, and then explore the accuracy of the MRCM compared with the MMMFEM and the MHM with same number of interface unknowns. Finally, we perform an exhaustive comparison study covering all the SPE10 layers.

3.4.1 The characteristic length scale

Dimensional analysis indicates that the Robin coefficient of subdomain i can be written in terms of a dimensionless α as

$$\beta_i(\mathbf{x}) = \frac{\alpha(\mathbf{x})L}{K(\mathbf{x})}.$$

In (GUIRALDELLO *et al.*, 2018b), we set $L = h$, h being the mesh size. Here we show that a better choice is $L = H$, where H is the size of $\Gamma_{ij} = \partial\Omega_i \cap \partial\Omega_j$. To see this we fix the decomposition of the computational region and perform a mesh refinement study inside subdomains. Although α could in general depend on $\mathbf{x}$, we adopt a *fixed* value for it that holds for all $\mathbf{x}$ and all i. For the choice $L = H$ the value of α for which the MRCM yields minimum error remains essentially unaltered under the refinement study. In order to illustrate our findings, we consider layer 36 (that contains a high contrast channel) divided into 22×6 rectangular subdomains with size $H \times H$, being $H = 1/6$. For this domain decomposition we consider a sequence of mesh refinements inside each subdomain starting with 10×10 (mesh size $h = H/10$) and increase each direction by a factor of 2 until we reach $h = H/80$. For the interface spaces we consider here polynomials of degree one, i.e., $\mathscr{U}_H = \mathscr{U}_H^{\text{pol},2}$ and $\mathscr{P}_H = \mathscr{P}_H^{\text{pol},2}$.

As can be seen in Fig. 16, where we report the errors against the parameter α, if one sets $L = h$ (solid lines) the optimal value for α increases for both pressure and fluxes as the mesh is refined. On the other hand, if one sets $L = H$ (dashed lines) the value of α for which the error is minimal turns out to be quite independent of h, with $\alpha \sim 0.3$ to minimize pressure error and $\alpha \sim 1$ to minimize flux error. This suggests that one could simply assign a fixed value to α.

To further confirm this, we solve the same problem with another decomposition given by 11×3 subdomains ($H = 1/3$) and a fixed mesh of 20×20 elements per subdomain (i.e., $h = H/20$). Further, we consider several permeability fields taken from different layers of the SPE10 data. As before, the interface spaces are $\mathscr{U}_H^{\text{pol},2}$ and $\mathscr{P}_H^{\text{pol},2}$ (piecewise linear polynomials). In Fig. 17 we illustrate the relative errors for pressure and flux as functions of α. Note that the minimum error remains close to $\alpha = 1$, especially for the flux error, in all cases.

Given the results reported above, from now on we adopt $L = H$ in the definition of the Robin parameter.

3.4.2 Comparison of multiscale mixed methods

Here we focus on numerical solutions computed with the MRCM, in comparison to those provided by the MMMFEM and the MHM. Through numerical simulations we have shown (see (GUIRALDELLO *et al.*, 2018b)) that as $\alpha \to +0$ the flux interface space $\mathscr{U}_H$ becomes irrelevant and the MRCM produces results that tend to those of the MMMFEM with the interface space $\mathscr{P}_H$. On the other hand, as $\alpha \to +\infty$, $\mathscr{P}_H$ becomes irrelevant and the MRCM produces results that tend to those computed with the MHM with the interface space $\mathscr{U}_H$. In conclusion, one can view the MRCM as a generalization of the two other known procedures.

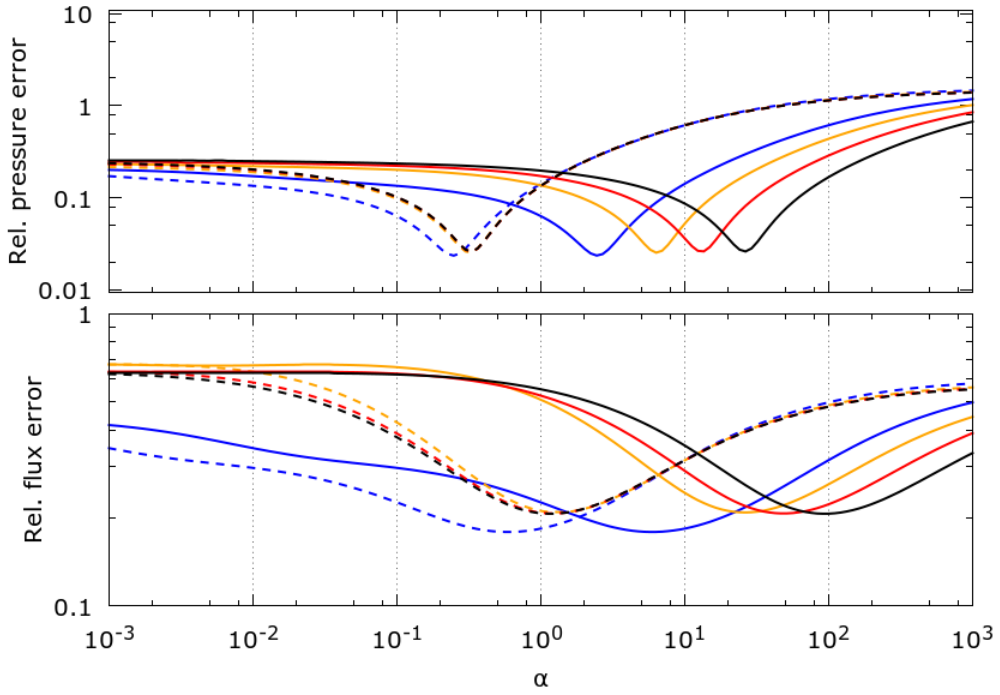

Source: Elaborated by the author.

$h = H/10, H/20, H/40, H/80.$

Figure 16 – Effect on α position for $L = h$ (solid lines) and $L = H$ (dashed lines) for a sequence of fine mesh refinement.

The comparison among the three methodologies will be conducted as follows: For each numerical study we fix a number k of degrees of freedom (*dof's*) per interface $\Gamma_{i,j}$ to be employed in solutions computed with all methods. For the MMMFEM we set $\mathscr{P}_H = \mathscr{P}_H^{\text{pol},k}$ in the case of piecewise polynomial spaces, and $\mathscr{P}_H = \mathscr{P}_H^{\text{inf},k}$ in the case of informed spaces. Similarly, for the MHM we set $\mathscr{U}_H$ equal to either $\mathscr{U}_H^{\text{pol},k}$ or $\mathscr{U}_H^{\text{inf},k}$. For the MRCM we take the interface spaces to be $\mathscr{P}_H^{\text{pol},k_P}$ (or $\mathscr{P}_H^{\text{inf},k_P}$ in the informed case) and $\mathscr{U}_H^{\text{pol},k_U}$ (or $\mathscr{U}_H^{\text{inf},k_U}$), with $k_U + k_P = k$.

Initially we set $k = 5$ *dof's* per interface and take some representative layers of the SPE10 database. We select layer 33 that does not exhibit a strong channelized structure, layer 36 with one well defined channel, and layers 42 and 45 with an intricate channel structure. In our studies we set $K_{max}/K_{min} \simeq 10^6$. In Figs. 18 and 19 we display the relative $L^2(\Omega)$ error norms for pressure and flux variables, respectively, as functions of α. When comparing the MRCM pressure with that of the MMMFEM (left dots) and that of the MHM (right dots) it is clear that one can always find a combination of (k_P, k_U) and α such that the MRCM produces a more accurate result than MMMFEM and MHM for both polynomial (solid lines) and informed (dashed lines) interface spaces. This observation is valid except for layer 45, for which the MMMFEM solution for the polynomial space is superior. This conclusion remains the same when comparing the flux errors. Exceptions to this finding occur on layers 33 and 42, for which the MHM produces the most accurate results for the case of informed spaces. In order to exhibit the quality of the

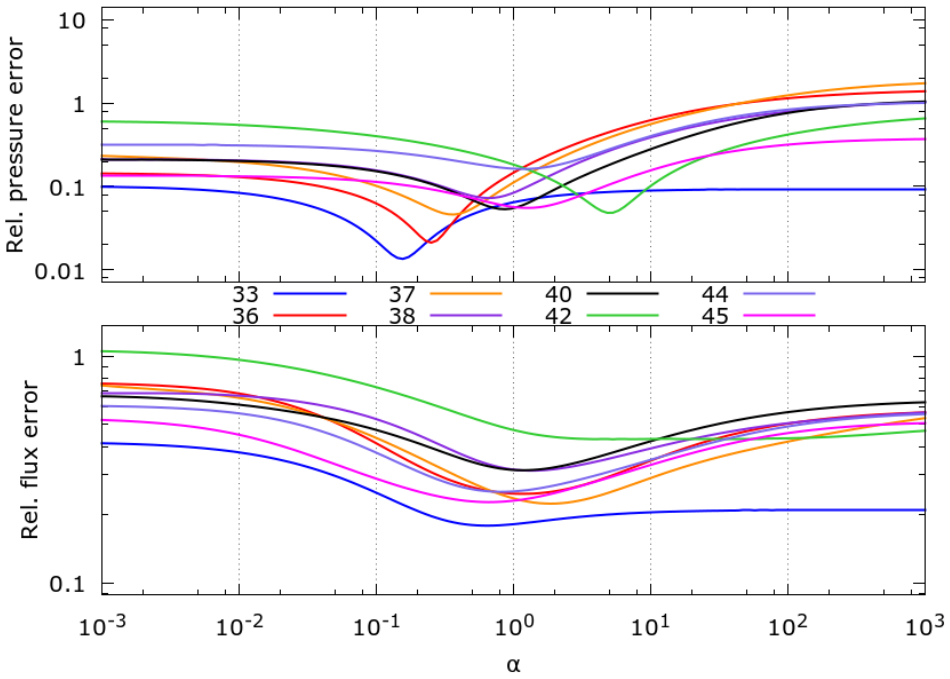

Source: Elaborated by the author.

Figure 17 – Relative pressure errors (top) and relative flux errors (bottom) for a collection of SPE10 layers with $L = H$.

solution, Figs. 20 and 21 display the pressure solution and the streamlines for the best global α compared to the fine solution for layer 36 for the polynomial case. In Figs. 22 and 23 we illustrate the relative $L^2(\Omega)$ error norms for pressure and flux variables, respectively, as a function of α for the case of $k = 4$ with layers 30, 63, 67 and 75, which were selected using the same criterion as adopted above, although none of the fields with channelized structure (layers ≥ 63) present one well-defined channel as in layer 36. In the numerical studies just discussed, that focus on global errors, we have shown that one can often find a combination of k_P, k_U and α for the MRCM that produces a better numerical solution than that provided by MMMFEM and MHM.

Next, we investigate how the error is distributed aiming at assessing the importance of informed spaces in approximating the velocity field in high-contrast realistic channelized formations. We take the permeability field with the most pronounced channel (layer 36), $k = 5$, and the best combination of (k_P, k_U) and α for polynomial and informed spaces that minimize the corresponding global error, as depicted on Figs. 18 and 19.

In Figs. 24 and 25 we show the pointwise absolute errors for pressure and flux, respectively. From these results one can see that both strategies provide comparable approximations for the pressure field (see Fig. 24). However, Fig. 25 indicates that informed spaces produce a better approximation of the flux variable than its polynomial counterpart. Moreover, the error is larger on the main channel structure of the permeability field for the polynomial compared to the informed case. Thus, informed spaces show great potential to be applied in reservoir simulation.

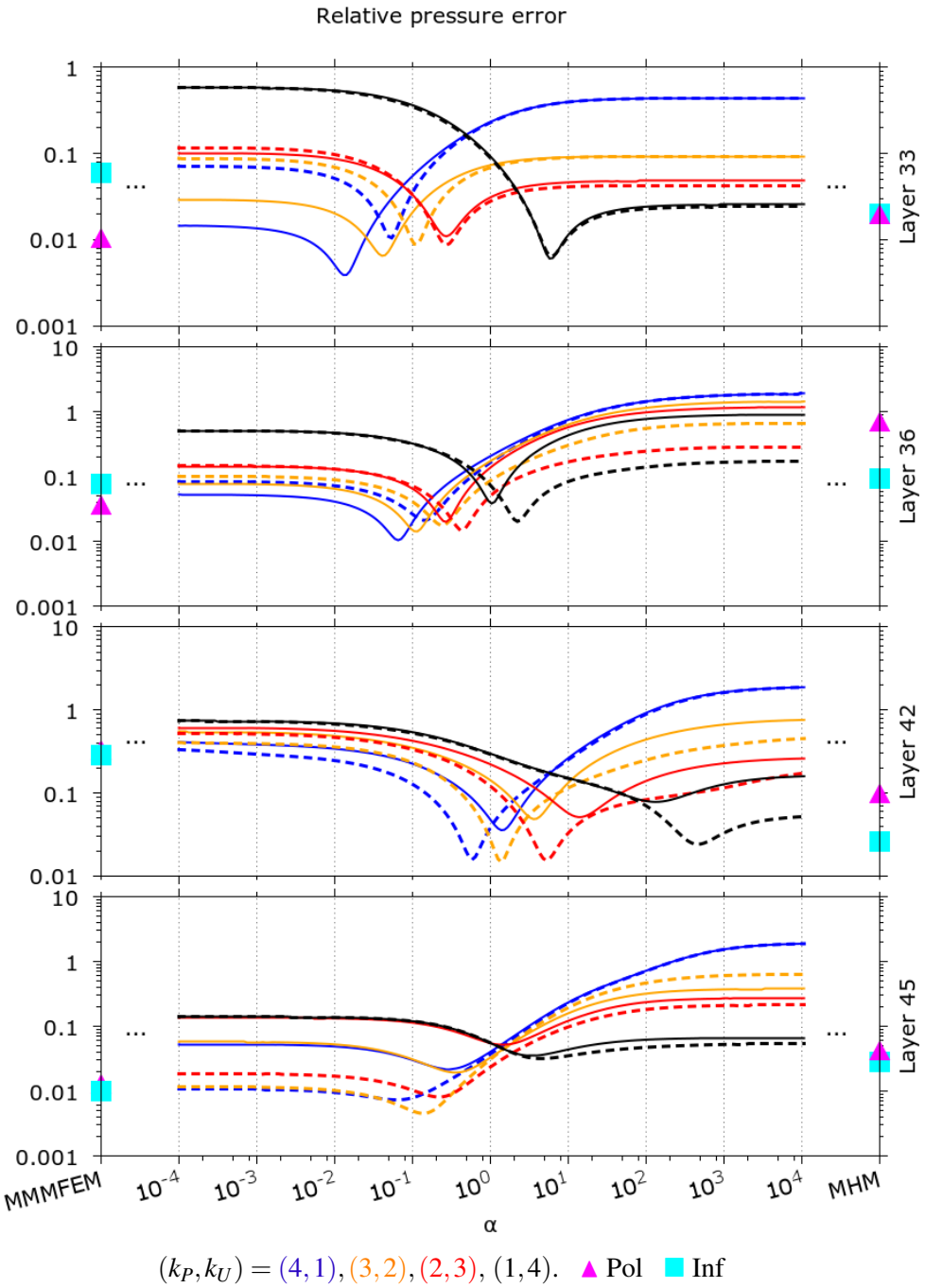

Source: Elaborated by the author.

Figure 18 – Relative pressure error as function of α for layers $33, 46, 42$ and 45 with 5 *dof's*. Solid lines: polynomial spaces; Dashed lines: informed spaces, for the MRCM formulation.

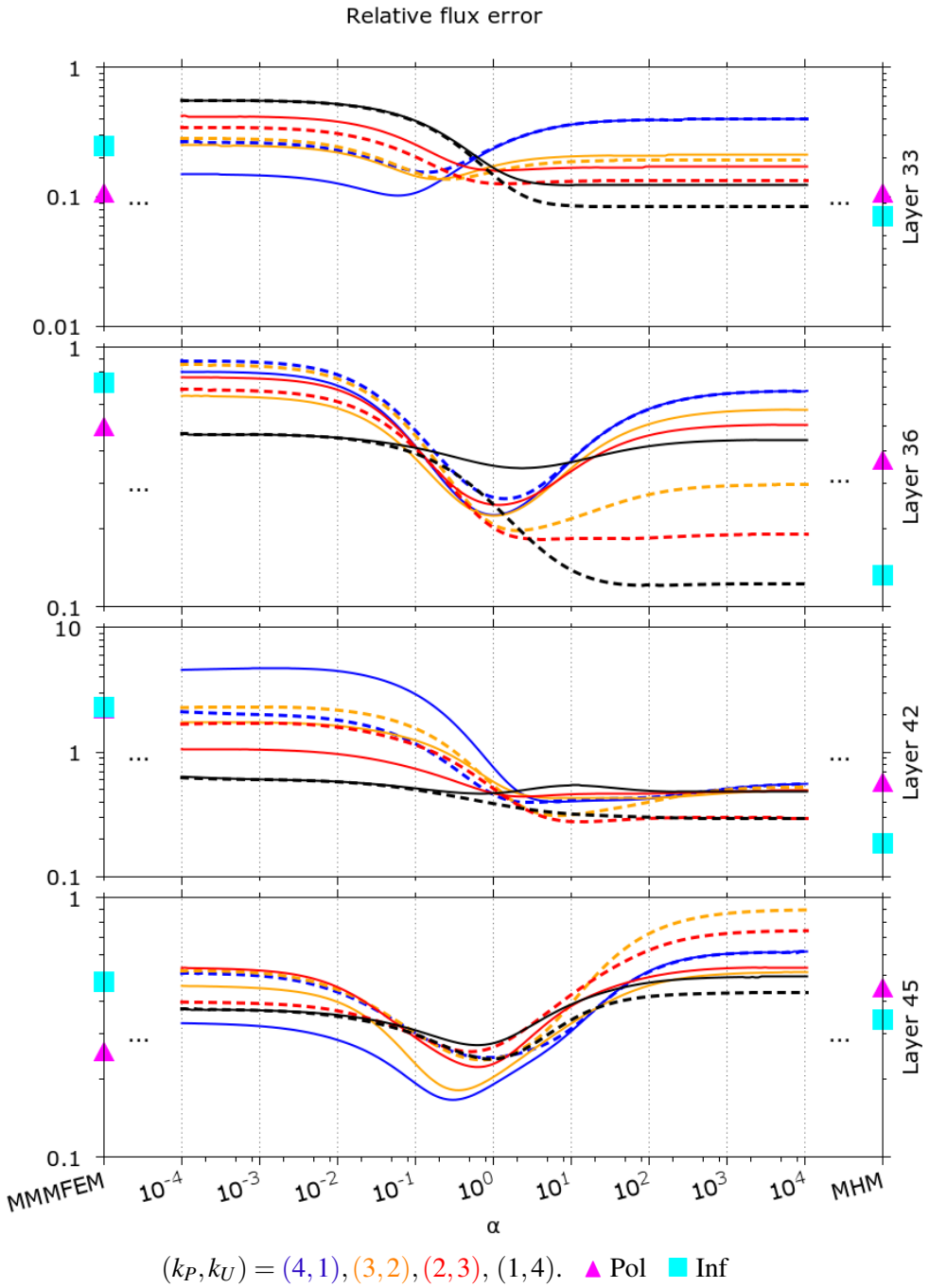

Source: Elaborated by the author.

Figure 19 – Relative flux error as function of α for layers 33, 46, 42 and 45 with 5 *dof's*. Solid lines: polynomial spaces; Dashed lines: informed spaces, for the MRCM formulation.

Layer 36 pressure solution

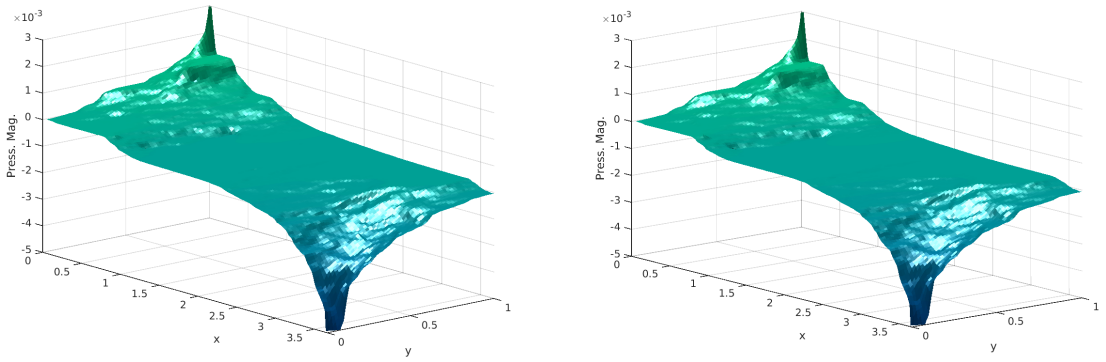

$(k_P, k_U) = (4,1)$ $\alpha = 6.527 \times 10^{-2}$ Fine Sol.

Source: Elaborated by the author.

Figure 20 – Pressure solution for the optimal global α and interface spaces with 5 *dof's* for polynomials and the fine pressure solution for layer 36.

Layer 36 streamlines

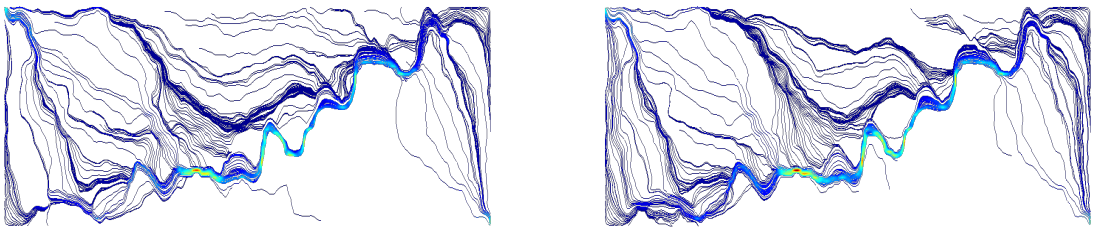

$(k_P, k_U) = (3,2)$ $\alpha = 1.035 \times 10^{0}$ Fine Sol.

Source: Elaborated by the author.

Figure 21 – Streamlines for the optimal global α and interface spaces with 5 *dof's* for polynomials and the fine solution for layer 36.

The studies discussed above illustrate that the accuracy of results produced by the MRCM depend on the choice of (k_P, k_U) and α. They also confirm, as noted by Guiraldello et al (GUIRALDELLO *et al.*, 2018b), that intermediate values of α are "safe", in the sense that they lead to errors that are *never* larger, and usually smaller, than the errors produced by the extreme values $\alpha = 0$ (MMMFEM) and $\alpha = +\infty$ (MHM). In order to avoid the need of selecting (k_P, k_U) and α at each run of the MRCM, we adopt the following strategy that has worked well in numerous tests:

- If k is even, we take $k_P = k_U = k/2$;
- if k is odd, we take $k_P = (k-1)/2$ and $k_U = k_P + 1 = k - k_P$;

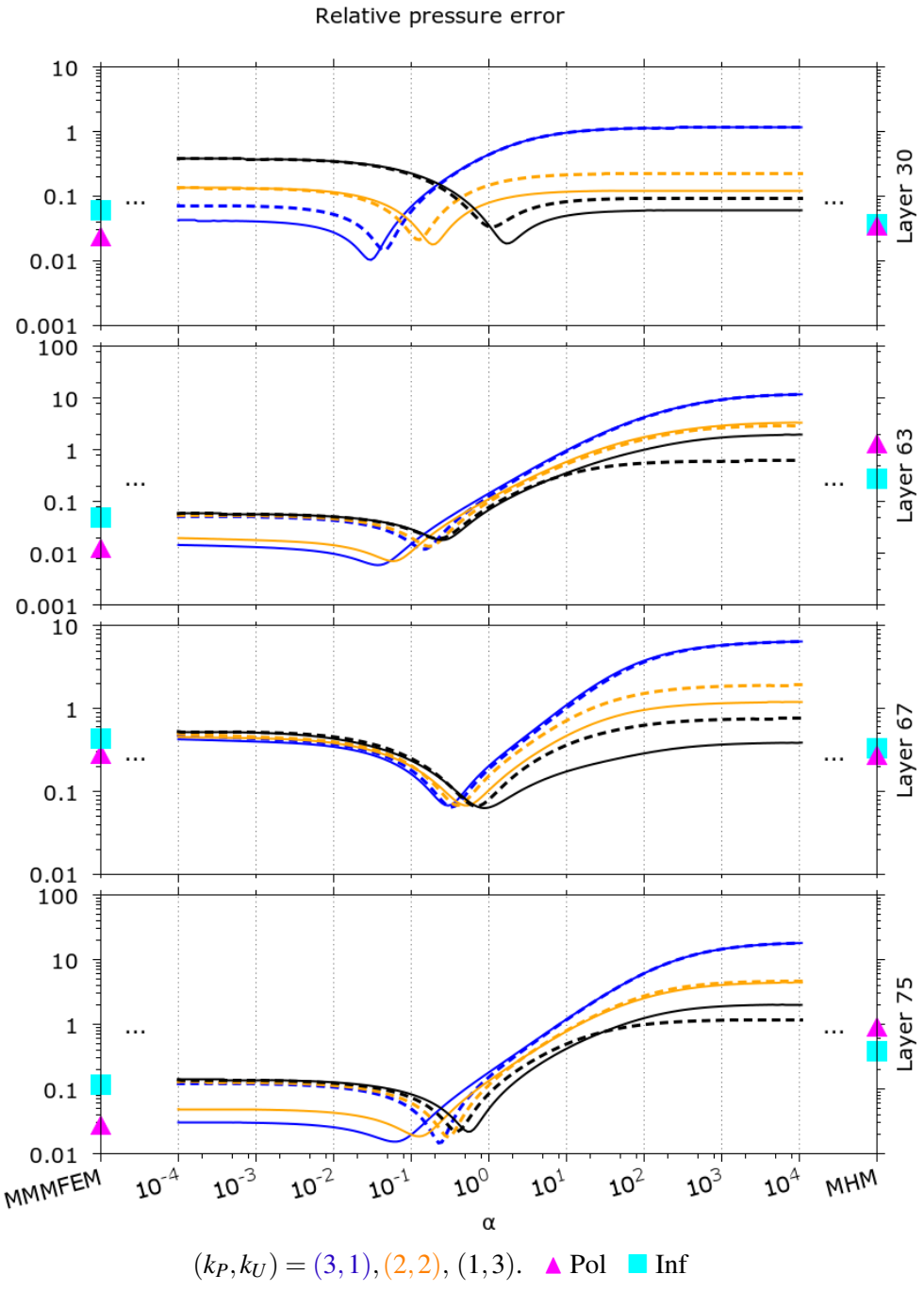

Source: Elaborated by the author.

Figure 22 – Relative pressure error as function of α for layers $30, 63, 67$ and 75 with 4 *dof's*. Solid lines: polynomial spaces; Dashed lines: informed spaces, for the MRCM formulation.

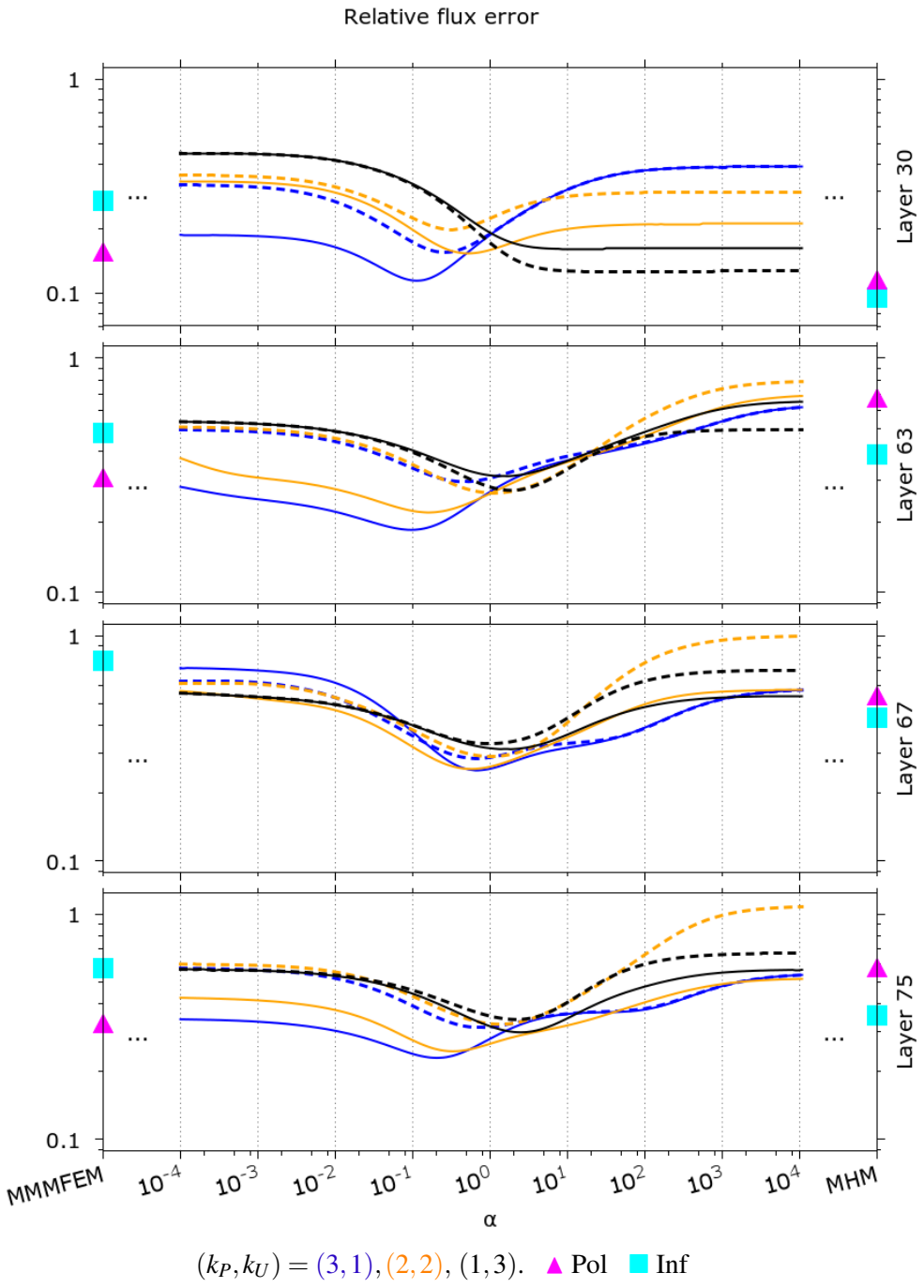

Source: Elaborated by the author.

Figure 23 – Relative flux error as function of α for layers $30, 63, 67$ and 75 with 4 *dof's*. Solid lines: polynomial spaces; Dashed lines: informed spaces, for the MRCM formulation.

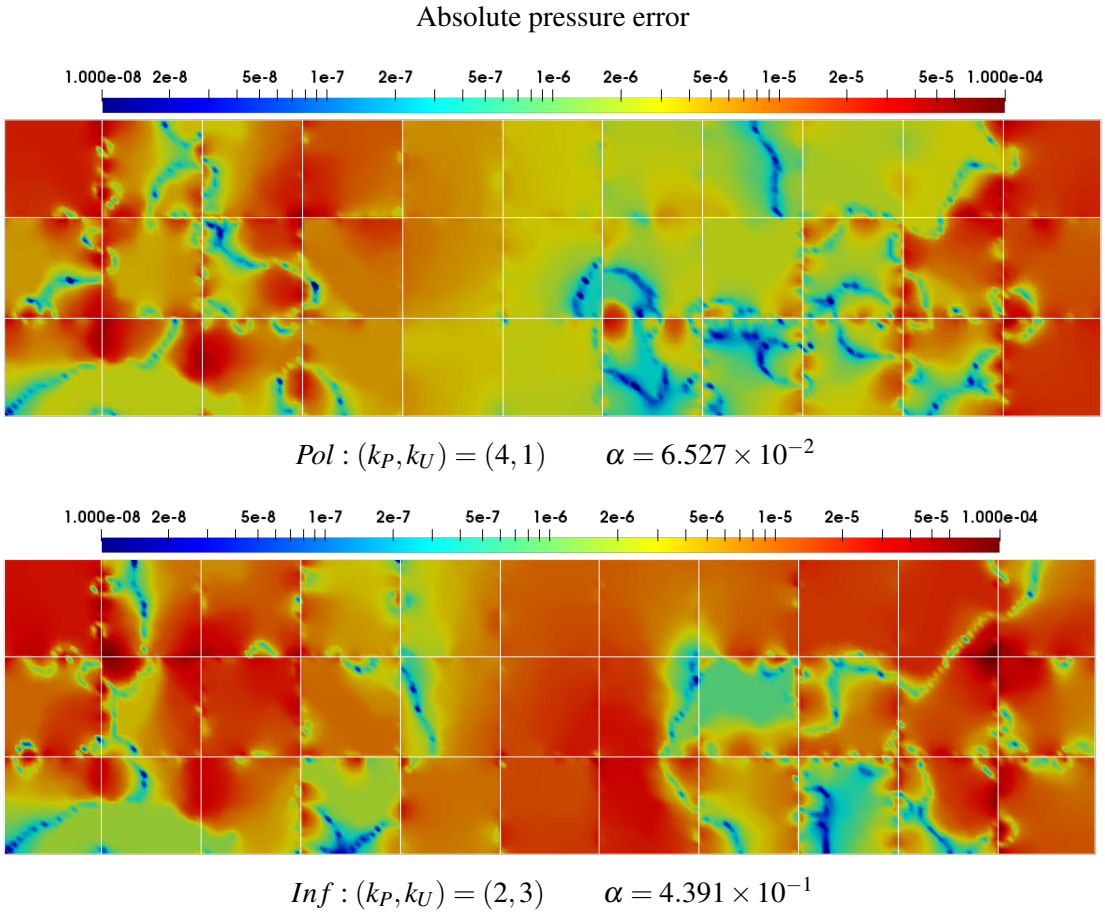

Source: Elaborated by the author.

Figure 24 – Absolute pressure error for the optimal global α and interface spaces with 5 *dof's* for polynomial and informed interface spaces for layer 36.

- set $\alpha = 1$.

In this way there are no free parameters for the MRCM. To justify such choices we perform an exhaustive comparison of MRCM, MHM and MMMFEM, with the same number k of *dof's* per interface for all methods, considering all SPE10 layers. Both polynomial and informed spaces are considered and the three methods can be compared on an equal footing. Figures 26 and 28 show, respectively, the results for $k = 4$ and $k = 5$ for polynomial interface spaces. Note that that when a curve corresponding to any of the methods appears in the shadowed region of another curve with a larger error, the color gets darker. For this choice of parameters the MHM is the least accurate method in the pressure variable for the channelized layers (layer number > 35), the MMMFEM being the most accurate. For the flux variable, however, the most accurate is the MRCM, while the MMMFEM behaves quite poorly for some of the layers around layer 40. The corresponding study for informed spaces is given in Figs. 27 and 29. For these spaces the MHM is again the least accurate procedure in the pressure variable (especially in layers 65-75), while the MMMFEM and MRCM behave similarly. For the flux variable the MHM and MRCM yield

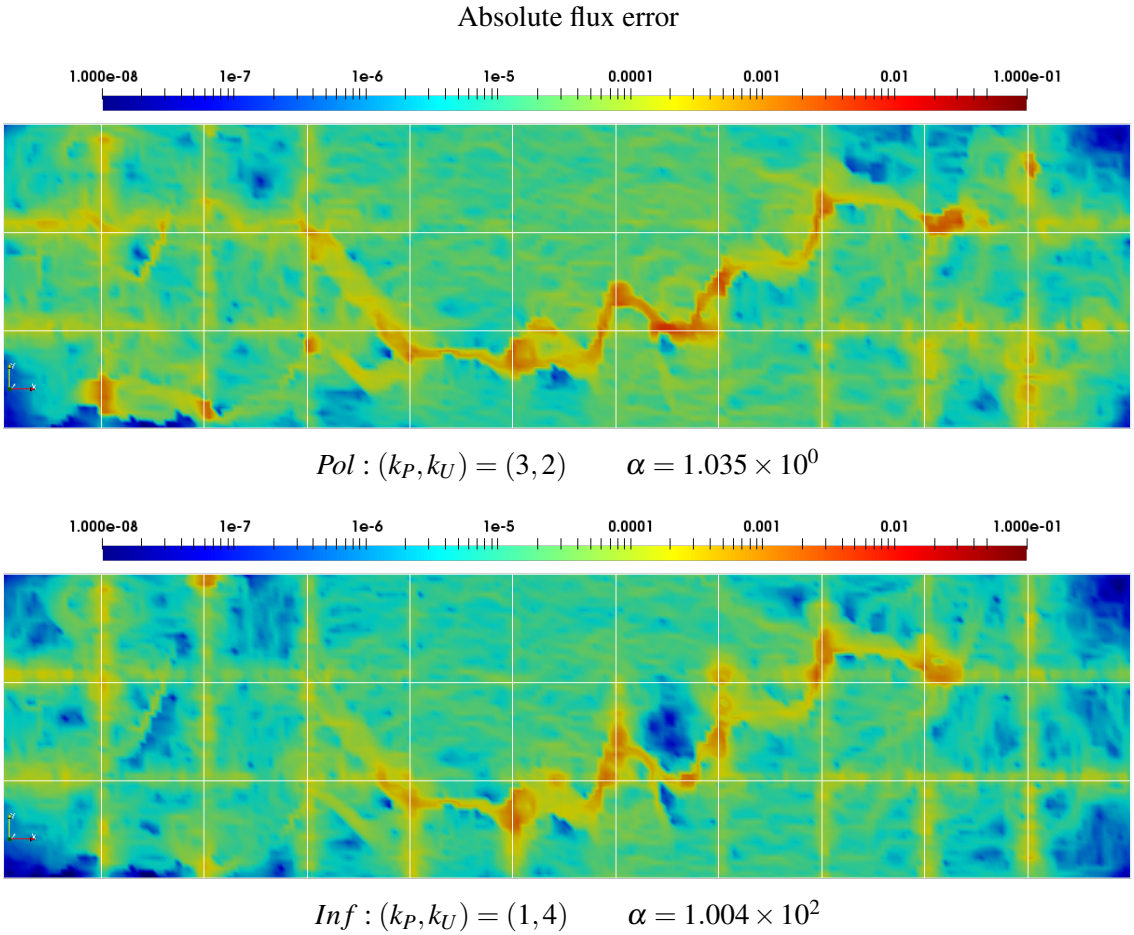

Source: Elaborated by the author.

Figure 25 – Absolute flux error for the optimal global α and interface spaces with 5 *dof's* for polynomial and informed interface spaces for layer 36.

similar accuracy, better than that of the MMMFEM, which again is considerably worse than the others for the layers around layer 40.

Although the focus of previous experiments is accuracy, another equally important aspect is the efficiency of the numerical methods. In order to illustrate this aspect, Figure 30 displays the number of GMRES iterations to convergence to solve the interface problem for each method with $k = 5$ for all the SPE10 layers with polynomial functions for the MMMFEM and MRCM and informed functions for the MHM. The GMRES was set with a relative tolerance of 10^{-9} and an ILU preconditioner with a drop tolerance of 10^{-4}. From the results one can observe that the MMMFEM and the MRCM have comparable number of GMRES iterations, with a slight advantage for the MRCM, and converge with half of the iterations required for the MHM. In these experiments the linear systems being solved have 260 unknowns. Another important point is that all of the above experiments are based on a fixed domain decomposition of 11×3 subdomains. In order to explorer other configurations, Figure 31 displays the relative error to convergence for many different domain decomposition geometries with $k = 5$ for layer 36. Notice

that, as the global fine mesh is fixed and each subdomain is a collection of fine elements, the number of elements for each domain decomposition geometry are different, e.g., each subdomain of the 5×6 domain decomposition geometry has a fine mesh of 44×10 elements.

The results shown in Figs. 26-31 allow us to conclude that the proposed MRCM is a competitive alternative to MMMFEM and MHM, both with polynomial and informed interface spaces. It should however be noted that the error obtained with informed spaces is roughly the same as that obtained with polynomial spaces. The only salient effect is the reduction of the pressure error, and just for the MHM.

Overall, the numerical results reported here indicate that the MRCM, with suitable choices for the spaces and parameters, is able to produce more accurate solutions than the other two procedures for problems defined for realistic, very heterogeneous permeability fields.

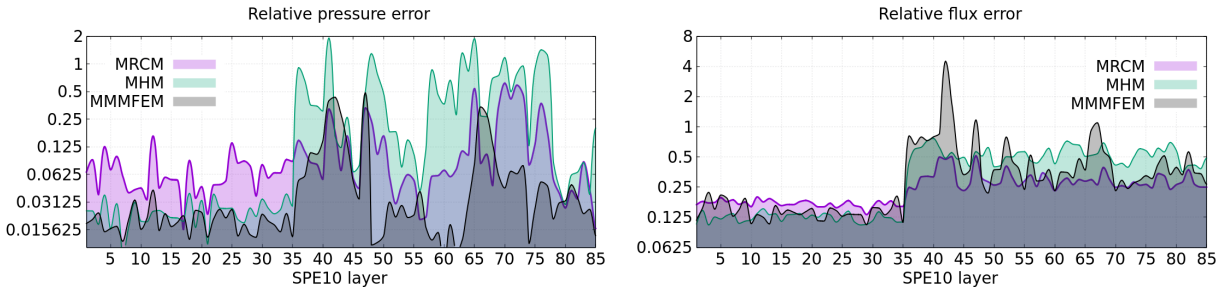

Source: Elaborated by the author.

Figure 26 – Relative pressure and flux error for all the SPE10 layers considering $k = 4$ and polynomial functions to build the interface spaces.

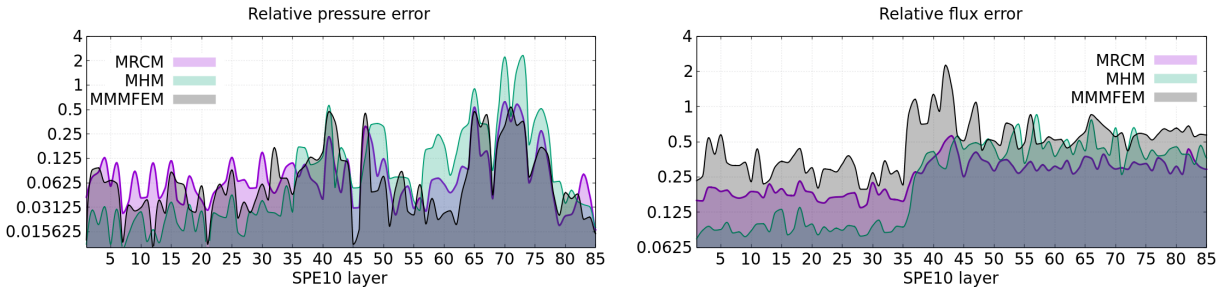

Source: Elaborated by the author.

Figure 27 – Relative pressure and flux error for all the SPE10 layers considering $k = 4$ and informed functions to build the interface spaces.

3.5 Concluding remarks

We have reviewed the recently introduced Multiscale Robin Coupled Method and described its implementation with informed spaces (or empirical interpolation spaces, obtained by oversampling) for the interface variables. We have compared the accuracy of the solutions of

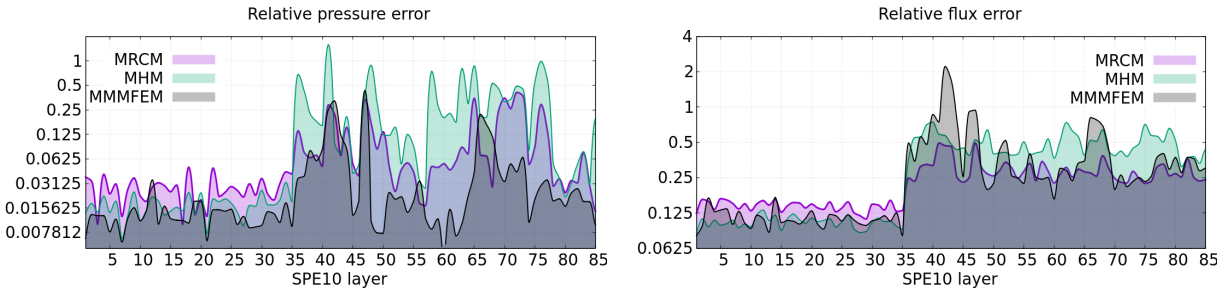

Source: Elaborated by the author.

Figure 28 – Relative pressure and flux error for all the SPE10 layers considering $k = 5$ and polynomial functions to build the interface spaces.

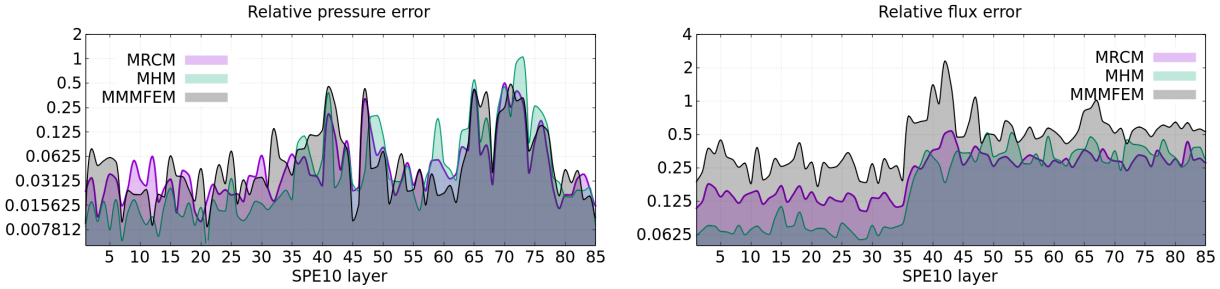

Source: Elaborated by the author.

Figure 29 – Relative pressure and flux error for all the SPE10 layers considering $k = 5$ and informed functions to build the interface spaces.

two well known multiscale methods, the Multiscale Mortar Mixed Finite Element Method and the Mixed Hybrid Method, with that of the MRCM in realistic, very heterogeneous permeability fields given by layers of the SPE10 project. The comparison was carried out with the same number of unknowns for all methods, with interface spaces given by polynomial and informed functions. It should be mentioned that no such comparison is available even if restricted to MMMFEM and MHM, and that no previous implementation or assessment of the MHM with informed spaces has been reported in the literature.

Our numerical results indicate that the MRCM, fixing its algorithmic parameter α to the value 1 and with a balanced distribution of the unknowns between interface pressures and interface fluxes, is a competitive alternative to the two previous methods. In fact, it is more accurate than MHM (which behaves better than MMMFEM) for the flux variable in highly channelized cases, without the large pressure errors produced by MHM.

Further work is needed to establish new, effective strategies for the construction of informed spaces. The simple procedures explored in this work have been useful for studying the optimal distribution of unknowns between interface pressures and fluxes, but the reduction in the solution global error was not significant, although it shows improved local approximations for the fluxes in channelized formations. Moreover, it was also shown that the MHM, when the

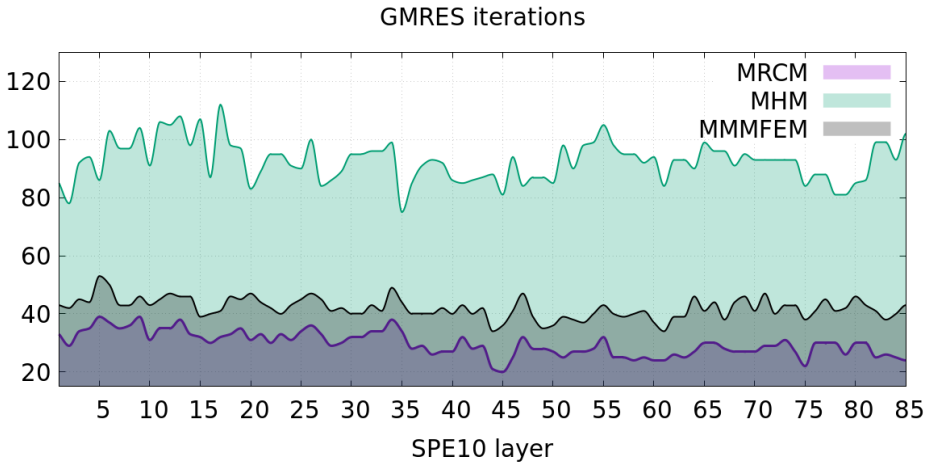

Source: Elaborated by the author.

Figure 30 – Number of GMRES iterations to convergence for all the SPE10 layers with $k = 5$.

interface spaces are switched from polynomial to informed (with the specific spaces proposed), exhibits essentially the same flux error but with a noticeable decrease of the pressure error. The identification of informed spaces with similar positive effects on the MRCM are left for future studies.

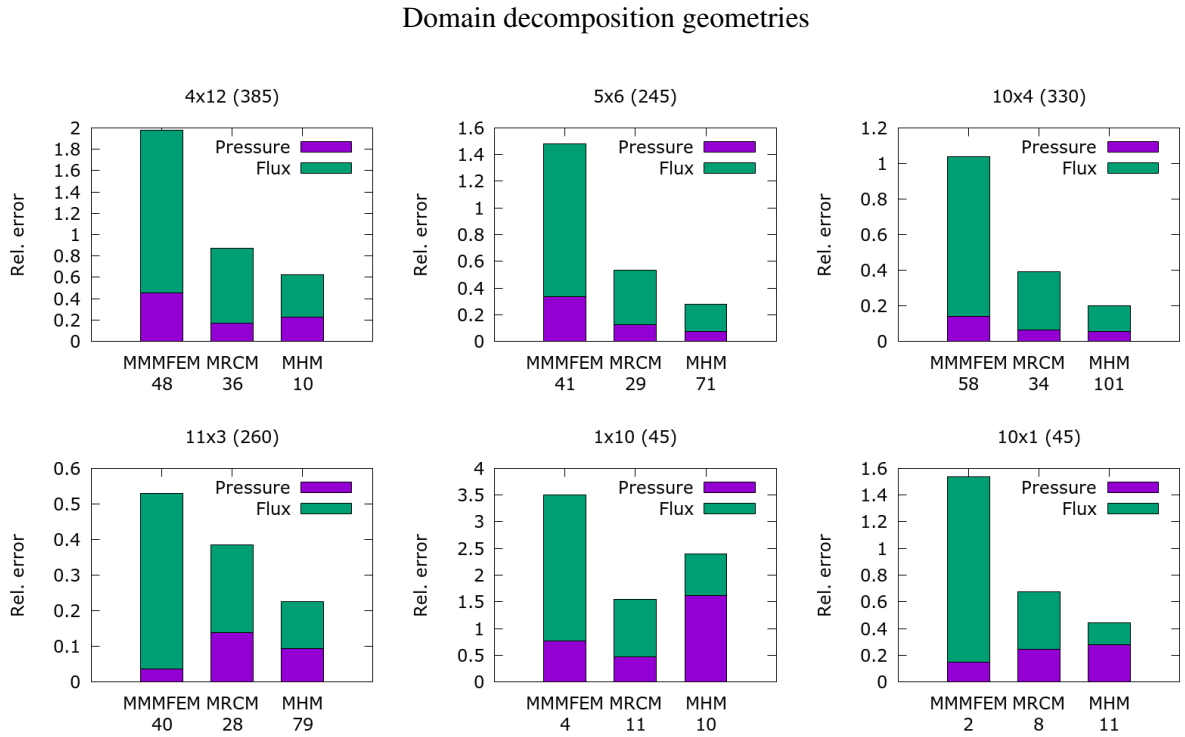

Source: Elaborated by the author.

Figure 31 – Relative pressure and flux errors and number of GMRES iterations, indicated below the labels, to convergence for different domain decomposition geometries,indicated at top of each graph with the number of unknowns being solved in parenthesis, for the layer 36 with $k = 5$.

CHAPTER

4

VELOCITY POSTPROCESSING SCHEMES FOR THE MULTISCALE ROBIN COUPLED METHOD FOR CONTAMINANT TRANSPORT IN SUBSURFACE FLOWS

We propose two postprocessing procedures (*Patch* method and *Stitch* method) to recover local conservation of velocity fields produced by multiscale approximations that are only conservative in coarse scales. These procedures operate on small overlapping regions and are designed to be implemented in parallel, that makes them relatively inexpensive. We investigate the applicability of such methods when tested on single-phase flow problems using the Multiscale Robin Coupled Method (MRCM) in highly heterogeneous permeability fields for modeling the contaminant transport in the subsurface. Numerical simulations are presented aiming to illustrate and compare the performance of the new methods with a standard procedure, the *Mean* method, in terms of accuracy in contaminant concentration. We show that for a collection of permeability fields taken as log-normal fields the new postprocessing procedures provide similar or better accuracy than the Mean method. Then we turn our attention to flows in high-contrast channelized porous formations, where the new methods robustly yield more accurate results and should thus be favored.

4.1 Introduction

We are concerned with flows in porous media. The model problem that we consider consists on the one hand of the second order elliptic Darcy model, whose mixed form is: find **u**

and p such that

$$\begin{cases} \mathbf{u} = -K\nabla p & \text{in } \Omega \\ \nabla\cdot\mathbf{u} = f & \text{in } \Omega \\ p = g & \text{on } \partial\Omega_p \\ \mathbf{u}\cdot\check{\mathbf{n}}_{\partial\Omega} = z & \text{on } \partial\Omega_u \end{cases} \tag{4.1}$$

where $\Omega \subset \mathbb{R}^d$, $d = 2$ or 3 is the computational domain, K is a symmetric, uniformly positive definite tensor with components in $L^\infty(\Omega)$, $\mathbf{u}$ is the Darcy velocity, p is the pressure, $f \in L^2(\Omega)$ the source, $g \in H^{\frac{1}{2}}(\partial\Omega_p)$ the pressure boundary data, $z \in H^{-\frac{1}{2}}(\partial\Omega_u)$ the normal velocity data and $\check{\mathbf{n}}_{\partial\Omega}$ is the outer normal to $\partial\Omega$. On the other hand, given the fluid velocity $\mathbf{u}$ as obtained from (4.1) we solve the transport of a passive tracer or contaminant which is governed by the scalar hyperbolic conservation law

$$\begin{cases} \dfrac{\partial\mathscr{C}}{\partial t} + \nabla\cdot(\mathbf{u}\mathscr{C}) = 0 & \text{in } \Omega \\ \mathscr{C}(\mathbf{x}, t=0) = \mathscr{C}_0(\mathbf{x}) & \text{in } \Omega \\ \mathscr{C}(\mathbf{x},t) = \mathscr{C}_D(\mathbf{x},t) & \text{in } \partial\Omega^- \end{cases} \tag{4.2}$$

where $\mathscr{C}$ is the concentration of the pollutant species, $\mathscr{C}_0$ its initial condition and $\mathscr{C}_D$ the concentration at the inlet boundaries $\partial\Omega^- = \{\mathbf{x} \in \partial\Omega,\ \mathbf{u}\cdot\check{\mathbf{n}}_{\partial\Omega} < 0\}$.

Nowadays applications of fluid flow in subsurface problems governed by (4.1)-(4.2) or some variant of it, such as those involving oil and gas production, compositional flow in oil reservoirs and pollutant transport in aquifers, may require over a billion computational cells to predict with reasonable accuracy the flow variables. Besides this enormous challenge, uncertainty quantification studies are necessary to deal with the stochastic nature of the permeability field and estimate relevant quantities with statistical significance. Multiscale domain decomposition methods for the simulation of transport in porous media, aiming for high performance and scalability, have been the focus of intensive research over the last years. The underlying idea is to decompose the computational domain into non-overlapping subdomains in which local small problems are solved. This is naturally done in parallel. Recently, in (GUIRALDELLO *et al.*, 2018b) and (GUIRALDELLO *et al.*, 2018a), we have proposed a new method named Multiscale Robin Coupled Method (MRCM) as a generalization to the Multiscale Mixed Method (MuMM) (FRANCISCO *et al.*, 2014), based on a domain decomposition technique introduced originally by Douglas et al (DOUGLAS *et al.*, 1993), in which the local problems are subject to Robin type boundary conditions. In the new method we introduce two unknown fields on the so called skeleton of the domain decomposition, namely, a flux U_H and a pressure P_H, belonging to some function spaces of low dimension $\mathscr{U}_H$ and $\mathscr{P}_H$ defined over the skeleton, such that continuity of pressure and flux are weakly enforced. This in turn leads to a system of equations of intermediate size that couples the solutions over the domains of the decomposition. In a multiscale formulation like ours, the compatibility conditions are only satisfied at some coarse scale $H \gg h$ in order to alleviate the computational burden. Denoting the skeleton of the decomposition by Γ and by

$(\mathbf{u}, p)$ the multiscale solution, this means that

$$\int_{\Gamma} \left(\mathbf{u}^{+} - \mathbf{u}^{-}\right) \cdot \check{\mathbf{n}}\, M_H \, d\Gamma \;=\; 0\,, \qquad \forall M_H \in \mathscr{P}_H\,, \tag{4.3}$$

$$\int_{\Gamma} (p^{+} - p^{-})\, V_H \, d\Gamma \;=\; 0\,, \qquad \forall V_H \in \mathscr{U}_H\,, \tag{4.4}$$

where the $+$ and $-$ superscripts refer to the two-sided limits approaching Γ and $\check{\mathbf{n}}$ is a unit vector normal to Γ. In the limit case when $H = h$ we recover the global fine grid solution and continuity of flux and pressure is satisfied pointwise. Two well known methods, the Multiscale Mortar Mixed Finite Element Method (MMMFEM) (ARBOGAST *et al.*, 2007) and the Multiscale Hybrid-Mixed Finite Element Method (MHM) (HARDER; PAREDES; VALENTIN, 2013) can be obtained as particular cases of the MRCM by suitably defining a parameter α in the Robin boundary condition that couples the subdomain solutions, i.e.,

$$-\frac{\alpha H}{K_i(\mathbf{x})}\, \mathbf{u}_h^i \cdot \check{\mathbf{n}}^i + p^i = -\frac{\alpha H}{K_i(\mathbf{x})}\, U_H\, \check{\mathbf{n}} \cdot \check{\mathbf{n}}^i + P_H \tag{4.5}$$

where $\mathbf{u}_h^i$ is the flux multiscale solution on subdomain Ω_i and $\check{\mathbf{n}}^i$ is the exterior normal to $\partial\Omega_i$. We can move from one method to the other in different parts of the domain without any implementation effort. Also, there is considerable freedom to select the numerical schemes to solve the local problems in the subdomains as well as to choose the interface spaces $\mathscr{U}_H$ and $\mathscr{P}_H$ independently from each other. All these features give the possibility of producing more accurate solutions as compared to other available techniques, as we have numerically shown in (GUIRALDELLO *et al.*, 2018b; GUIRALDELLO *et al.*, 2018a). The drawback of course is that fluxes are only conservative at the coarse scale given by the size of the subdomains H, i.e., for each interface Γ_{ij} between subdomains Ω_i and Ω_j the following holds

$$\int_{\Gamma_{ij}} \mathbf{u}_h^i \cdot \check{\mathbf{n}}\, d\Gamma = \int_{\Gamma_{ij}} \mathbf{u}_h^j \cdot \check{\mathbf{n}}\, d\Gamma. \tag{4.6}$$

Fluxes are not in general continuous at the fine level of the discretization on interfaces between adjacent domains. The velocity field produced by such methods is unsuitable to be used in the transport equation (4.2). Therefore, some post-processing or downscaling procedure becomes necessary.

Let us illustrate this with an example. Consider the highly heterogeneous permeability field displayed in Figure 32. This field exhibits a contrast $K_{\max}/K_{\min} \sim 10^5$ and corresponds to a log-normal field plus a central channelized region that has been inserted by hand to make the problem more challenging. In this example, the domain $\Omega = [0,1] \times [0,1]$ is discretized into 100×100 fine grid cells and decomposed into 2×2 subdomains.The skeleton of the decomposition is denoted by Γ, which in this particular case is made of the four internal interfaces between the subdomains. Figure 33 shows the multiscale solution (velocity and pressure) produced by our method in three different situations, considering interface spaces $\mathscr{P}_H$ and $\mathscr{U}_H$ of very low dimension made up of functions that are constant by parts on each interface.

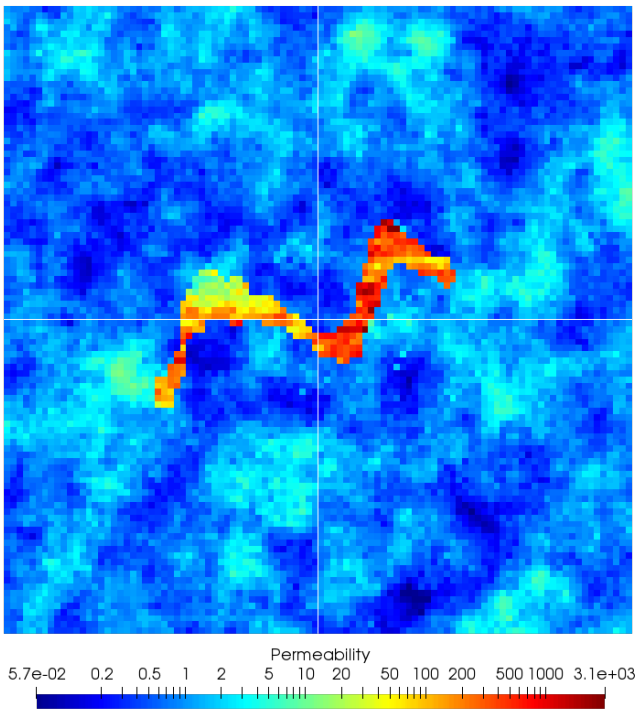

Source: Elaborated by the author.

Figure 32 – Permeability field used to illustrate the behavior of the multiscale method.

In the first case (top subfigure), we take the Robin condition parameter very large ($\alpha = 10^6$). In this situation the MRCM retrieves the MHM solution, in which continuity of fluxes is enforced pointwise, as observed in the insert, whereas continuity of pressure is weakly satisfied according to (4.4). This leads to a significant pressure jump at the interfaces, also clearly noticeable in the figure. In the second case we take $\alpha = 1$ (middle part). For such intermediate value of the Robin condition parameter neither flux nor pressure satisfy pointwise continuity. As a result, a small jump is observed at the interfaces in both multiscale velocity and pressure. For instance, this is clearly noticed in the right insert, where we have also plotted the flux jump along Γ_{13} which is one of the critical interfaces crossing the high permeability channel. Finally, we take the algorithmic parameter very small ($\alpha = 10^{-6}$), such that the method retrieves the MMMFEM solution, in which the pressure field is continuous, as observed at the bottom of Figure 33, while the velocity field exhibits very large jumps at the interfaces, also highlighted in the right insert that shows the flux jump along interface Γ_{13}. It becomes evident that in the last two cases some downscaling or postprocessing procedure on the velocity field is mandatory prior to its use in the resolution of the transport equation, be it in a multiphase (non-linear) problem or in the linear case of a passive tracer. This is addressed in this article where two new simple and relatively inexpensive procedures are proposed, namely the *Patch* method and the *Stitch* method, that are compared to the standard technique of computing the average velocity at interfaces between subdomains.

After this introduction, the plan of the article is as follows. First, we recall the MRCM

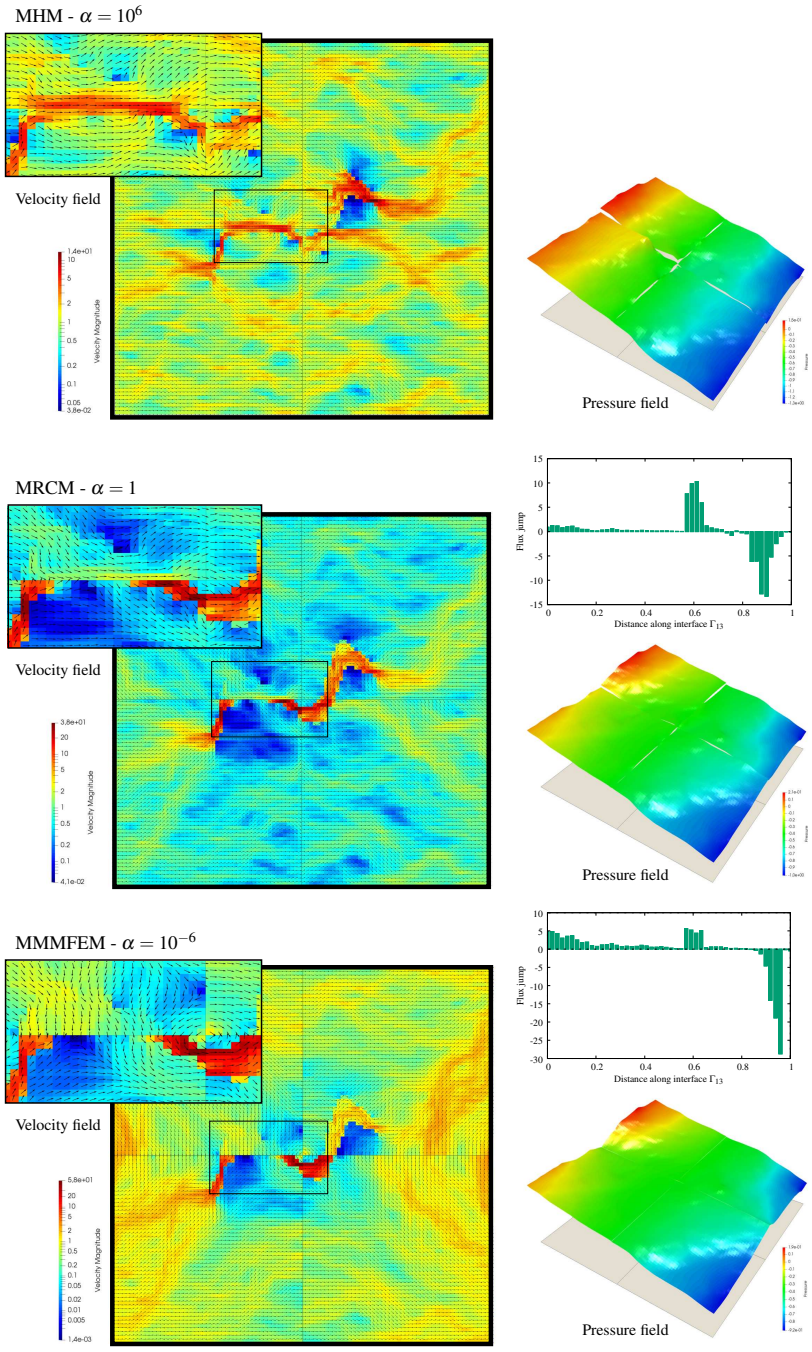

Source: Elaborated by the author.

Figure 33 – Multiscale solutions produced by the MRCM method considering different values of the Robin condition parameter: $\alpha = 10^{-6}$ (top), $\alpha = 1$ (middle), $\alpha = 10^6$ (bottom).

method by explaining with some level of detail how the previous example was actually computed. In section 4.3 the proposed downscaling methods are presented. In the numerical results section we extensively assess and compare them by solving the transport of a passive tracer by means of a finite volume method in highly heterogeneous permeability rock formations. Finally, some conclusions are drawn.

4.2 The Multiscale Robin Coupled method

In this section we recall the main ingredients and some implementation aspects of the Multiscale Robin Coupled Method method. For further details, such as well-posedness results, implementation in a variational setting and the possibility of using informed functions to build up the interface spaces $\mathscr{U}_H$ and $\mathscr{P}_H$ the reader is referred to (GUIRALDELLO *et al.*, 2018b; GUIRALDELLO *et al.*, 2018a).

We begin by introducing some notation. The key ingredient is the discrete solution of local Darcy problems. Let us consider a rectangular domain $\Omega \subset \mathbb{R}^d$, $d = 2,3$ and a subdivision $\mathscr{T}_h$ made of d-dimensional rectangles. We refer to this partition as the *fine grid*. The permeability K and source term f are functions belonging to the space $P_0(\mathscr{T}_h)$, i.e., functions that are constant by parts on this fine grid. In general, the boundary of Ω can be divided into disjoint parts denoted by $\Gamma_u, \Gamma_p, \Gamma_r$ in which flux, pressure and Robin boundary conditions are imposed. The problem reads: Find $(\mathbf{u}_h, p_h)$ such that

$$\left\{\begin{array}{rcll} \mathbf{u}_h & = & -K\nabla p_h & \text{in } \Omega \\ \nabla\cdot\mathbf{u}_h & = & f & \text{in } \Omega \\ p_h & = & g_p & \text{on } \Gamma_p \\ \mathbf{u}_h\cdot\mathbf{n} & = & g_u & \text{on } \Gamma_u \\ -\beta\mathbf{u}_h\cdot\mathbf{n}+p & = & g_r & \text{on } \Gamma_r \end{array}\right. . \tag{4.7}$$

The domain Ω can be the domain in which the global problem being considered is posed or any subdomain made of a collection of fine grid cells, as it will be the case later on when describing the downscaling procedures. Figure 34 shows the computational domain, the fine grid discretization and the domain decomposition. For the solution of the Darcy problems we adopt a standard cell-centered finite volume scheme on rectangular cartesian grids in which we solve for the cell pressure unknowns $p_{I,J}$ by eliminating the edge flux unknowns $u_{I\pm\frac{1}{2},J\pm\frac{1}{2}}$. A complete description can be found in (GUIRALDELLO *et al.*, 2018b). For further details and possible generalizations see e.g. (ARBOGAST; WHEELER; YOTOV, 1997). As mentioned, there is considerable freedom to choose the local solvers. In principle any finite volume, finite element or finite difference scheme that delivers the edge fluxes at subdomain interfaces, when requested by the multiscale method to be described below, can be used.

A non-overlapping domain decomposition of Ω into subdomains Ω_i, $i = 1,\ldots,N$ is considered. Let us denote by $\check{\mathbf{n}}^i$ the outer normal to $\partial\Omega^i$ and by $\check{\mathbf{n}}$ a unique normal to interface

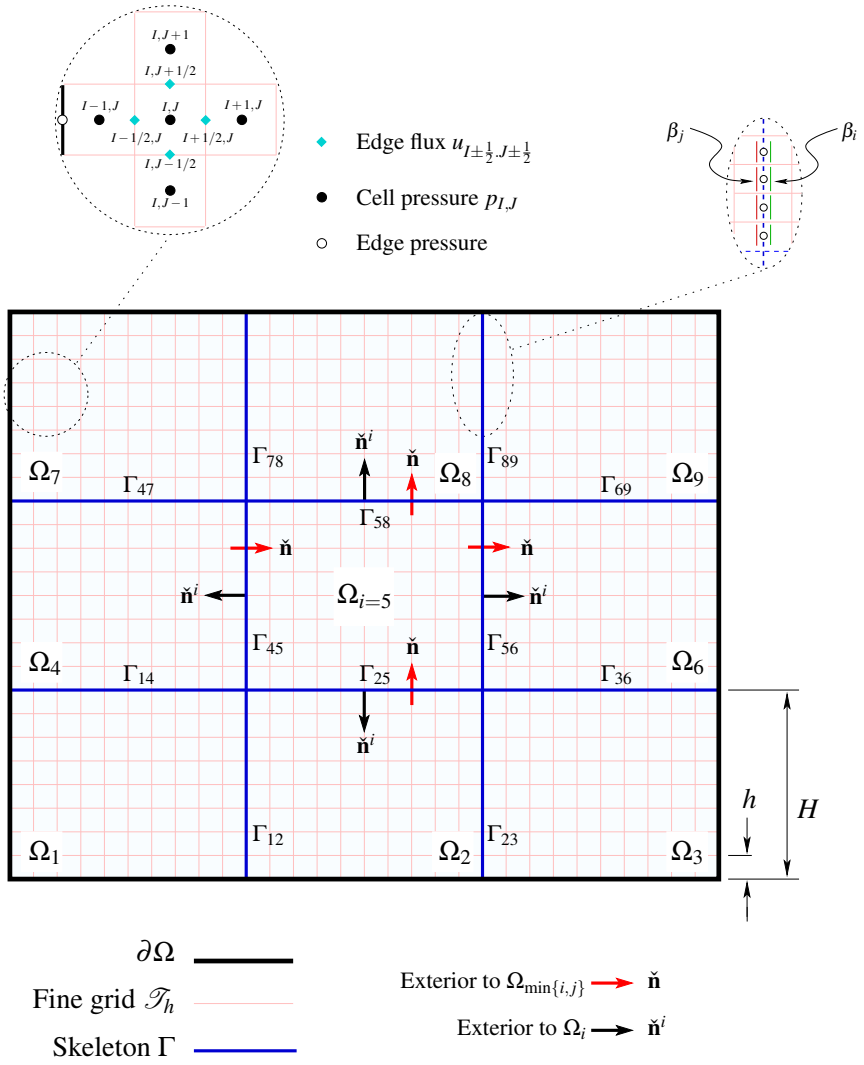

Source: Elaborated by the author.

Figure 34 – The computational domain along with the fine grid discretization and the domain decomposition adopted.

Γ_{ij} defined such that it points out from the domain with smallest index (i.e., $\check{\mathbf{n}} = \check{\mathbf{n}}^{\min(i,j)}$).

Our multiscale method can be written as: Find subdomain solutions $(\mathbf{u}_h^i, p_h^i)$, $i = 1, \ldots, N$ and interface fields (U_H, P_H) satisfying the local problems

$$\begin{cases} \mathbf{u}_h^i &= -K\nabla p_h^i & \text{in } \Omega_i \\ \nabla\cdot\mathbf{u}_h^i &= f & \text{in } \Omega_i \\ p_h^i &= g_p & \text{on } \partial\Omega_i \cap \Gamma_p \\ \mathbf{u}_h^i\cdot\check{\mathbf{n}}^i &= g_u & \text{on } \partial\Omega_i \cap \Gamma_u \\ -\beta_i\mathbf{u}_h^i\cdot\check{\mathbf{n}}^i + p_h^i &= -\beta_i U_H\,\check{\mathbf{n}}\cdot\check{\mathbf{n}}^i + P_H & \text{on } \partial\Omega_i \cap \Gamma \end{cases} \tag{4.8}$$

in which the differential operators are replaced by suitable discrete approximations, together

with the compatibility conditions on the skeleton Γ

$$\left\{\begin{array}{rcl} \displaystyle\sum_{i=1}^{N} \int\limits_{\partial\Omega_i\cap\Gamma} \left(\mathbf{u}_h^i\cdot\check{\mathbf{n}}^i\right)\,\psi\,d\Gamma &=& 0\,, \\ \displaystyle\sum_{i=1}^{N} \int\limits_{\partial\Omega_i\cap\Gamma} \beta_i\left(\mathbf{u}_h^i\cdot\check{\mathbf{n}}^i - U_H\,\check{\mathbf{n}}^i\cdot\check{\mathbf{n}}\right)\phi\,\check{\mathbf{n}}^i\cdot\check{\mathbf{n}}\,d\Gamma &=& 0\,, \end{array}\right. \tag{4.9}$$

which must hold for all functions $\psi\in\mathscr{P}_H$ and $\phi\in\mathscr{U}_H$. The interface flux U_H and interface pressure P_H are functions belonging to these spaces which are contained in $F_h(\mathscr{E}_h)$ defined as

$$F_h(\mathscr{E}_h)=\{f:\mathscr{E}_h\to\mathbb{R}\mid f|_e\in\mathbb{P}_0\,,\ \forall e\in\mathscr{E}_h\}\,, \tag{4.10}$$

where $\mathscr{E}_h$ is the set of all edges (in 2D) or faces (in 3D) of $\mathscr{T}_h$ contained in Γ. These spaces are made up at least of the constant function over Γ. Equation (4.9) in such case is nothing but the statement that fluxes and pressures are continuous over Γ in the mean sense. A smart definition of the interface spaces is essential for the resulting accuracy and convergence of the method. In this article we restrict ourselves to polynomial spaces for simplicity, however some better strategies were recently devised in (GUIRALDELLO *et al.*, 2018a). As for the Robin condition parameter β_i on each subdomain, several choices are possible. Based on our previous experience (see (GUIRALDELLO *et al.*, 2018a)), we adopt

$$\beta_i(\mathbf{x})=\frac{\alpha H}{K_i(\mathbf{x})} \tag{4.11}$$

where α is a dimensionless algorithmic parameter that is taken equal to 1 in the numerical experiments below, H is the characteristic size of the subdomains and $K_i(\mathbf{x})$ is a local permeability. By changing α we retrieve the MMMFEM method ($\alpha\to 0$) and the MHM method ($\alpha\to\infty$). This has been numerically shown in the authors' article (GUIRALDELLO *et al.*, 2018b).

Let us explain how the example of the previous section was actually computed by using the MRCM formulation. First, to solve the problem efficiently we must segregate the resolution of the subdomain problems from the resolution of the interface unknowns. To that end, on each subdomain Ω_i, the solution $(\mathbf{u}_h^i,p_h^i)$ of the Darcy problem is decomposed as the sum of two parts

$$\mathbf{u}_h^i=\hat{\mathbf{u}}_h^i+\bar{\mathbf{u}}_h^i,\qquad p_h^i=\hat{p}_h^i+\bar{p}_h^i, \tag{4.12}$$

satisfying the following problems

$$\left\{\begin{array}{rcll} \bar{\mathbf{u}}_h^i &=& -K\nabla\bar{p}_h^i & \text{in } \Omega_i \\ \nabla\cdot\bar{\mathbf{u}}_h^i &=& f & \text{in } \Omega_i \\ \bar{p}_h^i &=& g_p & \text{on } \partial\Omega_i\cap\Gamma_p \\ \bar{\mathbf{u}}_h^i\cdot\check{\mathbf{n}}^i &=& g_u & \text{on } \partial\Omega_i\cap\Gamma_u \\ -\beta_i\bar{\mathbf{u}}_h^i\cdot\check{\mathbf{n}}^i+\bar{p}_h^i &=& 0 & \text{on } \partial\Omega_i\cap\Gamma \end{array}\right.\,, \tag{4.13}$$

$$\left\{\begin{array}{rcll} \hat{\mathbf{u}}_h^i &=& -K\nabla\hat{p}_h^i & \text{in } \Omega_i \\ \nabla\cdot\hat{\mathbf{u}}_h^i &=& 0 & \text{in } \Omega_i \\ \hat{p}_h^i &=& 0 & \text{on } \partial\Omega_i\cap\Gamma_p \\ \hat{\mathbf{u}}_h^i\cdot\check{\mathbf{n}}^i &=& 0 & \text{on } \partial\Omega_i\cap\Gamma_u \\ -\beta_i\hat{\mathbf{u}}_h^i\cdot\check{\mathbf{n}}^i+\hat{p}_h^i &=& -\beta_i U_H\check{\mathbf{n}}\cdot\check{\mathbf{n}}^i+P_H & \text{on } \partial\Omega_i\cap\Gamma \end{array}\right. . \tag{4.14}$$

It is useful to think the solution $\hat{\mathbf{u}}_h^i$ as a function of the interface data (P_H,U_H). Abusing notation this will be denoted later on as $\hat{\mathbf{u}}_h^i(P_H,U_H)$. In the example above, the skeleton Γ in which the Robin boundary conditions are being imposed is made of the four internal interfaces as shown in Figure 32, which are numbered $\Gamma_{12},\Gamma_{34},\Gamma_{13}$ and Γ_{24}.

Now, consider $\mathscr{P}_H=\text{span}\{\psi_1,\ldots,\psi_{N_P}\}$ and $\mathscr{U}_H=\text{span}\{\phi_1,\ldots,\phi_{N_U}\}$, where N_P and N_U are the dimensions of the interface spaces. In general, we choose k_U and k_P degrees of freedom per interface, therefore the dimensions of these spaces are $N_P=k_P\times N_I$ and $N_U=k_U\times N_I$, being N_I the number of elements in the skeleton mesh. The simplest case corresponds to taking $k_P=k_U=1$ and one element per interface between subdomains, as we have done in the example above. In such case, the interface spaces are made up of functions that are constant on each interface Γ_{ij}. Let us write the interface fields as linear combinations of the basis functions

$$P_H=\sum_{k=1}^{N_P}P_k\,\psi_k,\quad U_H=\sum_{k=1}^{N_U}U_k\,\phi_k. \tag{4.15}$$

This leads to the linear system of equations to be satisfied by the vector of interface unknown coefficients $\underline{X}=(P_1,\ldots,P_{N_P},U_1,\ldots,U_{N_U})^\intercal$. This system consists of two blocks of rows and columns

$$\underline{\underline{A}}\,\underline{X}=\underline{b}\rightarrow\begin{bmatrix} A^{PP} & A^{PU} \\ A^{UP} & A^{UU}\end{bmatrix}\begin{bmatrix}\underline{P}\\ \underline{U}\end{bmatrix}=\begin{bmatrix}\underline{b}^P\\ \underline{b}^U\end{bmatrix}. \tag{4.16}$$

The first block of rows is obtained by taking $\psi=\psi_\ell,\ \ell=1,\ldots,N_P$ in the first equation of (4.9), i.e.,

$$\begin{aligned} &\sum_{i=1}^{N}\int_{\partial\Omega_i\cap\Gamma}\left(\mathbf{u}_h^i\cdot\check{\mathbf{n}}^i\right)\psi_\ell=\sum_{\substack{ij\\ i<j}}\int_{\Gamma_{ij}}\left(\mathbf{u}_h^i\cdot\check{\mathbf{n}}^i+\mathbf{u}_h^j\cdot\check{\mathbf{n}}^j\right)\psi_\ell= \\ &=\sum_{\substack{ij\\ i<j}}\int_{\Gamma_{ij}}\left[\left(\hat{\mathbf{u}}_h^i(P_H,U_H)+\bar{\mathbf{u}}_h^i\right)\cdot\check{\mathbf{n}}^i+\left(\hat{\mathbf{u}}_h^j(P_H,U_H)+\bar{\mathbf{u}}_h^j\right)\cdot\check{\mathbf{n}}^j\right]\psi_\ell= \\ &=\sum_{\substack{ij\\ i<j}}\int_{\Gamma_{ij}}\left(\hat{\mathbf{u}}_h^i(P_H,U_H)-\hat{\mathbf{u}}_h^j(P_H,U_H)\right)\cdot\check{\mathbf{n}}\,\psi_\ell+\sum_{\substack{ij\\ i<j}}\int_{\Gamma_{ij}}\left(\bar{\mathbf{u}}_h^i-\bar{\mathbf{u}}_h^j\right)\cdot\check{\mathbf{n}}\,\psi_\ell=0, \end{aligned} \tag{4.17}$$

where we have emphasized the dependence of $\hat{\mathbf{u}}_h^i$ with respect to (P_H,U_H) and omitted the

differential $d\Gamma$ for conciseness. Using (4.15) we obtain

$$\sum_{k=1}^{N_P} P_k \underbrace{\sum_{\substack{ij\\ i<j}} \int_{\Gamma_{ij}} \mathscr{J}_{ij}(\hat{\mathbf{u}}_h(\psi_k,0))\,\psi_\ell}_{A^{PP}_{\ell k}} + \sum_{k=1}^{N_U} U_k \underbrace{\sum_{\substack{ij\\ i<j}} \int_{\Gamma_{ij}} \mathscr{J}_{ij}(\hat{\mathbf{u}}_h(0,\phi_k))\,\psi_\ell}_{A^{PU}_{\ell k}} =$$
$$= \underbrace{-\sum_{\substack{ij\\ i<j}} \int_{\Gamma_{ij}} \mathscr{J}_{ij}(\bar{\mathbf{u}}_h)\,\psi_\ell}_{b^P_\ell}, \tag{4.18}$$

where the symbol $\mathscr{J}_{ij}(\cdot)$ stands for the jump operator at Γ_{ij} and is defined for any vector field $\mathbf{v}$ as $\mathscr{J}_{ij}(\mathbf{v}) = (\mathbf{v}^i - \mathbf{v}^j)\cdot\check{\mathbf{n}}$. The second block of rows is obtained similarly by taking $\phi = \phi_\ell$, $\ell = 1,\ldots,N_U$ in the second equation of (4.9), i.e.,

$$\begin{aligned}
&\sum_{i=1}^{N} \int_{\partial\Omega_i\cap\Gamma} \beta_i \left(\mathbf{u}^i_h\cdot\check{\mathbf{n}}^i - U_H\,\check{\mathbf{n}}^i\cdot\check{\mathbf{n}}\right)\phi_\ell\,\check{\mathbf{n}}^i\cdot\check{\mathbf{n}} = \\
&= \sum_{\substack{ij\\ i<j}} \int_{\Gamma_{ij}} \left(\beta_i\,\mathbf{u}^i_h + \beta_j\,\mathbf{u}^j_h\right)\cdot\check{\mathbf{n}}\,\phi_\ell - \sum_{\substack{ij\\ i<j}} \int_{\Gamma_{ij}} \left(\beta_i+\beta_j\right) U_H\,\phi_\ell = \\
&= \sum_{\substack{ij\\ i<j}} \int_{\Gamma_{ij}} \left(\beta_i\,\hat{\mathbf{u}}^i_h(P_H,U_H) + \beta_j\,\hat{\mathbf{u}}^j_h(P_H,U_H)\right)\cdot\check{\mathbf{n}}\,\phi_\ell + \\
&+ \sum_{\substack{ij\\ i<j}} \int_{\Gamma_{ij}} \left(\beta_i\,\bar{\mathbf{u}}^i_h + \beta_j\,\bar{\mathbf{u}}^j_h\right)\cdot\check{\mathbf{n}}\,\phi_\ell - \sum_{\substack{ij\\ i<j}} \int_{\Gamma_{ij}} \left(\beta_i+\beta_j\right) U_H\,\phi_\ell = 0.
\end{aligned} \tag{4.19}$$

Again, inserting (4.15) yields

$$\begin{aligned}
&\sum_{k=1}^{N_P} P_k \underbrace{\sum_{\substack{ij\\ i<j}} \int_{\Gamma_{ij}} \left(\beta_i\,\hat{\mathbf{u}}^i_h(\psi_k,0) + \beta_j\,\hat{\mathbf{u}}^j_h(\psi_k,0)\right)\cdot\check{\mathbf{n}}\,\phi_\ell}_{A^{UP}_{\ell k}} + \\
&+ \sum_{k=1}^{N_U} U_k \underbrace{\sum_{\substack{ij\\ i<j}} \int_{\Gamma_{ij}} \left[\left(\beta_i\,\hat{\mathbf{u}}^i_h(0,\phi_k) + \beta_j\,\hat{\mathbf{u}}^j_h(0,\phi_k)\right)\cdot\check{\mathbf{n}} - \left(\beta_i+\beta_j\right)\phi_k\right]\phi_\ell}_{A^{UU}_{\ell k}} \\
&= \underbrace{-\sum_{\substack{ij\\ i<j}} \int_{\Gamma_{ij}} \left(\beta_i\,\bar{\mathbf{u}}^i_h + \beta_j\,\bar{\mathbf{u}}^j_h\right)\cdot\check{\mathbf{n}}\,\phi_\ell}_{b^U_\ell}.
\end{aligned} \tag{4.20}$$

Remark 5. Two remarks can be made about (4.18) and (4.20):

i. The functions $\hat{\mathbf{u}}^i_h(\psi_k,0)$ and $\hat{\mathbf{u}}^i_h(0,\phi_k)$ are the solutions to the subdomain problems (4.14) taking as Robin boundary data $(P_H,U_H) = (\psi_k,0)$ and $(P_H,U_H) = (0,\phi_k)$, respectively. These are, in fact, the so called multiscale basis functions that we have described before in (GUIRALDELLO *et al.*, 2018b).

ii. Although not necessary, in this article each of the basis functions ψ_l and ϕ_ℓ that span $\mathscr{P}_H$ and $\mathscr{U}_H$ is chosen to have as support one single interface Γ_{ij} of the mesh skeleton Γ, greatly simplifying the system assembly and leading to a sparse matrix $\underline{\underline{A}}$. Moreover, such choice for the space $\mathscr{P}_H$ allows us to obtain a conservative solution at the coarse scale H for $\beta < +\infty$, a fact easily verified through expression (4.18).

4.3 The velocity postprocessing schemes

First, let us recall that the multiscale solutions produced by the MRCM are mass-conserving at the coarse scale of the domain decomposition, i.e., for each interface Γ_{ij} between subdomains Ω_i and Ω_j, it holds

$$\int_{\Gamma_{ij}} \left(\mathbf{u}_h^i \cdot \check{\mathbf{n}} - \mathbf{u}_h^j \cdot \check{\mathbf{n}} \right) = 0, \ \forall\, i, j. \tag{4.21}$$

The solution is, however, discontinuous at the fine level, except when the algorithmic parameter α is taken very large as we have illustrated (see Figure 33). Some postprocessing or downscaling procedure on the velocity field becomes thus essential if transport of any quantity such as a fluid saturation or the concentration of a passive tracer is to be solved. A natural and simple way to deal with such discontinuous field is to take the average value of the two-sided solution at the interfaces between subdomains so as to define a unique flux on the fine grid over the skeleton of the domain decomposition. Given the multiscale solutions $\mathbf{u}_h^i$, $i = 1, \ldots, N$, this amounts to computing in a first step for each Γ_{ij} a new interface field defined as

$$\bar{\mathbf{U}}_h^{ij} \doteq \frac{1}{2} \left(\mathbf{u}_h^i|_{\Gamma_{ij}} + \mathbf{u}_h^j|_{\Gamma_{ij}} \right). \tag{4.22}$$

Notice that the new velocity $\bar{\mathbf{U}}_h^{ij}$ transfers the same mass through the interfaces as the two-sided multiscale solution, i.e.,

$$\int_{\Gamma_{ij}} \mathbf{u}_h^i \cdot \check{\mathbf{n}} = \int_{\Gamma_{ij}} \mathbf{u}_h^j \cdot \check{\mathbf{n}} = \int_{\Gamma_{ij}} \bar{\mathbf{U}}_h^{ij} \cdot \check{\mathbf{n}}. \tag{4.23}$$

Once the flux values on every Γ_{ij} are updated, we proceed to the second step: for each subdomain Ω_i, solve

$$\begin{cases} \widetilde{\mathbf{u}}_h^i &= -K \nabla \widetilde{p}_h^i & \text{in } \Omega_i, \\ \nabla \cdot \widetilde{\mathbf{u}}_h^i &= f & \text{in } \Omega_i, \\ \widetilde{\mathbf{u}}_h^i \cdot \check{\mathbf{n}}^i &= \mathbf{u}_h^i \cdot \check{\mathbf{n}}^i & \text{on } \partial\Omega_i \cap \partial\Omega, \\ \widetilde{\mathbf{u}}_h^i \cdot \check{\mathbf{n}}^i &= \bar{\mathbf{U}}_h^{ik} \cdot \check{\mathbf{n}}^i & \text{on } \Gamma_{ik}, \forall k, \end{cases} \tag{4.24}$$

where index k above runs over all subdomain neighbors to Ω_i. After these two steps we end up with a flux field which is conservative on the fine grid and therefore suitable for transport. We refer to this method as the Mean method. Notice in (4.24) that along $\partial\Omega_i \cap \partial\Omega$ the original velocity multiscale solution is being imposed as boundary condition. This approach is quite simple to implement and relatively cheap. The only operation that involves some additional cost is the solution of subdomain problems (4.24), which can clearly be done in parallel.

The question considered here is whether alternative methods can be designed that have complexity similar to that of the Mean method while exhibiting better accuracy. The aim of this article is precisely to propose two new alternatives to the Mean method, namely, the Patch and the Stitch methods, which are now explained and later on assessed in the results section.

4.3.1 The Patch method

Let us consider oversampling regions around each interface Γ_{ij} covering the skeleton of the domain decomposition. These regions are called patches and they are made up of a collection of fine grid cells of the underlying discretization. In our implementation each one covers one single interface Γ_{ij} and has a thickness in the directions perpendicular to Γ_{ij} tipically formed by 1 to 3 layers of fine cells, as illustrated in Figure 35. Notice, these regions may intersect each other. The idea is to solve local Darcy problems on these patches so as to define a unique velocity

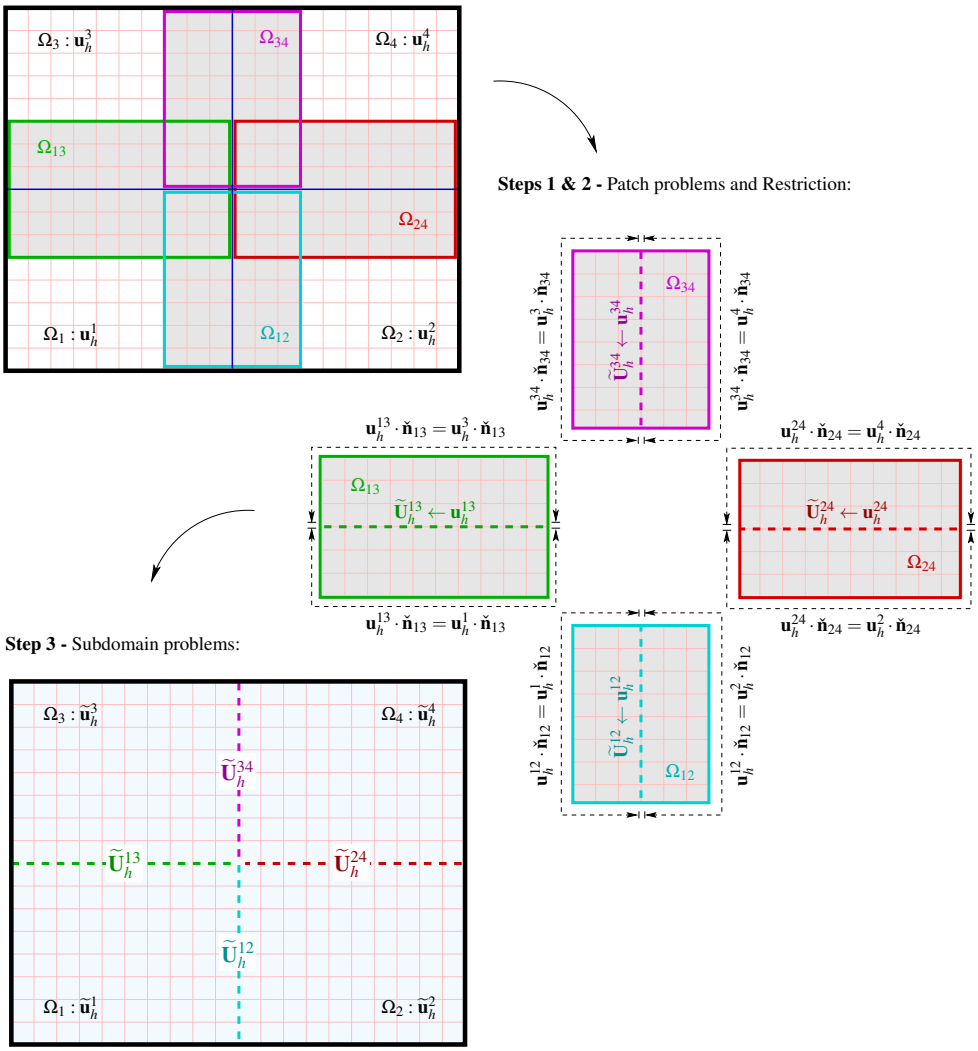

Source: Elaborated by the author.

Figure 35 – The Patch method.

field on each interface Γ_{ij}. The procedure can be divided into three steps:

Step 1 - Patch problems: For each Γ_{ij} define a patch Ω_{ij} that encloses the interface, formed by a collection of fine grid elements of Ω_i and Ω_j and solve:

$$\left\{\begin{array}{rcll} \mathbf{u}_h^{ij} & = & -K\nabla p_h^{ij} & \text{in } \Omega_{ij} \\ \nabla\cdot\mathbf{u}_h^{ij} & = & f & \text{in } \Omega_{ij} \\ \mathbf{u}_h^{ij}\cdot\mathbf{n}_{ij} & = & \left\{\begin{array}{ll} \mathbf{u}_h^{i}\cdot\mathbf{n}_{ij} & \text{if } \mathbf{x}\in\Omega_i \\ \mathbf{u}_h^{j}\cdot\mathbf{n}_{ij} & \text{if } \mathbf{x}\in\Omega_j \end{array}\right. & \text{on } \partial\Omega_{ij} \end{array}\right. , \tag{4.25}$$

where $\mathbf{n}_{ij}$ is the exterior normal vector to $\partial\Omega_{ij}$.

Step 2 - Restriction: For each interface define a new interface field as the restriction of $\mathbf{u}_h^{ij}$ to Γ_{ij}, i.e.,

$$\widetilde{\mathbf{U}}_h^{ij} \doteq \mathbf{u}_h^{ij}|_{\Gamma_{ij}}. \tag{4.26}$$

Step 3 - Subdomain problems: Foreach Ω_i, solve:

$$\left\{\begin{array}{rcll} \widetilde{\mathbf{u}}_h^{i} & = & -K\nabla\widetilde{p}_h^{i} & \text{in } \Omega_i, \\ \nabla\cdot\widetilde{\mathbf{u}}_h^{i} & = & f & \text{in } \Omega_i, \\ \widetilde{\mathbf{u}}_h^{i}\cdot\check{\mathbf{n}}^i & = & \mathbf{u}_h^{i}\cdot\check{\mathbf{n}}^i & \text{on } \partial\Omega_i\cap\partial\Omega, \\ \widetilde{\mathbf{u}}_h^{i}\cdot\check{\mathbf{n}}^i & = & \widetilde{\mathbf{U}}_h^{ik}\cdot\check{\mathbf{n}}^i & \text{on } \Gamma_{ik}, \forall k, \end{array}\right. \tag{4.27}$$

where index k above runs over all subdomain neighbors to Ω_i. This is exactly the same as in (4.24) with $\bar{\mathbf{U}}_h^{ij}$ replaced by $\widetilde{\mathbf{U}}_h^{ij}$. After steps 1-3, we end up with a mass-conserving flux field. The extension to three dimensions is straightforward. One can easily check that the new interface velocity satisfies

$$\int_{\Gamma_{ij}} \mathbf{u}_h^{i}\cdot\check{\mathbf{n}} = \int_{\Gamma_{ij}} \mathbf{u}_h^{j}\cdot\check{\mathbf{n}} = \int_{\Gamma_{ij}} \widetilde{\mathbf{U}}_h^{ij}\cdot\check{\mathbf{n}}, \tag{4.28}$$

since the solutions of the local problems are obtained by a mass-conserving method and satisfies the compatibility condition

$$\int_{\partial\Omega_{ij}} \mathbf{u}_h^{ij}\cdot\mathbf{n}_{ij} = \int_{\Omega_{ij}} f. \tag{4.29}$$

Also notice that problems (4.25) and (4.27) are undefined up to a pressure constant. The indeterminacy is in practice removed by imposing the average pressure field to be zero.

Interestingly, this method can be turned into an iterative scheme by repeating the process and taking in equation (4.25) (in **Step 1**) the last computed $\widetilde{\mathbf{u}}_h^i$ instead of the multiscale solution $\mathbf{u}_h^i$. A few iterations have shown to provide a more accurate result when compared to the fine grid solution, however, based on our numerical experimentation we have concluded the benefit brought by such iterative method does not justify the additional computational cost involved.

In the Mean method, the only necessary operation to define a unique flux at the interfaces is the averaging of the original multiscale flux solution, whereas in the Patch method this is acomplished by executing **Steps 1** and **2**, that obviously involve an additional cost. However, the

local patch problems are in general small as compared to the subdomain problems, whose resolution is part of both methods and dominates the overall computational cost of the downscaling procedures. All these tasks can always be executed efficiently in parallel.

4.3.2 The Stitch method

We propose another method based on the idea of solving local problems on patches around the interfaces of the domain decomposition. Informally speaking, in this method, instead of recomputing the solutions over the subdomains, we simply “stitch" the local patch solutions to the global multiscale solution. In order to proceed we must first distinguish two situations: (i) Overlapping patches; and (ii) Non-overlapping patches. The first case, is the one to be adopted if using non-simplicial grids for discretization in the subdomains, as is the case in our implementation that uses rectangular cartesian grids. The second case is feasible when using simplicial grids for discretization. These two situations are illustrated in Figure 36.

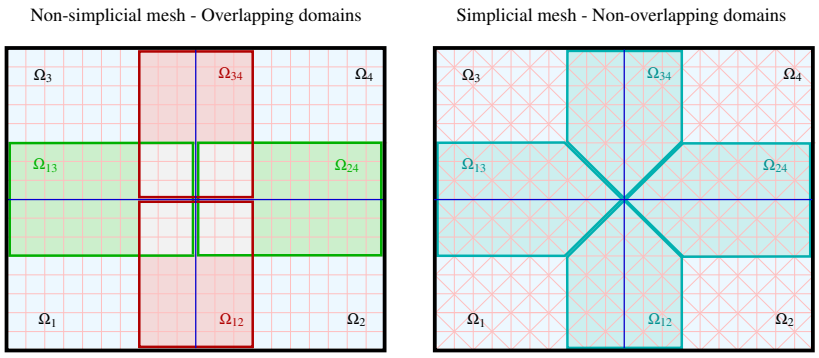

Source: Elaborated by the author.

Figure 36 – Examples of patch definitions for the Stitch method. Overlapping domains with non-simplicial mesh (left) and non-overlapping domains with simplicial mesh (right).

Let us consider the first case of overlapping patches. In such case, in order to produce a mass-conserving solution, the local patches need to be separated into disjoint sets. This can in principle be done in an arbitrary way. In our implementation, for the sake of simplicity we separate into two sets: the sets of horizontal and vertical patches, as displayed in Figure 37. In this case, the downscaling method proceeds as follows:

Step 1 - Horizontal patch problems: For each horizontal interface Γ_{ij} define a patch Ω_{ij}^{H} that encloses the interface, formed by a collection of fine grid elements of Ω_i and Ω_j and solve:

$$\begin{cases} \mathbf{u}_h^{ij,\mathrm{H}} = -K\nabla p_h^{ij,\mathrm{H}} & \text{in } \Omega_{ij}^{\mathrm{H}} \\ \nabla\cdot\mathbf{u}_h^{ij,\mathrm{H}} = f & \text{in } \Omega_{ij}^{\mathrm{H}} \\ \mathbf{u}_h^{ij,\mathrm{H}}\cdot\mathbf{n}_{ij} = \begin{cases} \mathbf{u}_h^{i}\cdot\mathbf{n}_{ij} & \text{if } \mathbf{x}\in\Omega_i \\ \mathbf{u}_h^{j}\cdot\mathbf{n}_{ij} & \text{if } \mathbf{x}\in\Omega_j \end{cases} & \text{on } \partial\Omega_{ij}^{\mathrm{H}} \end{cases}, \tag{4.30}$$

where $\mathbf{n}_{ij}$ is exterior normal vector to $\partial\Omega_{ij}^{\mathrm{H}}$.

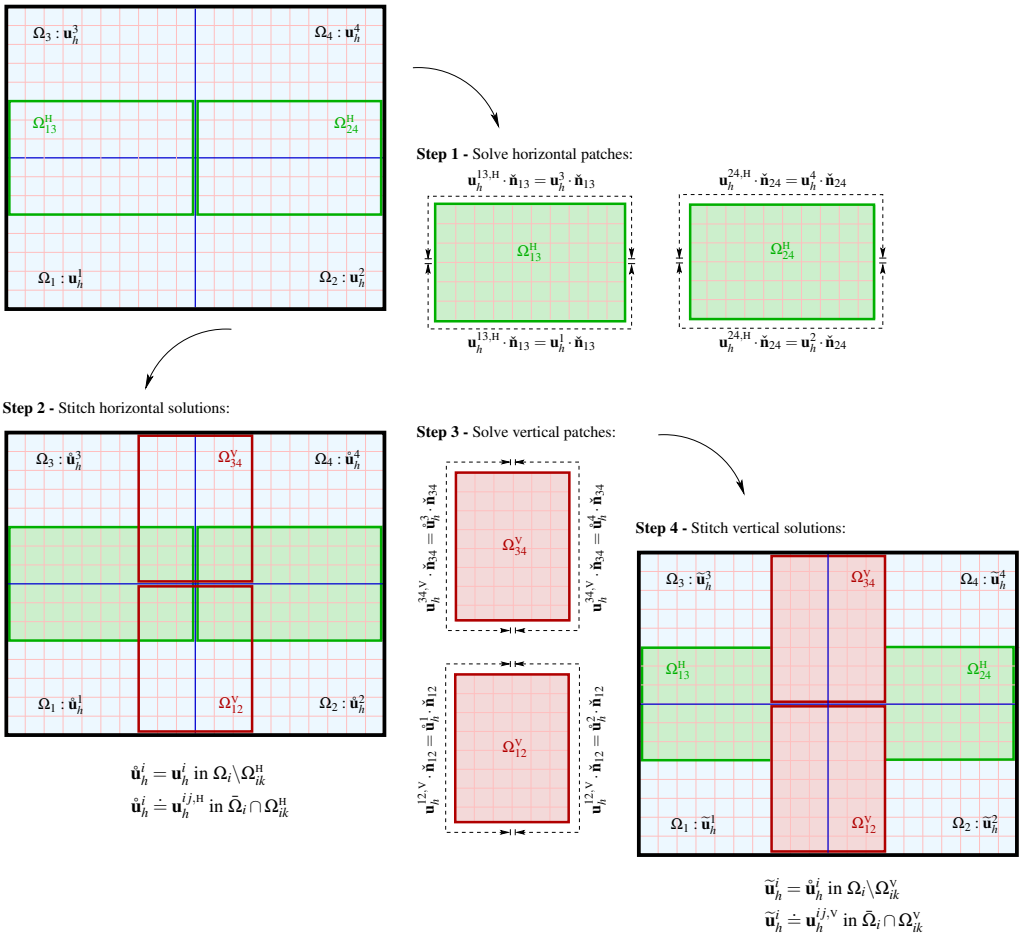

Source: Elaborated by the author.

Figure 37 – The Stitch method.

Step 2 - Stitch horizontal solutions: For each subdomain Ω_i, take:

$$\begin{aligned} \mathring{\mathbf{u}}_h^i &\doteq \mathbf{u}_h^i \text{ in } \Omega_i \backslash \Omega_{ik}^{\mathrm{H}}, \\ \mathring{\mathbf{u}}_h^i &\doteq \mathbf{u}_h^{ij,\mathrm{H}} \text{ in } \bar{\Omega}_i \cap \Omega_{ik}^{\mathrm{H}}, \end{aligned} \quad \forall k \tag{4.31}$$

where index k runs over all horizontal patches that intersect with Ω_i.

Step 3 - Vertical patch problems: For each vertical interface Γ_{ij} define a patch Ω_{ij}^{V} that encloses the interface, formed by a collection of fine grid elements of Ω_i and Ω_j and solve:

$$\left\{ \begin{array}{rcll} \mathbf{u}_h^{ij,\mathrm{V}} & = & -K\nabla p_h^{ij,\mathrm{V}} & \text{in } \Omega_{ij}^{\mathrm{V}} \\ \nabla \cdot \mathbf{u}_h^{ij,\mathrm{V}} & = & f & \text{in } \Omega_{ij}^{\mathrm{V}} \\ \mathbf{u}_h^{ij,\mathrm{V}} \cdot \mathbf{n}_{ij} & = & \left\{ \begin{array}{ll} \mathring{\mathbf{u}}_h^i \cdot \mathbf{n}_{ij} & \text{if } \mathbf{x} \in \Omega_i \\ \mathring{\mathbf{u}}_h^j \cdot \mathbf{n}_{ij} & \text{if } \mathbf{x} \in \Omega_j \end{array} \right. & \text{on } \partial\Omega_{ij}^{\mathrm{V}} \end{array} \right. , \tag{4.32}$$

Step 4 - Stitch vertical solutions: For each subdomain Ω_i, take:

$$\begin{aligned} \widetilde{\mathbf{u}}_h^i &\doteq \mathring{\mathbf{u}}_h^i \text{ in } \Omega_i \backslash \Omega_{ik}^{\mathrm{V}}, \\ \widetilde{\mathbf{u}}_h^i &\doteq \mathbf{u}_h^{ij,\mathrm{V}} \text{ in } \bar{\Omega}_i \cap \Omega_{ik}^{\mathrm{V}}, \end{aligned} \quad \forall k \tag{4.33}$$

where index k runs over all vertical patches that intersect with Ω_i. After steps 1-4 we end up with a velocity field $\widetilde{\mathbf{u}}_h^i$ which is mass-conserving on the fine grid and continuous at subdomain interfaces. The extension to three dimensions is straightforward.

In the second aforementioned situation of non-overlapping patches the computation can be done all at once, i.e., in a first step all patches are solved simultaneously and, in a second step, the solutions are stitched in order to produce a mass-conserving global solution. This last case has not been implemented and its assessment is left for future works.

This method is perhaps the most attractive one in regards to computational cost, since it does not require solution of the subdomain problems, but only resolution of local small patch problems around the interfaces.

4.4 Numerical set-up

In order to compare the downscaling schemes under the same conditions we consider the transport of a passive tracer in highly heterogeneous permeability fields $K(\mathbf{x})$. Two types of absolute permeability fields are considered here, the first being the log-normal, $K(\mathbf{x}) = \exp(\gamma\xi(\mathbf{x}))$, in which $\xi(\mathbf{x})$ is a Gaussian field and γ a constant value chosen that controls the contrast, i.e., $K_{\max}/K_{\min}$. Here, $\xi(\mathbf{x})$ is characterized by its mean value μ_ξ and an exponential anisotropic covariance function given by

$$C_\xi(\mathbf{r}) = \sigma_\xi^2 e^{(-\mathbf{r})},$$

where σ_ξ is a constant variance and $\mathbf{r} = \sqrt{r_1^2/I_x + r_2^2/I_y}$ with I_x and I_y being correlation lengths and r_1 and r_2 the two-point separation distance in longitudinal and transverse direction, respectively. To generate these log-conductivity fields we have used the Hydro-Gen package (BELLIN; RUBIN, 1996). The second type considered are the layers of the SPE10 project that is highly heterogeneous and presents channelized structures.

In all the numerical experiments the domain is a 2D region $\Omega = [0, L_x] \times [0, L_y]$. For the Darcy problem no-flow boundary conditions are considered at $y = 0$ and $y = L_y$ and inflow-outflow boundary conditions are imposed at $x = 0$ and $x = L_x$, respectively.

For the MRCM we have considered piecewise polynomial functions both for the pressure space $\mathscr{P}_H$ and for the flux space $\mathscr{U}_H$. In fact, we use elementwise constant fine grid representation of polynomials over the interface elements

$$\begin{aligned}
\mathscr{U}_H &= \{V_H,\ V_H|_e = \Pi_0(q), q \in \mathbb{P}_{k_U-1}(e),\ e \in \mathscr{T}_H\},\\
\mathscr{P}_H &= \{M_H,\ M_H|_e = \Pi_0(q), q \in \mathbb{P}_{k_P-1}(e),\ e \in \mathscr{T}_H\},
\end{aligned}$$

where $\mathbb{P}_l$, is the space of polynomials of degree $\leq l$ and Π_0 is the L^2–projection of a function $\mathbb{P}_l(e)$ onto the space $F_h(e),\ e \in \mathscr{T}_H$. In the numerical results section the experiments are performed

by choosing a total number of degrees of freedom per interface $k = k_U + k_P$. Although not mandatory, this number will be the same for all interfaces. Also, for simplicity, the number of fine grid elements per interface N_f is chosen to be the same for all interfaces. In such case the order reduction obtained by our multiscale method is simply computed as $100 \times (N_f - k)/N_f$.

For the transport problem we assume a water saturated field ($\mathscr{C}(\mathbf{x}, t_0) = 0, \mathbf{x} \in \Omega$) with a passive tracer injected on $x = 0$ at time $t = t_0$, carried by the flow for $t > t_0$. In order to solve the transport equation a classical upwind scheme combined with a TVD Runge-Kutta of second order in time is adopted for discretization. Let us provide some details about the scheme. Given the fine grid partition $\mathscr{T}_h$ of Ω, a cell-centered finite volume scheme is considered for the concentration unknowns. For each fine grid element of $\mathscr{T}_h$, V_i, $i = 1, \ldots, m$, the discrete concentration field $\mathscr{C}_h$ satisfies

$$\frac{d}{dt} \int_{V_i} \mathscr{C}_h \, dV = - \sum_{E \in \partial V_i} \int_E \mathscr{C}_h|_E \, \widetilde{\mathbf{u}}_h \cdot \nu \, dS, \tag{4.34}$$

where $\widetilde{\mathbf{u}}_h$ is the postprocessed multiscale velocity field, which is already given at the edges of V_i and ν is the outer normal to ∂V_i. As mentioned, for the edge concentration $\mathscr{C}_h|_E$ the upwind value is taken. This leads to the semi-discrete system

$$\frac{d}{dt} \underline{C} = \mathscr{F}(\underline{C}),$$

where $\underline{C} \in \mathbb{R}^m$ and $C_i = \frac{1}{|V_i|} \int_{V_i} \mathscr{C}_h \, dV$. Applying a TVD Runge-Kutta scheme of second order ((GOTTLIEB; SHU, 1998)) a fully-discrete system is obtained. Defining the time step δt, the unknown vector at time level $n+1$ is obtained from

$$\underline{C}^{(n+1)} = \frac{1}{2} \underline{C}^n + \frac{1}{2} \underline{C}^* + \frac{1}{2} \, \delta t \, \mathscr{F}(\underline{C}^*), \tag{4.35}$$

where

$$\underline{C}^* = \underline{C}^n + \delta t \, \mathscr{F}(\underline{C}^n). \tag{4.36}$$

4.5 Numerical Results

We begin this section by assessing the coupling between the multiscale solution of the MRCM and the postprocessing schemes. Two types of domain decomposition are considered in combination with different interface spaces. These results allow us to define the MRCM parameters and evaluate the error produced by increasing the size of the patches in the postprocessing schemes. Based on these results, we choose a patch size and repeat the previous experiment for a collection of permeability fields with the same covariance function as well as for permeability fields taken from the SPE10 project. From these we obtain some metrics for the error of the schemes. Finally, we evaluate the error and the convergence order of downscaling schemes coupled with the MMMFEM, the MHM, and the MRCM with enriched interface spaces for permeability fields with and without channel structures.

In this section the downscaling methods are assessed in terms of the $L^2(\Omega)$ relative error norm of the tracer concentration, defined as

$$E_c(\tilde{t}) = \frac{\|\mathscr{C}_{msc}(\mathbf{x},\tilde{t}) - \mathscr{C}_{fine}(\mathbf{x},\tilde{t})\|_{L^2(\Omega)}}{\|\mathscr{C}_{fine}(\mathbf{x},\tilde{t})\|_{L^2(\Omega)}},$$

in which $\mathscr{C}_{msc}(\mathbf{x},t)$ is the result obtained by using the postprocessed flux multiscale solution and $\mathscr{C}_{fine}(\mathbf{x},t)$ is the result obtained by using the fine grid flux solution.

4.5.1 First approach

We start by considering a domain Ω with dimensions $L_x = L_y = 1$ and square fine elements of size $h = 1/120$. For the absolute permeability field $K(\mathbf{x}) = \exp(\gamma\xi(\mathbf{x}))$, we set $\xi(\mathbf{x})$ with $I_x = 5 \times h$, $I_y = 12 \times h$, $\mu_\xi = 0$ and $\sigma_\xi = 1$ and take $\gamma = 2$, leading to a contrast of order $K_{max}/K_{min} \simeq 10^6$. The domain is decomposed into 4×4 and 8×8 square subdomains of size $H = 30h$ and $H = 15h$, respectively. For the interface spaces we have considered $k = 2,3,4$. Table 2 displays the order reduction obtained by the multiscale method for the above cases.

	# of dof's per interface k		
	2	3	4
4×4	93.3%	90.0%	86.7%
8×8	86.7%	80.0%	73.3%

Table 2 – Order reduction for the multiscale solutions of the first numerical experiment.

Source: Elaborated by the author.

The degrees of freedom (*dof's*) are distributed in the possible combinations such that $k_P + k_U = k$ and the patches' thicknesses are taken as two fine elements in the downscaling schemes. The transport equation is solved with $\delta t = 10^{-5}$, that satisfies a CFL condition for all the problems considered here, from $t_0 = 0$ to $t_{MAX} = 1$. Figure 38 displays the concentration transported by the fine solution and the concentration transported by the multiscale solution with $k = 2$ and the downscaling schemes at time $t = 0.5$ for the 4×4 decomposition. The relative errors from t_0 to t_{MAX} are shown in Figure 39. One can note in the considered cases that the Patch scheme consistently has the smallest errors when compared to the other two schemes. Also, the Stitch scheme presents larger errors when the multiscale method has $k_P = k_U = 1$ for the 4×4 domain decomposition and $k_U > k_P$ and presents similar errors to the Mean scheme in all other cases.

From our experience, the precision of the postprocessing schemes depends on the accuracy of the multiscale solution. With this observed we set the MRCM with $k_P = k_U = 2$ and a 4×4 domain decomposition, where the schemes have similar errors and the multiscale solution has a reduced computational cost, to further assess the downscaling schemes.

Now we evaluate the impact of the patch thickness on the error of the Patch and Stitch schemes. We take the problem defined above and increase the thickness from 2 fine elements to

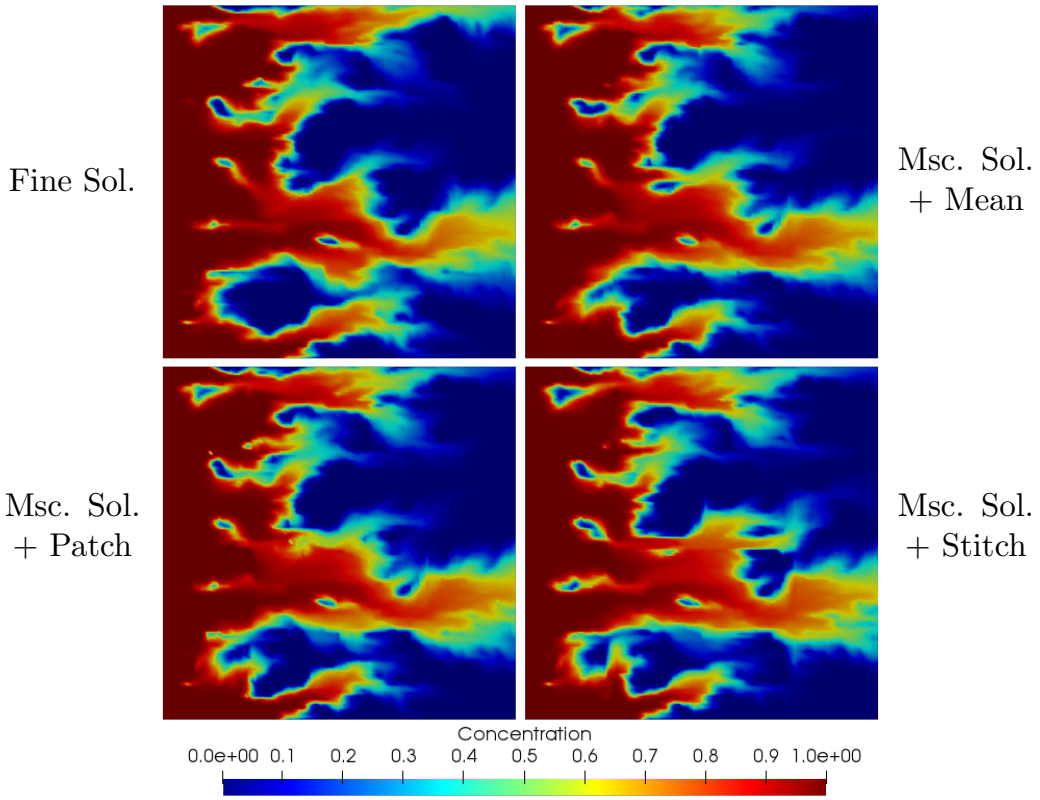

Source: Elaborated by the author.

Figure 38 – Concentration at time $t = 0.5$ for the fine solution and multiscale solution with $k = 2$.

10 fine elements. Results are shown in Figure 40. Larger patches lead to smaller errors in both schemes, but the gain in accuracy is not significant after about 6 fine elements. To keep the patch problems small relative to the subdomain problems, we set patches with 4 elements.

Figure 41 displays the relative error of the flux field for the multiscale solution and the relative errors after the postprocessing schemes. As is well known, multiscale methods based on non-overlapping domain decomposition have larger errors at the interfaces between subdomains, where the coupling is done through low order spaces, as shown in the left top of Figure 41. From this experiment we observed that the Mean scheme, despite generating a continuous field, maintains existing errors at the interfaces. The scenario is different for the Patch and Stitch schemes, in which the patches include information from within the subdomains. The errors are greatly reduced at the interfaces and only remain concentrated at the corners of the domain decomposition.

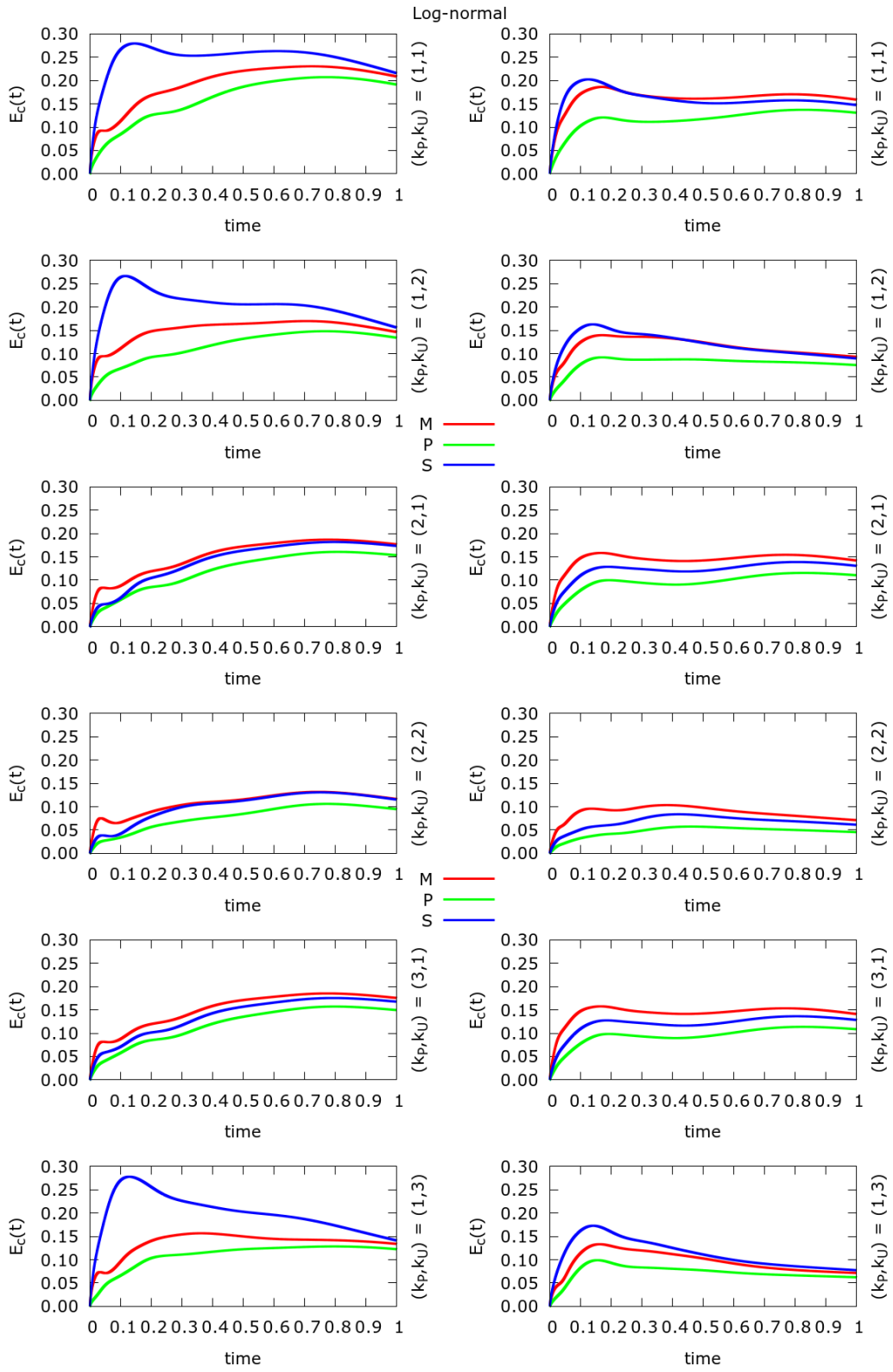

Source: Elaborated by the author.

Figure 39 – Relative concentration errors for $k = 2, 3, 4$ and two domain decomposition: 4×4 (left column) and 8×8 (right column) for the downscaling schemes, the Mean (red line), the Patch (green line) and the Stitch (blue line).

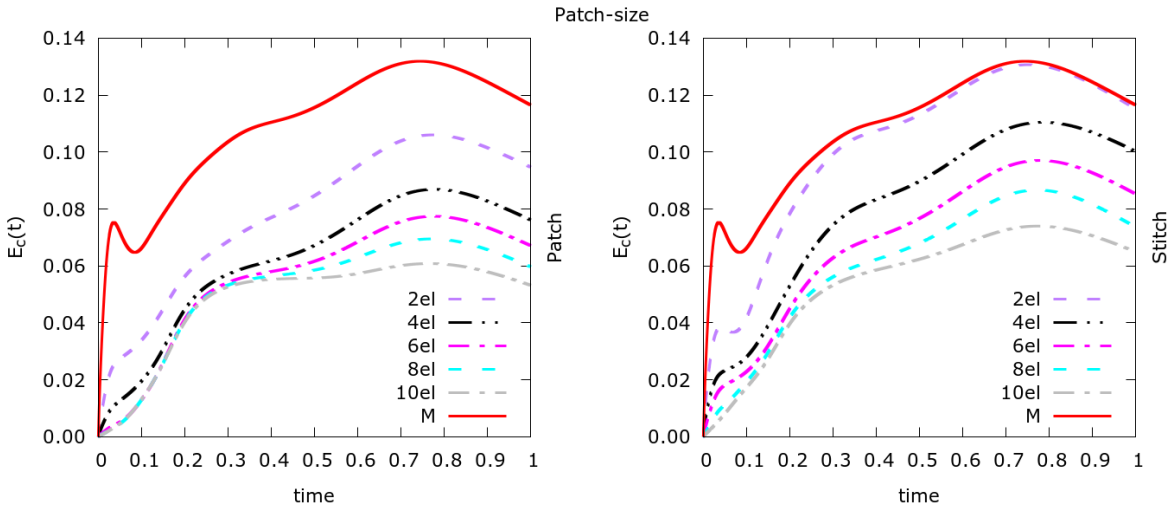

Source: Elaborated by the author.

Figure 40 – Relative errors of the Patch (left) and the Stitch (right) for different patch sizes and the relative error of the Mean scheme (red line).

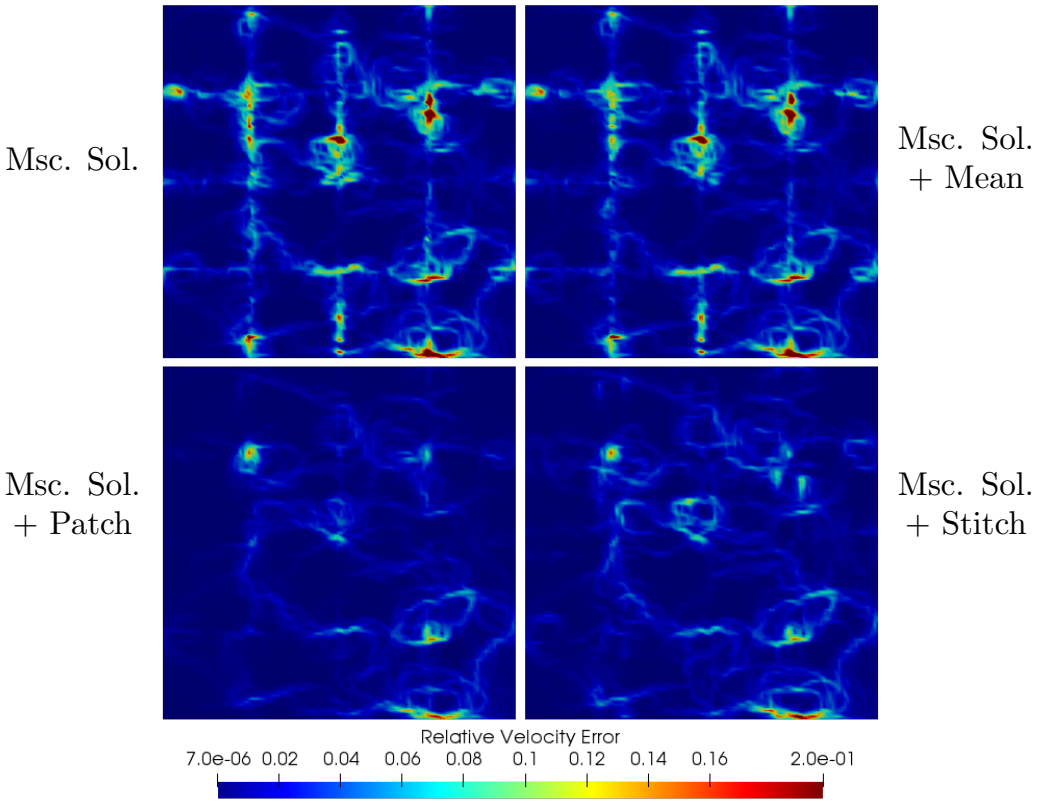

Source: Elaborated by the author.

Figure 41 – Relative velocity field error to the maximum absolute velocity value of the fine solution w/o downscaling.

4.5.2 Robustness

To check the robustness of the downscaling schemes we generate new log-conductivity fields, $\xi_j(\mathbf{x}), j = 1,\ldots,100$, with the same properties described in the last section for different seeds, thus generating fields with similar structures distributed in spatially distinct patterns. With that we define new permeability fields $K_j(\mathbf{x})$, also taking $\gamma = 2$ and redo the last experiment from the previous section for each $j = 1,\ldots,100$. In Figure 42 we show some examples of these fields. Figure 43 displays the mean error of all these simulations for each time t as well as the

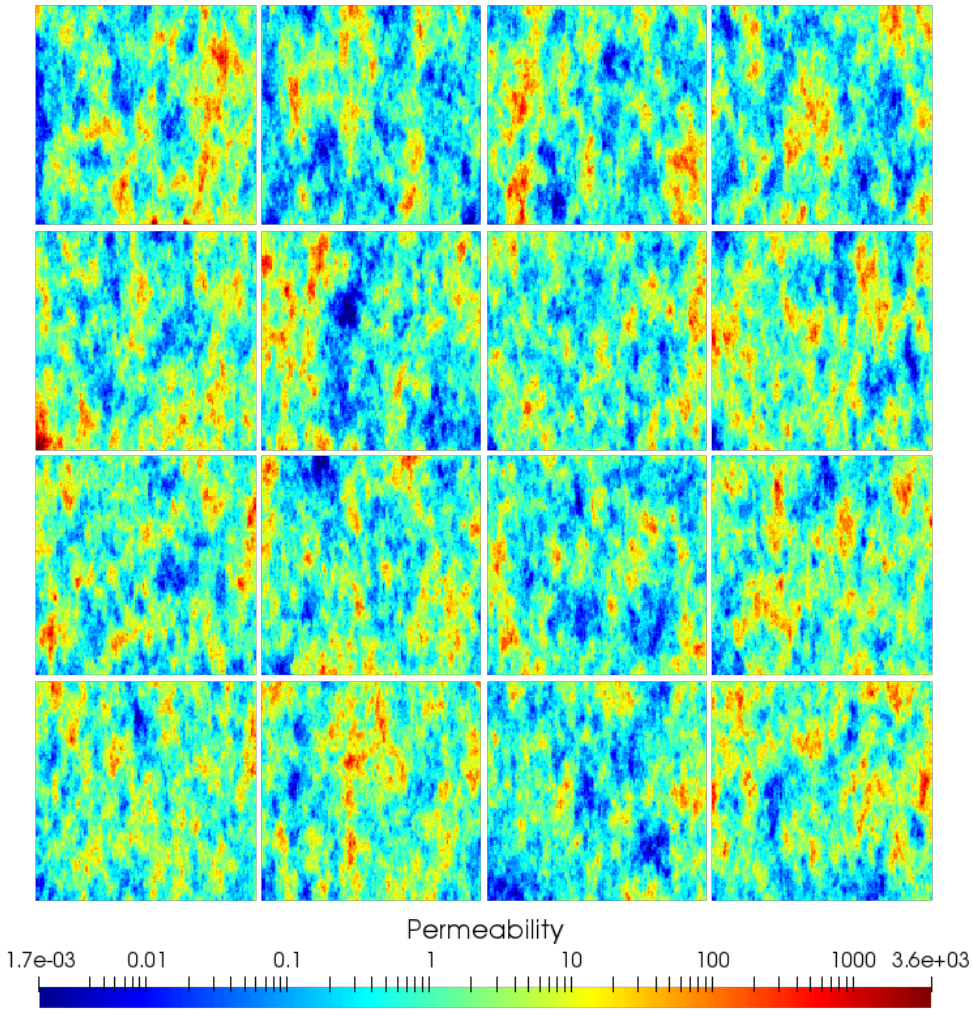

Source: Elaborated by the author.

Figure 42 – Examples of permeability fields generated by the log-conductivity functions with different seeds.

maximum and minimum errors and the maximum standard deviation over all the time steps.

The Patch scheme still displays smaller errors than the other two schemes for all error measures. Similar errors in average for the Stitch and the Mean schemes are observed, although the Stitch has larger maximum errors and a standard deviation almost 1.5 times larger than the other schemes.

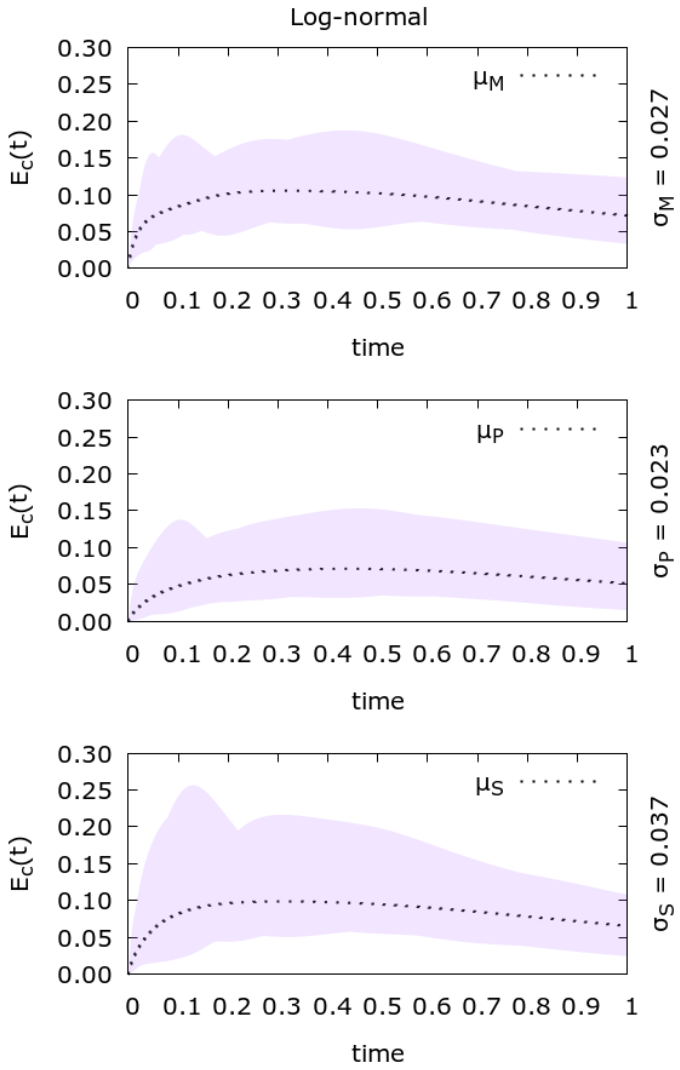

Source: Elaborated by the author.

Figure 43 – Relative mean error μ at each time t for the permeability fields $K_j(\mathbf{x}), j = 1,\ldots,100$, and the maximum standard deviation σ over t. Shaded area denotes the maximum and minimum error region.

For the next numerical experiment we take 2D layers of the SPE10 project (CHRISTIE; BLUNT, 2001) as permeability fields in a rectangular domain with dimensions $L_x = 11/3$ and $L_y = 1$. There are 85 highly heterogeneous layers in the SPE10 project. Layers 1 to 35 have structures similar to those of the fields previously explored and layers 36 to 85 have high correlation channels that pose realistic challenges and are commonly used for the evaluation of numerical methods in oil reservoir simulation. In Figure 44 we show two examples of these layers, with and without channel structures.

These fields are defined in a fine mesh with 220×60 elements. For the multiscale method the domain is decomposed into 11×3 subdomains, each one with a fine mesh of 20×20 square elements of size $h = 1/60$. In this case the order reduction of the multiscale method is 80%. Figure 45 shows the solution of the transport equation at the breakthrough time for the fine

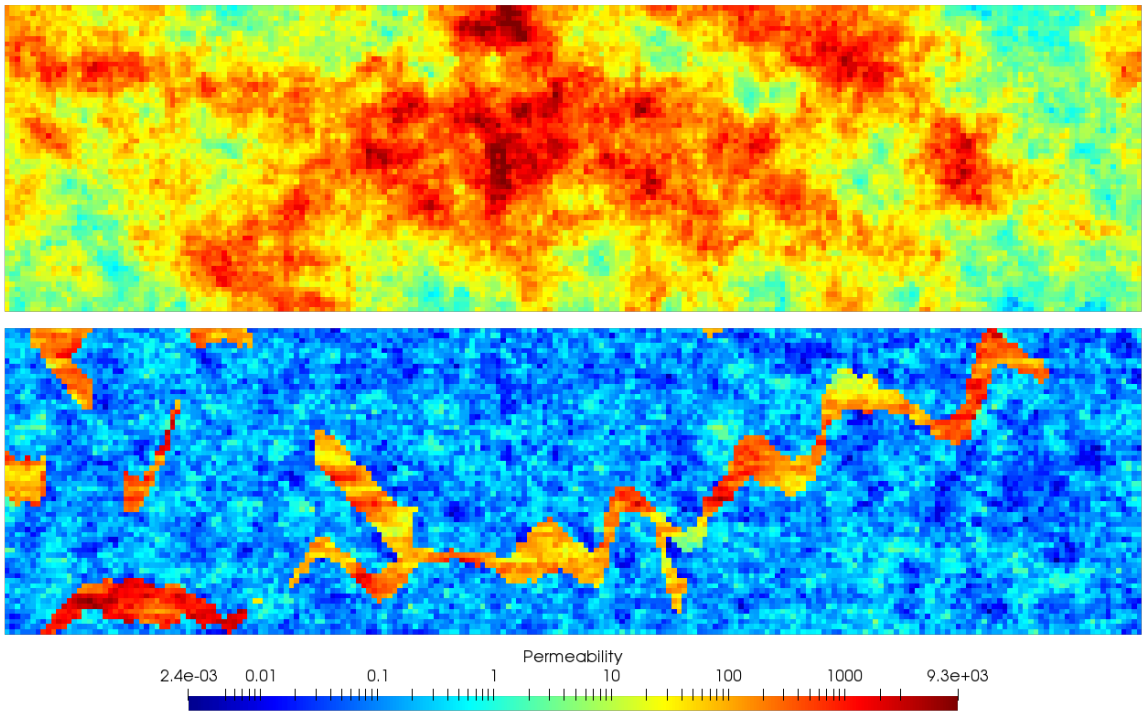

Source: Elaborated by the author.

Figure 44 – Examples of permeability fields from SPE10 project: layer 20 (top) and layer 36 (bottom).

solution and for the multiscale solution with the Stitch scheme. Figure 46 shows the maximum relative error among all time steps, t_o to t_{MAX} for each layer.

By looking at the concentration error it is easy to note the transition from layers without channels, where errors stay between 5% and 10%, to layers with channels, where errors range from 10% to 30%, as displayed in Figure 46. For the downscaling schemes, the Patch shows the smallest errors and the Stitch provides intermediate errors between the Patch and Mean for all layers, although the errors for layers with channelized structures are similar. In Table 3 we show the mean error and the standard deviation for the cases with and without channels.

	Layers ≤ 35		Layers ≥ 36	
	μ	σ	μ	σ
Patch	0.0330	0.0104	0.1245	0.0479
Stitch	0.0488	0.0137	0.1438	0.0486
Mean	0.0855	0.0170	0.1958	0.0467

Table 3 – Mean μ errors and the standard deviation σ of the SPE10 layers.

Source: Elaborated by the author.

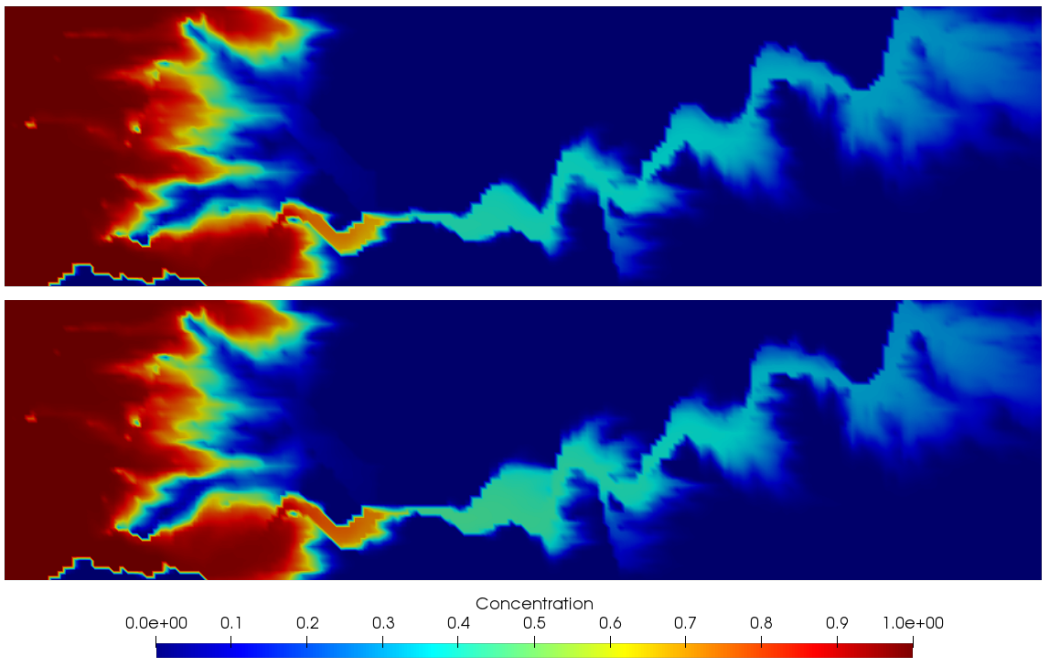

Source: Elaborated by the author.

Figure 45 – Concentrations at breakthrough time for the fine solution (top) and the multiscale solution with $k = 4$ and the Stitch scheme (bottom) for layer 36.

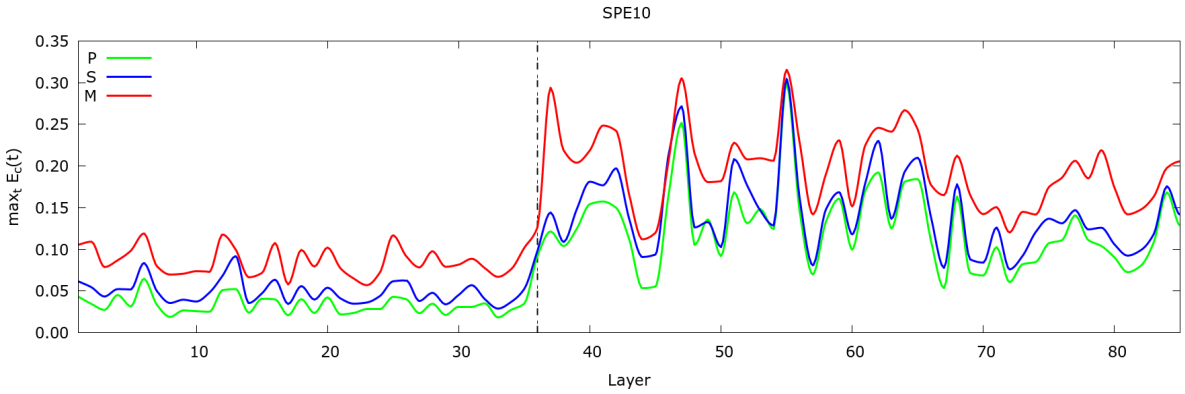

Source: Elaborated by the author.

Figure 46 – Maximum relative error over t of the downscaling schemes, the Mean (red line), the Patch (green line) and the Stitch (blue line) for all layers of the SPE10 project. The dashed line indicates where the layers with channels begins.

4.5.3 Comparison of multiscale methods

As mentioned earlier, the MRCM generalizes a family of multiscale methods and among them are the MMMFEM ($\beta = 0$) and the MHM ($\beta \to +\infty$). Taking advantage of this fact, we now compare the concentration errors of the postprocessing schemes when combined with the above multiscale methods for a collection of k values. From these results we will estimate a convergence

order of the schemes when combined with these multiscale methods. Although the MHM multiscale solution has naturally a continuous flux field without the need of a postprocessing scheme, we apply them in order to assess whether there is an improvement in terms of accuracy. Note that the Mean scheme does not change the MHM multiscale solution.

For the MRCM, we choose to keep the equidistribution of degrees of freedom between pressure and flux interface spaces, i.e., if we take $k = 4$, both pressure and flux interface spaces have linear functions per interface. On the other hand, the MMMFEM and the MHM with $k = 4$ are defined with cubic functions by interfaces in the pressure interface space and in the flux interface space, respectively. The experiment is performed using two types of permeability fields. For the first we use $\xi(x)$ with $\gamma = 2$ to define the permeability field $K(\mathbf{x}) = \exp(\gamma\xi(\mathbf{x}))$ in $\Omega = [0,1] \times [0,1]$ decomposed into 8×8 subdomains, each subdomain with a fine mesh of 15×15 square elements of size $h = 1/120$. For the second type we take layer 36 of the SPE10 project and use the same configuration as the last experiment of the previous section. Figure 47 shows the maximum concentration error over time from $k = 2$ until $k = 10$ for the above permeability fields. Table 4 displays the order reduction obtained by the multiscale methods.

	# of dof's per interface k				
	2	4	6	8	10
Log-normal	86.7%	73.3%	60.0%	46.7%	33.3%
Layer 36	90.0%	80.0%	70.0%	60.0%	50.0%

Table 4 – Order reduction obtained by the multiscale method by enriching the interface spaces.

For the log-normal field (left column on Fig.47) the smallest errors are obtained by the MMMFEM with all the downscaling schemes followed by the MRCM, with similar errors for $k = 2$ in all multiscale methods. In this type of permeability field the MMMFEM shows a quadratic convergence order when combined with the Patch and Stitch schemes that drops to 1.5 when combined with the Mean scheme. On the other hand, the MRCM shows a 1.5 convergence order when combined with the Patch and Stitch schemes that drops to linear when combined with the Mean scheme and the MHM shows a convergence order of 0.5 when combined with all the downscaling schemes.

For layer 36 (right column of Fig.47) the MMMFEM shows a quadratic numerical convergence when combined with the Patch scheme, that drops to 1.5 with the Stitch scheme and again drops to 0.5 when combined with the Mean scheme. The convergence order for the MRCM drops to 0.5 in combination with all the downscaling schemes, the same convergence order obtained for the MHM. A summary of convergence orders are depicted in Table 5.

4.6 Concluding remarks

We have started by recalling the main ingredients and implementation aspects of the recently proposed Multiscale Robin Coupled Method (MRCM). After that, we have proposed

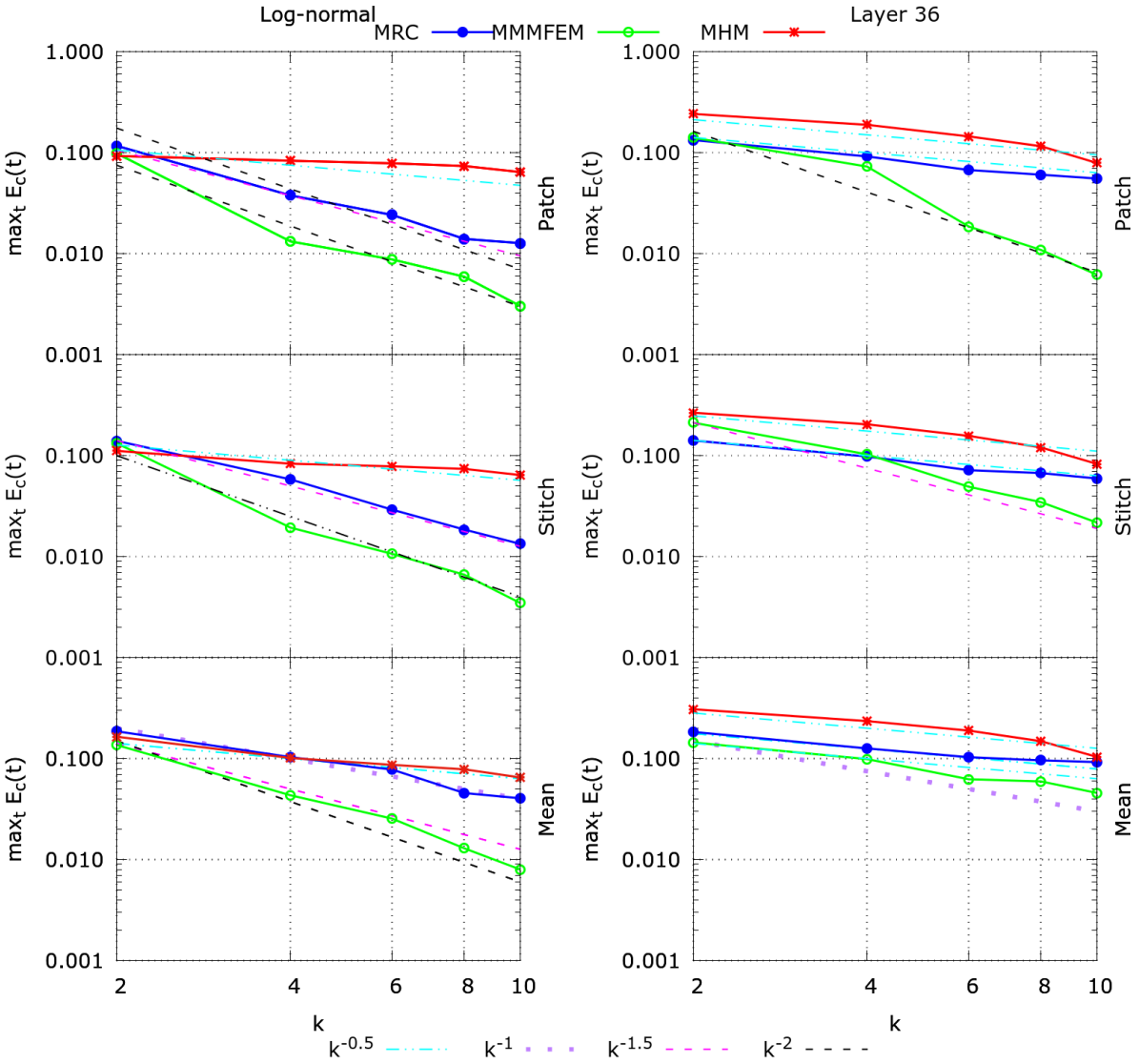

Source: Elaborated by the author.

Figure 47 – Maximum relative errors over time t of the MRCM, MMMFEM and MHM for the log-normal field (left column) and the Layer 36 (right column) for enriched interface spaces.

two postprocessing methods to recover mass-conserving velocity fields from multiscale solutions that are only conservative in coarse scales. The new methods were compared with a standard method of the literature in terms of accuracy of the transport of contaminant in subsurface. Two types of very heterogeneous permeability fields were considered, the ones generated with the Hydro-Gen package and the fields given by the SPE10 project. Initially, the comparison was carried out with solutions produced by the MRCM with a set of predefined parameters. Thereafter, by suitable choices of the parameter β, we have compared the performance of the postprocessing procedures with solutions produced by the MMMFEM, the MRCM and the MHM with the same order reduction.

The numerical results indicate that the Patch method consistently has the smallest errors,

	Log-normal			Layer 36		
	Patch	Stitch	Mean	Patch	Stitch	Mean
MRCM	$\mathscr{O}(k^{-1.5})$	$\mathscr{O}(k^{-1.5})$	$\mathscr{O}(k^{-1.0})$	$\mathscr{O}(k^{-0.5})$	$\mathscr{O}(k^{-0.5})$	$\mathscr{O}(k^{-0.5})$
MMMFEM	$\mathscr{O}(k^{-2})$	$\mathscr{O}(k^{-2.0})$	$\mathscr{O}(k^{-1.5})$	$\mathscr{O}(k^{-2.0})$	$\mathscr{O}(k^{-1.5})$	$\mathscr{O}(k^{-0.5})$
MHM	$\mathscr{O}(k^{-0.5})$	$\mathscr{O}(k^{-0.5})$	$\mathscr{O}(k^{-0.5})$	$\mathscr{O}(k^{-0.5})$	$\mathscr{O}(k^{-0.5})$	$\mathscr{O}(k^{-0.5})$

Table 5 – Convergence order on concentration for the multiscale methods in two types of permeability fields.

Source: Elaborated by the author.

followed by the Stitch method (which is the least expensive of the three) and then the Mean method. These results were very robust for the two types of permeability fields considered. Furthermore, the new methods have reduced the velocity error at subdomain interfaces of the multiscale approximations, a task not accomplished by the Mean method.

Combining the Patch method with the MMMFEM proved to be the most accurate procedure in channelized fields, although significant differences in accuracy with other postprocessing schemes were only attained for multiscale solutions with order reduction less than or equal to 65%. In the more interesting cases with order reduction above 75% the Stitch method provides comparable accuracy and thus provides the best compromise between computational cost and precision.

CHAPTER

5

MAIN RESULTS AND FUTURE WORK

In this section the main result obtained are summarized and future works are discussed.

5.1 Main contributions

The main contributions of this project can be summarized as:

- A new multiscale mixed method was proposed, the Multiscale Robin Coupled Method for subsurface flows.
  - Formal well-posedness is proved;
  - Provides a variational formulation for the Two-Lagrange-Multiplier domain decomposition method;
  - Allows for independent choices for interface spaces;
  - *Generalize existing multiscale methods of the literature*;
  - First assessment of the MHM with $H(\mathrm{div})$ subelement grid discretization;
  - Suitable choice of the parameter β produces more accurate results when compared to existing methods in realistic high-channelized porous formations.
- The accuracy of the MRCM is assessed for two types of interface spaces: piecewise polynomial and *informed spaces*.
  - Provides a strategy to build-up the informed spaces;
  - Show improved local approximations for fluxes in channelized formations;
  - First comparison of the MMMFEM, MRCM and MHM in terms of accuracy with polynomial and informed spaces;
  - First assessment of the MHM with informed spaces;

  - Fully defines the parameters of the MRCM ($\beta, \mathscr{P}_H, \mathbb{U}_H$) given a multiscale reduction, *k dof's* in this case, leading to a competitive method when compared to similar methods of the literature.
  - MRCM shows less iterations of GMRES to attain a given tolerance when compared to the MMMFEM and the MHM.

- Two new strategies to recover local mass conservation of multiscale solution that are only conservative on coarse scales were proposed and compared with a standard method of the literature in terms of accuracy in contaminant transport.

  - New methods reduce the flux error between subdomains of the multiscale approximations;
  - Improved precision compared to the Mean method with similar/reduced computational cost.

5.1.1 Future work

Recently, in (GUIRALDELLO *et al.*, 2018b) and (GUIRALDELLO *et al.*, 2018a), an exhaustive assessment of the MRCM has been presented. However, several improvements are still under investigation, some of them we intend to address in a postdoc project. The main topics we are concerned are: (i) improved choices of interface spaces; (ii) extension of the method to a multilevel/multigrid context so as to accelerate convergence of iterative methods; (iii) 3D HPC implementation of the MRCM. In what follows we provide an overview of what we intend to survey and some of the expected results.

5.1.1.1 New informed spaces - LOD

In the original implementation of the MRCM (see (GUIRALDELLO *et al.*, 2018b)), we have considered piecewise polynomial spaces over the skeleton Γ of the domain decomposition, both for pressure $\mathscr{P}_H$ and flux $\mathscr{U}_H$. This choice is standard for a first exploration of a multiscale method, since it allows rigorous analysis. For highly heterogeneous media an alternative are *informed spaces*, in which fine-mesh solutions are precomputed at some neighborhood (*oversampling*) of the subdomain and/or the interface between subdomains. From these solution, some dimensionality reduction technique is applied to build $\mathscr{P}_H$ and $\mathscr{U}_H$. The MRCM with informed spaces was first explored in (GUIRALDELLO *et al.*, 2018a).

We intend to study and establish new strategies for the construction of informed spaces by exploring new regions of oversampling, new strategies to compute the offline spaces and basis reduction methods, seeking for accuracy improvements for the 2D case and possibly extending to 3D.

The informed spaces described above are constructed in an *offline* stage. Recently in the literature the concept of *online spaces* has been explored (CHUNG; EFENDIEV; LEUNG, 2018) where the informed spaces are constructed from multiscale solutions of low computational cost, so as to include global information as boundary condition in the oversampling problem. This in turn leads to procedures that allow to enrich the interface spaces iteratively.

5.1.1.2 A Multilevel MRCM

The size of the interface linear system involved in the MRCM depends on the dimensions of the coarse interface spaces $\mathscr{U}_H$ and $\mathscr{P}_H$. A reasonable multiscale approximation to the true (fine grid) solution can be obtained by suitably choosing the interface spaces to be of sufficiently large dimension (see (ARBOGAST; XIAO, 2015)). In the three dimensional case this may end up leading to a linear system of intermediate size whose resolution still requires an efficient linear solver. Available linear algebra packages, generally provides several preconditioned Krylov based iterative methods that can be used for such purpose.

We intend to explore other alternatives that have the potential to solve the problem more efficiently, namely

(i) Multilevel/Multigrid linear solvers based on successive refinements/coarsening of the interface spaces $\mathscr{U}_H$ and $\mathscr{P}_H$;

(ii) Use of the MRCM as a preconditioner of the fine grid problem into a Krylov based iterative solver.

5.1.1.3 3D HPC implementation

In (GUIRALDELLO *et al.*, 2018b) and (GUIRALDELLO *et al.*, 2018a) the implementation has been restricted to the two dimensional case. An important point is the extension of these methods to three-dimensional case into a high-performance environment aiming to solve large size reservoirs, containing up to 1 billion computational cells, so as to deal with the unusual thick Brazil's reservoirs in the pre-salt layer and capture the severe heterogeneity of the permeability field.

BIBLIOGRAPHY

AARNES, J. E. On the Use of a Mixed Multiscale Finite Element Method for Greater Flexibility and Increased Speed or Improved Accuracy in Reservoir Simulation. **SIAM Multiscale Model. Simul.**, v. 2, n. 3, p. 421–439, 2006. Citation on page 27.

ARAYA, R.; HARDER, C.; PAREDES, D.; VALENTIN, F. Multiscale hybrid-mixed method. **SIAM J. Numer. Anal.**, v. 51, n. 6, p. 3505–3531, 2013. Citations on pages 31, 37, and 70.

ARBOGAST, T. Analysis of a Two-scale, Locally Conservative Subgrid Upscaling for Elliptic Problems. **SIAM J. Numer. Anal.**, v. 42, p. 576–598, 2004. Citation on page 28.

ARBOGAST, T.; COWSAR, L. C.; WHEELER, M. F.; YOTOV, I. Mixed finite element methods on nonmatching multiblock grids. **SIAM J. Numer. Anal.**, v. 37, n. 4, p. 1295–1315, 2000. Citations on pages 31, 32, 39, 43, 50, and 55.

ARBOGAST, T.; PENCHEVA, G.; WHEELER, M. F.; YOTOV, I. A multiscale mortar mixed finite element method. **SIAM Multiscale Model. Simul.**, v. 6, n. 1, p. 319–346, 2007. Citations on pages 28, 30, 32, 36, 55, 70, and 95.

ARBOGAST, T.; WHEELER, M. F.; YOTOV, I. Mixed finite elements for elliptic problems with tensor coefficients as cell-centered finite differences. **SIAM J. Numer. Anal.**, v. 34, n. 2, p. 828–852, 1997. Citations on pages 31, 32, 45, 46, and 98.

ARBOGAST, T.; XIAO, H. Two-level mortar domain decomposition preconditioners for heterogeneous elliptic problems. **Computer Methods in Applied Mechanics and Engineering**, v. 292, p. 221 – 242, 2015. ISSN 0045-7825. Special Issue on Advances in Simulations of Subsurface Flow and Transport (Honoring Professor Mary F. Wheeler). Available: <http://www.sciencedirect.com/science/article/pii/S0045782514004198>. Citation on page 123.

BABUSKA, I.; OSBORN, E. Generalized finite element methods: Their performance and their relation to mixed methods. **SIAM J. Numer. Anal.**, v. 31, p. 510–536, 1983. Citations on pages 27 and 71.

BARANGER, J.; MAITRE, J.-F. c.; OUDIN, F. Connection between finite volume and mixed finite element methods. **ESAIM: Mathematical Modelling and Numerical Analysis - Modélisation Mathématique et Analyse Numérique**, Dunod, v. 30, n. 4, p. 445–465, 1996. Available: <http://www.numdam.org/item/M2AN_1996__30_4_445_0>. Citations on pages 31 and 32.

BELGACEM, F. The mortar finite element method with Lagrange multipliers. **Numer. Math.**, v. 84, n. 2, p. 173–197, 1999. Citations on pages 31, 37, and 43.

BELLIN, A.; RUBIN, Y. Hydro_gen: A spatially distributed random field generator for correlated properties. **Stochastic Hydrology and Hydraulics**, v. 10, n. 4, p. 253–278, Nov 1996. ISSN 1435-151X. Available: <https://doi.org/10.1007/BF01581869>. Citation on page 108.

BERNARDI, C.; MADAY, Y.; PATERA, A. T. A new nonconforming approach to domain decomposition: The mortar element method. In: **Nonlinear Partial Differential Equations**

and their Applications. Collège de France Seminar, volume XI. Lectures presented at the weekly seminar on applied mathematics, Paris, France, 1989-1991. [S.l.]: Harlow: Longman Scientific & Technical; New York: John Wiley & Sons, Inc., 1994. p. 13–51. ISBN 0-582-23800-5/pbk; 0-470-23367-2/pbk. Citations on pages 31 and 37.

BLANCO, P.; LEIVA, J.; BUSCAGLIA, G. C. A black-box decomposition approach for coupling heterogeneous components in hemodynamics simulations. **Int. J. Numer. Method. Biomed. Eng.**, John Wiley & Sons, Ltd, v. 29, n. 3, p. 408–427, 2013. ISSN 2040-7947. Available: <http://dx.doi.org/10.1002/cnm.2519>. Citation on page 40.

BOSMA, S.; HAJIBEYGI, H.; TENE, M.; TCHELEPI, H. Multiscale finite volume method for discrete fracture modeling on unstructured grids (MS-DFM). **Journal of Computational Physics**, v. 351, p. 145 – 164, 2017. ISSN 0021-9991. Available: <http://www.sciencedirect.com/science/article/pii/S0021999117306927>. Citations on pages 28 and 71.

BREZZI, F.; DOUGLAS, J.; DURÁN, R.; FORTIN, M. Mixed finite elements for second order elliptic problems in three variables. **Numerische Mathematik**, v. 51, n. 2, p. 237–250, 1987. ISSN 0945-3245. Available: <http://dx.doi.org/10.1007/BF01396752>. Citation on page 31.

BREZZI, F.; DOUGLAS, J.; FORTIN, M.; MARINI, L. D. Efficient rectangular mixed finite elements in two and three space variables. **ESAIM: Mathematical Modelling and Numerical Analysis - Modélisation Mathématique et Analyse Numérique**, Dunod, v. 21, n. 4, p. 581–604, 1987. Available: <http://eudml.org/doc/193515>. Citation on page 31.

BREZZI, F.; DOUGLAS, J.; MARINI, L. D. Two families of mixed finite elements for second order elliptic problems. **Numer. Math.**, v. 47, p. 217–236, 1985. Citations on pages 31 and 37.

BREZZI, F.; FORTIN, M. **Mixed and Hybrid Finite Elements Methods**. Springer-Verlag, 1991. (Springer series in computational mathematics). ISBN 9780387975825. Available: <https://books.google.com.br/books?id=yYwZAQAAIAAJ>. Citation on page 31.

CALO, V. M.; EFENDIEV, Y.; GALVIS, J.; GHOMMEM, M. Multiscale empirical interpolation for solving nonlinear pdes using generalized multiscale finite element methods. **arXiv preprint arXiv:1407.0103v1**, 2014. Citation on page 72.

CALO, V. M.; EFENDIEV, Y.; GALVIS, J.; LI, G. Randomized oversampling for generalized multiscale finite element methods. **SIAM Multiscale Model. Simul.**, v. 14, n. 1, p. 482–501, 2016. Citations on pages 72 and 77.

CHAVENT, G.; JAFFRÉ, J. **Mathematical Models and Finite Elements for Reservoir Simulation - Single phase, Multiphase and Multicomponent Flows through Porous Media**. [S.l.]: North-Holland, 1986. (Studies in Mathematics and its Applications). Citations on pages 26, 31, and 32.

CHEN, W.; GUNZBURGER, M.; HUA, F.; WANG, X. A Parallel Robin-Robin Domain Decomposition Method for the Stokes-Darcy System. **SIAM J. Numer. Anal.**, v. 49, n. 3, p. 1064–1084, 2011. Citation on page 30.

CHEN, Z. **Finite Element Methods and Their Applications**. Springer Berlin Heidelberg, 2005. (Scientific Computation). ISBN 9783540240785. Available: <https://books.google.com.br/books?id=DEGlOJ1KZOwC>. Citation on page 26.

____. **Mathematical Techniques in Oil Recovery**. [S.l.]: Siam, 2007. (Reservoir Simulation). Citation on page 26.

CHEN, Z.; HOU, T. Y. A Mixed Multiscale Finite Element Method for Elliptic Problems with Oscillating Coefficients. **Math. Comp**, v. 72, p. 541–576, 2003. Citation on page 28.

CHEN, Z.; HUAN, G.; MA, Y. **Computational Methods for Multiphase Flows in Porous Media**. [S.l.]: Computational Science & Engineering. Society for Industrial and Applied Mathematics (SIAM), Philadelphia, PA, 2006. Citation on page 26.

CHRISTIE, M.; BLUNT, M. Tenth SPE comparative solution project: A comparison of upscaling techniques. **SPE-66599-MS,Society of Petroleum Engineers**, 2001. Citations on pages 58, 77, and 115.

CHUNG, E. T.; EFENDIEV, Y.; HOU, T. Adaptive multiscale model reduction with generalized multiscale finite element methods. **J. Comp. Phys.**, v. 320, p. 69–95, 2016. Citation on page 71.

CHUNG, E. T.; EFENDIEV, Y.; LEUNG, W. T. Fast online generalized multiscale finite element method using constraint energy minimization. **Journal of Computational Physics**, v. 355, p. 450 – 463, 2018. ISSN 0021-9991. Available: <http://www.sciencedirect.com/science/article/pii/S0021999117308604>. Citations on pages 71 and 123.

CHUNG, E. T.; FU, S.; YANG, Y. An enriched multiscale mortar space for high contrast flow problems. **arXiv preprint arXiv:1609.02610**, 2016. Citations on pages 44 and 71.

CORREA, M.; LOULA, A. F. D. Stabilized velocity post-processings for Darcy flow in heterogeneous porous media. **Commun. Numer. Methods Eng.**, John Wiley & Sons, Ltd., v. 23, n. 6, p. 461–489, 2007. ISSN 1099-0887. Available: <http://dx.doi.org/10.1002/cnm.904>. Citation on page 37.

COUSSY, O. **Mechanics and Physics of Porous Solids**. [S.l.]: Wiley, 2010. ISBN 978-0-470-72135-3. Citation on page 26.

COWSAR, L. C.; WHEELER, M. F. Parallel Domain Decomposition Method for Mixed Finite Elements for Elliptic Partial Differential Equations. **Fourth International Symposium on Domain decomposition methods for partial differential equations, Philadelphia, PA**, p. 358–372, 1991. Citation on page 30.

DOUGLAS, J.; PAES-LEME, P. J.; ROBERTS, J.; WANG, J. P. A parallel iterative procedure aplicable to the approximate solution of second order partial differential equations by mixed finite element methods. **Numer. Math.**, v. 65, n. 1, p. 95–108, 1993. Citations on pages 31, 37, 38, 42, 70, and 94.

DURLOFSKY, L. J.; GERRITSEN, M. G. Modeling Fluid Flow in Oil Reservoirs. **Annu. Rev. Fluid Mech**, v. 37, n. 37, p. 211–238, 2006. Citation on page 26.

EFENDIEV, Y.; HOU, T. **Multiscale Finite Element Methods. Theory and Applications.** [S.l.]: Springer, 2008. Citation on page 26.

EYMARD, R.; GALLOUËT, T.; HERBIN, R. **Finite Volume Methods**. [S.l.]: Elsevier Science B.V., Amsterdam, 2000. 713-1020 p. (Handbook of Numerical Analysis, 7). Citations on pages 31 and 32.

FRANCISCO, A.; GINTING, V.; PEREIRA, F.; RIGELO, J. Design and implementation of a multiscale mixed method based on a nonoverlapping domain decomposition procedure. **Math. Comput. Simul.**, v. 99, p. 125–138, 2014. Citations on pages 31, 37, 49, 58, 62, 70, 74, and 94.

GANIS, B.; YOTOV, I. Implementation of a mortar mixed finite element method using a multiscale flux basis. **Comput. Methods Appl. Mech. Engrg.**, v. 198, p. 3989–3998, 2009. Citations on pages 30, 43, 44, 48, and 73.

GELHAR, L. W. **Flow and Transport in Porous Formations**. [S.l.]: Springer, New York, 1989. Citation on page 25.

____. **Stochastic Subsurface Hydrology**. [S.l.]: Prentice-Hall, Englewood Cliffs, NJ, 1993. Citation on page 25.

GINTING, V.; PEREIRA, F.; RAHUNANTHAN, A. A Prefetching Technique for Prediction of Porous Media Flows. **Computa. Geosci.**, v. 18, n. 5, p. 661–675, 2014. Citation on page 25.

GLOWINSKI, R.; WHEELER, M. F. Domain decomposition and mixed finite element methods for elliptic problems. **First international symposium on domain decomposition methods for partial differential equations**, p. 144–172, 1988. Citations on pages 30, 33, 39, and 43.

GOTTLIEB, S.; SHU, C.-W. Total variation diminishing runge-kutta schemes. **Math. Comput.**, American Mathematical Society, Boston, MA, USA, v. 67, n. 221, p. 73–85, Jan. 1998. ISSN 0025-5718. Available: <http://dx.doi.org/10.1090/S0025-5718-98-00913-2>. Citation on page 109.

GUIRALDELLO, R. T.; AUSAS, R. F.; SOUSA, F. S.; PEREIRA, F.; BUSCAGLIA, G. C. Interface spaces for the multiscale Robin coupled method in reservoir simulation. **Math. Comput. Simul.**, 2018. Citations on pages 33, 94, 95, 98, 100, 122, and 123.

____. The multiscale Robin coupled method for flows in porous media. **J. Comput. Phys.**, v. 355, p. 1–21, 2018. Citations on pages 31, 33, 70, 73, 74, 78, 83, 94, 95, 98, 100, 102, 122, and 123.

HAJIBEYGI, H.; BONFIGLI, G.; HESSE, M. A.; JENNY, P. Iterative multiscale finite-volume method. **Journal of Computational Physics**, v. 227, n. 19, p. 8604 – 8621, 2008. ISSN 0021-9991. Available: <http://www.sciencedirect.com/science/article/pii/S002199910800332X>. Citation on page 71.

HAJIBEYGI, H.; TCHELEPI, H. A. Compositional Multiscale Finite-Volume Formulation. **Society of Petroleum Engineers**, v. 19, n. 2. Citations on pages 28 and 71.

HARDER, C.; PAREDES, D.; VALENTIN, F. A family of multiscale hybrid-mixed finite element methods for the Darcy equation with rough coefficients. **J. Comput. Phys.**, v. 245, p. 107 – 130, 2013. Citations on pages 31, 37, 43, 49, 50, 55, and 95.

____. On a multiscale hybrid-mixed method for advective-reactive dominated problems with heterogeneous coefficients. **SIAM Multiscale Model. Simul.**, v. 13, n. 2, p. 491–518, 2015. Citation on page 70.

HOU, T. Y.; WU, X. H. A Multiscale Finite Element Method for Elliptic Problems in Composite Materials and Porous Media. **J. Comput. Phys.**, v. 134, p. 169–189, 1997. Citations on pages 26 and 27.

HUGHES, T. Multiscale Phenomena: Green's Functions, the Dirichlet-to-Neumann Formulation, Subgrid Scale Models, Bubbles and the Origins of Stabilized Methods. **Comput. Methods Appl. Mech. Engrg.**, v. 127, p. 387–401, 1995. Citation on page 28.

HUGHES, T.; FEIJOO, G.; MAZZEI, L.; QUINCY, J. The Variational Multiscale Method - A Paradigm for Computational Mechanics. **Comput. Methods Appl. Mech. Engrg.**, v. 166, p. 3–24, 1998. Citation on page 28.

JENNY, P.; LEE, S. H.; TCHELEPI, H. A. Multi-scale finite-volume method for elliptic problems in subsurface flow simulation. **J. Comput. Phys.**, v. 187, p. 47–67, 2003. Citations on pages 28, 37, and 71.

KIPPE, V.; AARNES, J. E.; LIE, K. A Comparison of Multiscale Methods for Elliptic Problems in Porous Media Flow. **Comput Geosci.**, v. 12, n. 3, p. 377–398, 2008. Citation on page 28.

KöNNö, J.; SCHOETZAU, D.; STENBERG, R. Mixed finite element methods for problems with Robin boundary conditions. **SIAM J. Numerical Analysis**, v. 49, p. 285–308, 2011. Citation on page 27.

LAW, K.; STUART, A.; ZYGALAKIS, K. **Data Assimilation: A Mathematical Introduction**. [S.l.]: Springer. (Texts in Applied Mathematics, 62). Citation on page 25.

LEE, S. H.; ZHOU, H.; TCHELEPI, H. A. Adaptive multiscale finite-volume method for nonlinear multiphase transport in heterogeneous formations. **Journal of Computational Physics**, v. 228, n. 24, p. 9036 – 9058, 2009. ISSN 0021-9991. Available: <http://www.sciencedirect.com/science/article/pii/S002199910900494X>. Citations on pages 28 and 71.

LEIVA, J.; BLANCO, P.; BUSCAGLIA, G. C. Iterative strong coupling of dimensionally heterogeneous models. **Int. J. Numer. Methods Eng.**, John Wiley & Sons, Ltd., v. 81, n. 12, p. 1558–1580, 2010. ISSN 1097-0207. Available: <http://dx.doi.org/10.1002/nme.2741>. Citation on page 40.

LIONS, P. L. On the schwars alternating method iii: A variant for nonoverlapping subdomains. In: ____. **Third International Symposium on Domain Decomposition Methods for Partial Differential Equations**. Society for Industrial and Applied Mathematics, 1990. (Domain decomposition methods - international symposium), chap. 11, p. 202–223. ISBN 9780898712537. Available: <https://books.google.com.br/books?id=_GJ1DXrAyJ8C>. Citation on page 30.

LOISEL, S. Condition number estimates for the nonoverlapping optimized Schwarz method and the 2-Lagrange multiplier method for general domains and cross points. **SIAM J. Numer. Anal.**, v. 51, n. 6, p. 3062–3083, 2013. Citations on pages 31, 38, and 42.

LOISEL, S.; NGUYEN, H.; SCHEICHL, R. Optimized Schwarz and 2-Lagrange multiplier methods for multiscale elliptic PDEs. **SIAM J. Sci. Comput.**, v. 37, n. 6, p. A2896–A2923, 2015. Citation on page 42.

LUNATI, I.; JENNY, P. Multiscale finite-volume method for compressible multiphase flow in porous media. **Journal of Computational Physics**, v. 216, n. 2, p. 616 – 636, 2006. ISSN 0021-9991. Available: <http://www.sciencedirect.com/science/article/pii/S0021999106000039>. Citations on pages 28 and 71.

MADAY, Y.; MAGOULÈS, F. Absorbing interface conditions for domain decomposition methods: A general presentation. **Comput. Methods Appl. Mech. Engrg.**, v. 195, p. 3880–3900, 2006. Citation on page 42.

MATHEW, T. **Domain Decomposition Methods for the Numerical Solution of Partial Differential Equations**. Springer Berlin Heidelberg, 2008. (Lecture Notes in Computational Science and Engineering). ISBN 9783540772095. Available: <https://books.google.com.br/books?id=9n9PTTvimG4C>. Citation on page 29.

NEDELEC, J. C. Mixed finite elements in r3. **Numerische Mathematik**, v. 35, n. 3, p. 315–341, 1980. ISSN 0945-3245. Available: <http://dx.doi.org/10.1007/BF01396415>. Citation on page 31.

QUARTERONI, A.; VALLI, A. **Domain Decomposition Methods for Partial Differential Equations**. [S.l.]: Clarendon press - Oxford, 1999. Citations on pages 29 and 31.

RAVIART, P. A.; THOMAS, J. M. A mixed finite element method for 2nd order elliptic problems. In: **Mathematical Aspects of the Finite Elements Method**. [S.l.]: Springer, Berlin, 1977, (Lecture Notes in Mathematics, 606). p. 292–315. Citations on pages 31 and 37.

ROBERTS, J. E.; THOMAS, J. M. Mixed and hybrid methods. In: CIARLET, P.; LIONS, J. (Ed.). **Handbook of Numerical Analysis, Vol. II**. [S.l.]: North-Holland, Amsterdam, 1991. p. 523–639. Citation on page 31.

RUSSEL, T. F.; WHEELER, M. F. **Chapter II: Finite Element an Finite Difference Methods for Continuous Flows in Porous Media**. [S.l.]: SIAM, 1983. (The Mathematics of Reservoir Simulation). Citations on pages 31 and 32.

SILVA, R. C. C.; LOULA, A. F. D. Local residual error estimator and adaptive finite element analysis of poisson problems. **Comput. Struct.**, v. 80, p. 2027 – 2034, 2002. ISSN 0045-7949. Available: <http://www.sciencedirect.com/science/article/pii/S0045794902002602>. Citation on page 37.

SMITH, R. C. **Uncertainty Quantification: Theory, Implementation, and Applications**. [S.l.]: Siam, 2013. (Computational Science and Engineering). ISBN 978-1611973211. Citation on page 25.

TRANGENSTEIN, J. A.; BELL, J. B. Mathematical Structure of Compositional Reservoir Simulation. **SIAM J. Appl. Math.**, v. 10, n. 5, p. 817–845, 1989. Citation on page 26.

____. Mathematical Structure of the Black Oil Model for Petroleum Reservoir Simulation. **SIAM J. Appl. Math.**, v. 49, n. 3, p. 749–783, 1989. Citation on page 26.

VOHRALÍK, M. Equivalence between lowest order mixed finite element and multipoint finite volume methods on simplicial meshes. **ESAIM**, v. 40, n. 2, 2006. Citations on pages 31, 32, and 46.

ZHANG, D.; LU, Z. An Efficient, High-order Perturbation Approach for Flow in Random Porous Media via Karhunen-Loéve and Polynomial Expansions. **J. Comput. Phys.**, v. 194, p. 773–794, 2004. Citation on page 25.


ICMC
USP
SÃO CARLOS